Diversity in cytokinesis and the regulation of cytokinesis across cell types

Imge Ozugergin

A Thesis
In the Department
of
Biology

Presented in Partial Fulfillment of the Requirements
For the Degree of
Doctor of Philosophy (Biology) at
Concordia University
Montreal, Quebec, Canada

July 2022

CONCORDIA UNIVERSITY

School of Graduate Studies

This is to certify that the thesis prepared

By: Imge Ozugergin
Entitled: Diversity in cytokinesis and the regulation of cytokinesis across cell types

and submitted in partial fulfillment of the requirements for the degree of

Doctor of Philosophy (Biology)

complies with the regulations of the University and meets the accepted standards with respect to originality and quality.

Signed by the final examining committee:

_____Chair
Dr.

_____Thesis Supervisor
Dr. Alisa Piekny

_____Examiner
Dr. Stephanie Crane Weber

_____Examiner
Dr. Malcolm Whiteway

_____External Examiner
Dr. Peter Darlington

_____External Examiner
Dr. Abigail Gerhold

Approved by _____
Dr. Robert Weladji, Graduate Program Director

July 2022 _____
Dr. Pascale Sicotte, Dean
Faculty of Arts and Science

ABSTRACT

Diversity in cytokinesis and the regulation of cytokinesis across cell types

Imge Ozugergin, Ph.D.

Concordia University, 2022

Cytokinesis physically cleaves a cell into two through the assembly and constriction of an actomyosin ring. This process is crucial for growth and development, and the core machinery is highly conserved across metazoans. Studies in different systems have shown that both spindle-dependent and -independent mechanisms control this machinery. However, these mechanisms appear to vary widely among organisms and cell types. In addition, most of our knowledge of cytokinesis has been generated using only a couple of transformed cell types cultured *in vitro*, or in early embryos before cells adopt fates. This raises the question of how cytokinesis is regulated in diverse cell types and developmental contexts. This thesis characterizes cytokinesis in cells with different fates in *C. elegans*, and in mammalian cultured cell lines that have not been studied in this context before. In Chapter 2, we provide the first in-depth description of cytokinesis in AB and P_1 cells with different fates in the two-cell *C. elegans* embryo. We found that each cell type has unique cytokinesis kinetics, driven by different thresholds of myosin. Our results revealed that cell fate, size and/or ploidy are contributing factors that regulate myosin levels and/or organization to influence these kinetics. We also demonstrated how a chromatin-dependent mechanism regulates cytokinesis differently in the two cell types. In Chapter 3, we compare cytokinesis kinetics for the first time in 5 different cultured mammalian cell types by studying the localization of endogenously tagged machinery. We found that this machinery has distinct spatiotemporal

localization which reflects differences in cytokinesis kinetics among the cell types. Overall, this thesis highlights the diversity in cytokinesis and cytokinesis regulation, and explores the criteria that should be considered when conducting or interpreting cytokinesis research.

ACKNOWLEDGEMENTS

Firstly, I would like to thank my supervisor, Dr. Alisa Piekny. I have gained more during my time in the Piekny lab than I thought possible, and there is no doubt that it is thanks to the scientific curiosity you encourage, and the compassionate workplace environment you have created. I would also like to acknowledge the support and encouragement of my committee members, Drs. Stephanie Crane Weber and Malcolm Whiteway, whose insight and advice over the years has been invaluable. I would also like to thank Dr. Zerges, who has contributed greatly to my learning since I joined Concordia.

I would like to especially thank Dr. Chris Law for his help throughout my graduate studies. I am very grateful for the training you have provided and the tools you have developed for me over the years. Without these, this thesis would have looked very different.

Last, but certainly not least, I would like to thank my support system; I have made lifelong friends in the lab, and many past and present Piekny lab members (or affiliated members) have made the lab a place I did not want to miss out on. In particular, I thank Mathieu Husser, Nhat Pham, Kevin Larocque, as well as Su Pin Koh, Björn Tam and the incomparable Holladay for their moral and academic support over the years. I would also like to thank my non-colleague friends, especially Yiğithan Özden and Yunus Thurston; growing up together has been an adventure, and I appreciate your encouragement and bizarreness throughout this chapter of my life. We know that it is not the pandemic, but the contents of this thesis that has kept our friendship virtual for many years.

DEDICATIONS

This thesis is dedicated to my husband, Mathieu (not that I have other husbands). It makes perfect sense that our life together started in the lab, and that even our work complements each other. I am sorry that my ability to accurately convey my appreciation for you is as good as my ability to rhyme (subpar, I am told), but it is challenging to describe the fortune of having such a supporting, helpful and resourceful partner.

As a self-permitted bonus dedication, I would like to also dedicate this thesis to my Turkish and French families. In particular, thank you to my mother, father, sister and grandparents, who taught me the values that push me to work for myself and others. Thank you for your sustained consciousness as I talked about the infinite number of circles and lines that I have drawn over these past years, and thank you for always being there. One of my fondest memories of graduate school is when some of you were able to visit. The many facial expressions I witnessed as you tried to figure out what to do with yourselves in the lab will be an accurate summary of the past years.

CONTRIBUTION OF AUTHORS

Chapter 2: Diverse mechanisms regulate contractile ring assembly for cytokinesis in the two-cell *Caenorhabditis elegans* embryo

Alisa Piekny supervised the project and edited the manuscript.

Imge Ozugergin wrote the manuscript, prepared all figures, and performed the majority of experiments and data analysis.

Chris Law wrote macros for FIJI and MATLAB and performed data analysis. These contributions apply to all figures except Figure 12, and Figures S1, S5B-D, and S6.

Karina Mastronardi contributed to some of the imaging experiments using confocal microscopy. These contributions apply to all figures except Figures 9 and 12, and Figures S2-4, and S6.

Daniel Beaudet performed the pull-down experiments in Figure 11 and Figure S7.

Chapter 3: Cytokinetic diversity across cultured mammalian cells

Alisa Piekny and Vincent J.J. Martin supervised the project, and edited the manuscript.

Mathieu Husser generated the tagged cell lines, wrote the majority of the manuscript, prepared figures, and performed data analysis. These contributions apply to all figures except the analysis shown in Figure 16.

Imge Ozugergin wrote part of the manuscript, edited figures, performed experiments and data analysis. These contributions apply to all figures except Figures 13 and S8, and the analysis shown in Figures 14 and S9.

TABLE OF CONTENTS

List of Figures ..... **xii**

List of Tables ..... **xiv**

List of Supplemental Figures ..... **xv**

List of Supplemental Tables ..... **xvi**

List of Abbreviations ..... **xvii**

Chapter 1. Introduction **1**

1.1 Overview of cytokinesis and spindle-dependent regulation **1**

1.2 Differences in cytokinesis among cell types **10**

1.3 Spindle-independent regulation of cytokinesis **15**

1.3.1 Cortical mechanisms 16

1.3.1.1 Cortical mechanisms in asymmetrically dividing cells 18

1.3.2 Kinetochores 20

1.3.3 Chromatin 21

1.3.3.1 Cortical regulation by the Ran/importin system 22

1.3.3.2 The Ran/importin system during cytokinesis 26

1.4 Thesis overview **28**

Chapter 2. Diverse mechanisms regulate contractile ring assembly for cytokinesis in the two-cell *Caenorhabditis elegans* embryo **31**

2.1 Preamble **31**

2.2 Abstract 31

2.3 Introduction 32

2.4 Materials and Methods 36

2.4.1 Strains 36

2.4.2 RNA interference 36

2.4.3 Microscopy 37

2.4.4 Image analysis 38

2.4.5 Quantitative data analysis 40

2.4.6 Pull-down assays and western blots 42

2.4.7 Statistical analysis 43

2.5 Results 44

2.5.1 Cytokinesis occurs differently in AB and P_1 cells 44

2.5.2 Contractility controls the rate of ring assembly 48

2.5.3 Cell fate determines the rate of ring assembly 52

2.5.4 Cell size and ploidy influence the rate of ring assembly 55

2.5.5 The Ran pathway regulates cytokinesis differently in AB and P_1 cells 60

2.5.6 Ran regulation occurs through different components in AB and P_1 cells 64

2.6 Discussion 68

2.6.1 AB and P_1 cells have distinct cytokinesis kinetics 68

2.6.2 Differences in AB and P_1 ring assembly are fate dependent 69

2.6.3 Size and ploidy govern differences in AB and P_1 ring closure kinetics 72

2.6.4 The Ran pathway regulates cytokinesis differently in AB and P_1 cells 73

Chapter 3. Cytokinetic diversity among cultured mammalian cells 76

3.1 Preamble 76

3.2 Abstract 77

3.3 Introduction 77

3.4 Materials and Methods 84

3.4.1 Cell culture 84

3.4.2 Transfection 84

3.4.3 Microscopy 85

3.4.4 Image analysis 85

3.4.5 Statistical analysis 87

3.5 Results 88

3.5.1 Visualization of endogenously tagged cytokinesis proteins 88

3.5.2 Cytokinetic diversity across mammalian cell lines 93

3.6 Discussion 100

Chapter 4. Conclusion and Future Directions 104

4.1 Overview 104

4.2 Cytokinesis kinetics differ between AB and P_1 cells in *C. elegans* embryos 105

4.3 The role of the chromatin pathway differs in AB and P_1 cells in *C. elegans* embryos 108

4.4. Cytokinesis diversity among mammalian cells 112

4.5 Future directions 115

References **118**

Supplemental Figures **144**

Supplemental Tables **164**

Appendix **165**

LIST OF FIGURES

Figure 1. Mitosis and cytokinesis 2

Figure 2. Multiple pathways regulate cytokinesis 4

Figure 3. An overview of the cell components regulating cytokinesis 7

Figure 4. Division and ingression can occur symmetrically or asymmetrically 13

Figure 5. Ran regulation of cytokinesis 23

Figure 6. AB and P_1 cells have unique cytokinesis kinetics 45

Figure 7. Cytokinesis still occurs uniquely in AB and P_1 cells after perturbing actomyosin contractility 49

Figure 8. Differences in ring assembly between AB and P_1 cells are fate dependent 53

Figure 9. Cell size and ploidy contribute to differences in ring assembly between AB and P_1 cells 57

Figure 10. Ran regulates ring assembly in AB and P_1 cell cytokinesis 62

Figure 11. Ran differently regulates ring assembly in AB and P_1 cells 66

Figure 12. Myosin levels and organization in addition to the pathways of regulation contribute to differences in cytokinesis 70

Figure 13. Endogenous tagging of cytokinesis using CRISPR/Cas9 79

Figure 14. Comparison of endogenous anillin, Ect2 and RhoA localization in HeLa cells during cytokinesis 89

Figure 15. Endogenous tagging of anillin reveals cytokinetic differences between different cell lines 94

Figure 16. Ingression occurs with variable symmetry in MDCK cells 98

Figure 17. Different models for Ran gradient function during cytokinesis 110

LIST OF TABLES

Table 1. Mean size of cells in the two-cell embryo across different conditions 56

LIST OF SUPPLEMENTAL FIGURES

Figure S1. Comparison of cytokinesis in AB and P_1 cells 144

Figure S2. AB and P_1 cells have distinct cytokinesis phases 146

Figure S3. Characterization of cytokinesis shows differences in actomyosin, and asymmetric ring closure in AB and P_1 cells 148

Figure S4. Symmetry of ring closure is similar between influenced and influence-free P_1 cells 150

Figure S5. Myosin filaments are less-well organized and aligned in *ect-2(RNAi)* AB and P_1 cells 152

Figure S6. There is no correlation between the duration of ring assembly and cell size after ECT-2 depletion, disruption of cell fate or lowering Ran-GTP in P_1 cells 154

Figure S7. Different thresholds of importin-α and -β control cytokinesis in AB and P_1 cells ...156

Figure S8. Comparison of endogenous tags with transient overexpression 158

Figure S9. Characterization of endogenous mNeonGreen-anillin, Ect2 and RhoA localization during cytokinesis 160

Figure S10. Comparison of HeLa cells expressing high and low levels of mNeonGreen-anillin 162

LIST OF SUPPLEMENTAL TABLES

Table S1. *C. elegans* strains used in this study 164

LIST OF ABBREVIATIONS

14-3-3	Protein family named after their elution and migration pattern (*C. elegans* PAR-5)
AHD	Anillin Homology domain
ANI-1	*C. elegans* anillin
Arp2/3	Actin Related Protein 2/3 complex
BHK	Baby hamster kidney cells
BSA	Bovine serum albumin
C-term	C (carboxyl)-terminus
C2	Lipid-binding domain
Cas9	CRISPR associated protein 9
CCS	Cosmic calf serum
CCM-3	Cerebral cavernous malformation-3
Cdc42	Cell division control protein 42
Cdk1	Cyclin-dependent kinase 1
CLIC4	Chloride Intracellular Channel 4
CRISPR	Clustered regularly interspaced short palindromic repeats
Cyk4	Cytokinesis defect 4 (also called MgcRacGAP [Male germ cell RacGAP (Rac GTPase activating protein), or RACGAP1; *C. elegans* CYK-4]
Dlg	Discs large
DMEM	Dulbecco's Modified Eagle Medium
DMSO	Dimethyl sulfoxide

DNA	Deoxyribonucleic acid
DSB	Double-stranded break
dsRNA	Double stranded ribonucleic acid
DTT	Dithiothreitol
Ect2	Epithelial cell transforming 2 (*C. elegans* ECT-2, *Drosophila* Pebble)
EMEM	Eagle's Minimum Essential Medium
ERM	Ezrin/Radixin/Moesin
F-actin	Filamentous actin
FBS	Fetal bovine serum
GAP	GTPase-activating protein
GCK-1	Germinal center kinase-1 (human GCK III)
GEF	Guanosine nucleotide exchange factor
GFP	Green fluorescent protein
GST	Glutathione S-transferase
GTP	Guanosine triphosphate
H2B	Histone H2B
HCT116	Human colorectal carcinoma cell line
HDR	Homology-directed repair
HEK293	Human embryonic kidney cell line
HeLa	Human cervical cancer cell line taken from Henrietta Lacks
HepG2	Human hepatocellular carcinoma cell line
HILO	Highly inclined and laminated optical sheet microscopy
HIS-58	*C. elegans* histone H2B

HRP	Horseradish peroxidase
IMA-1/-2/-3	*C. elegans* importin-α-1, -2, -3
IMB-1	*C. elegans* importin-β
IPTG	Isopropyl β-D-1-thiogalactopyranoside
Kc167	Cell line derived from *Drosophila melanogaster* embryos
L4	Fourth larval stage of *C. elegans* development
LB	Luria broth
MBP	Maltose-binding protein
MDCK	Madin-Darby canine kidney cells
MKLP1	Mitotic kinesin-like protein 1 (KIF23 [Kinesin family member 23]; *C. elegans* ZEN-4)
MP-GAP	M-phase GTPase-activating protein
NGM	Nematode growth medium
ns	Not significant
NHEJ	Non-homologous end joining
NLS	Nuclear localization signal
NMY-2	Non-muscle myosin heavy chain II
NOP-1	No Pseudocleavage-1
OD	Optical density
PAR-1/-2/-3/-6	Abnormal embryonic *par*titioning of cytoplasm -1, -2, -3, -6
PGL-1	P-granule abnormality-1
PH	Pleckstrin Homology

Pins	Partner of Inscuteable (mammalian LGN [protein with ten Leucine-Glycine-Asparagine repeats], *C. elegans* GPR-1/2 [G Protein Regulator-1/2])
PKC-3	Protein kinase C-3
Plk1	Polo-like kinase 1
PMSF	Phenylmethanesulfonyl fluoride
PP1	Protein phosphatase 1
PRC1	Protein regulator of cytokinesis 1
Rac	Ras-related C3 botulinum toxin substrate
Ran	Ras-related nuclear protein
RAN-3	*C. elegans* RCC1
RBD	RhoA-GTP binding domain
RCC1	Regulator of chromosome condensation 1
REC-8	Recombination abnormal-8
RGA-3/4	Rho GTPase activating protein-3, -4
RFP	Red fluorescent protein
RhoA	Ras homolog family member A
RNA	Ribonucleic acid
RNAi	Ribonucleic acid interference
ROCK	RhoA kinase
Rpe1	Retinal pigment epithelium cells
s.e.m.	Standard error of the mean
S2	Schneider 2 cells (derived from *Drosophila melanogaster* embryos)

Sds22	PP1 regulatory subunit (homolog of suppressor of Dis2 mutant 2)
SDS-PAGE	Sodium dodecyl sulfate-polyacrylamide gel electrophoresis
sgRNA	Single guide RNA
TBB-2	β-tubulin-2
TCA	Trichloroacetic acid
TIRF	Total internal reflection fluorescence microscopy
TPXL-1	*C. elegans* ortholog of TPX2 (Targeting Protein for *Xenopus* kinesin-like protein 2)
tsBN2	temperature sensitive RCC1 mutants of baby hamster kidney cells

CHAPTER ONE

Introduction

This chapter will be modified and submitted as a manuscript to Frontiers in Cell and Developmental Biology for their upcoming collection on the mechanics and regulation of mitotic exit and cytokinesis. Another review was previously published and is attached as an appendix.

1.1 OVERVIEW OF CYTOKINESIS AND SPINDLE-DEPENDENT REGULATION

Metazoan cytokinesis occurs due to the ingression of an actomyosin ring that pulls in the overlying membrane to physically separate the daughter cells. This process must be coordinated with mitosis to ensure the correct segregation of chromosomes and cell fate determinants, and requires a high level of spatial and temporal regulation to prevent developmental defects or pathologies **(Fig. 1)**. A wholistic view of cytokinesis considers that multiple pathways functioning at different times and originating from different places within the cell create a highly robust system that can accommodate perturbations **(Fig. 2)**. The relative role of these pathways is expected to vary with cell type, especially with differences in cell geometry, fate, size and/or ploidy. However, it is not clear how these pathways are coordinated, as most of our knowledge of cytokinesis has been acquired from studies using only a few cell types: cultured *Drosophila* cells (S2, Kc167), cultured human cells (HeLa), or undifferentiated cells in early embryos (*C. elegans*, echinoderms and *Xenopus*).

The core machinery is well-conserved among metazoans. An actomyosin ring forms in the division plane in response to active RhoA **(Fig. 2)**. RhoA is a small GTPase that is active when bound to GTP, which is generated by the guanine nucleotide exchange factor Ect2 (ECT-2 in *C.*

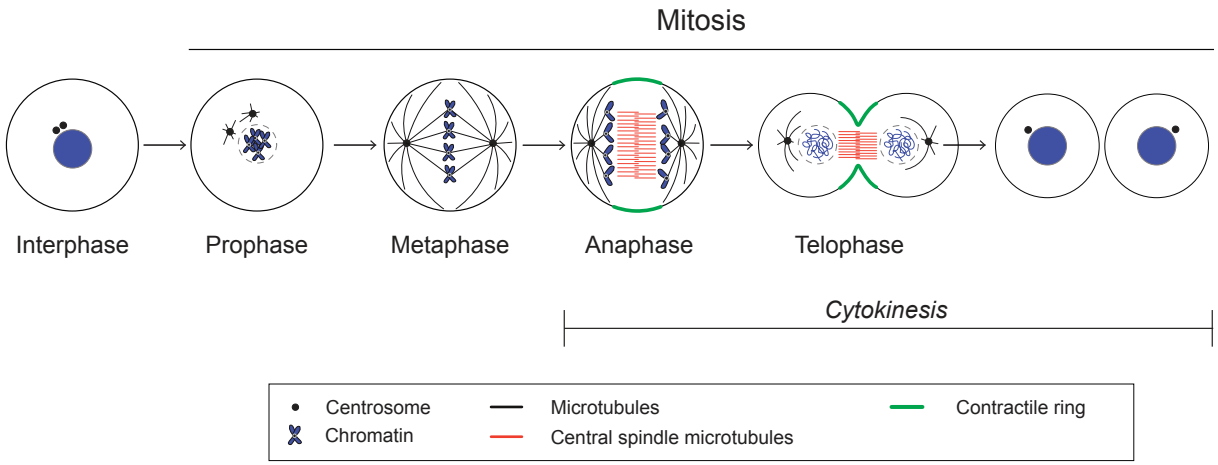
Mitosis
Interphase
Prophase
Metaphase
Anaphase
Telophase
Cytokinesis
Centrosome
Chromatin
Microtubules
Central spindle microtubules
Contractile ring

Figure 1. Mitosis and cytokinesis. The cartoon schematic shows a cell undergoing mitosis. Chromosome condensation and nuclear envelope breakdown occur during prophase. In metaphase, chromosomes (blue) are aligned at the equator of the cell by the spindle (black). The final steps of mitosis overlap with cytokinesis, which begins at anaphase onset, when the sister chromatids move towards the opposite poles of the cell. The spindle consists of astral microtubules which extend from the centrosomes (black circles) and the central spindle which are overlapping, bundled microtubules that form between the segregating chromosomes (red). The contractile ring (green) assembles in the plane that bisects the central spindle. The ring constricts in telophase and pulls in the overlying membrane to divide the cytosol of the cell. The nuclear membrane reassembles during telophase. After the ring ingresses, a midbody forms that controls abscission to separate the two daughter cells.

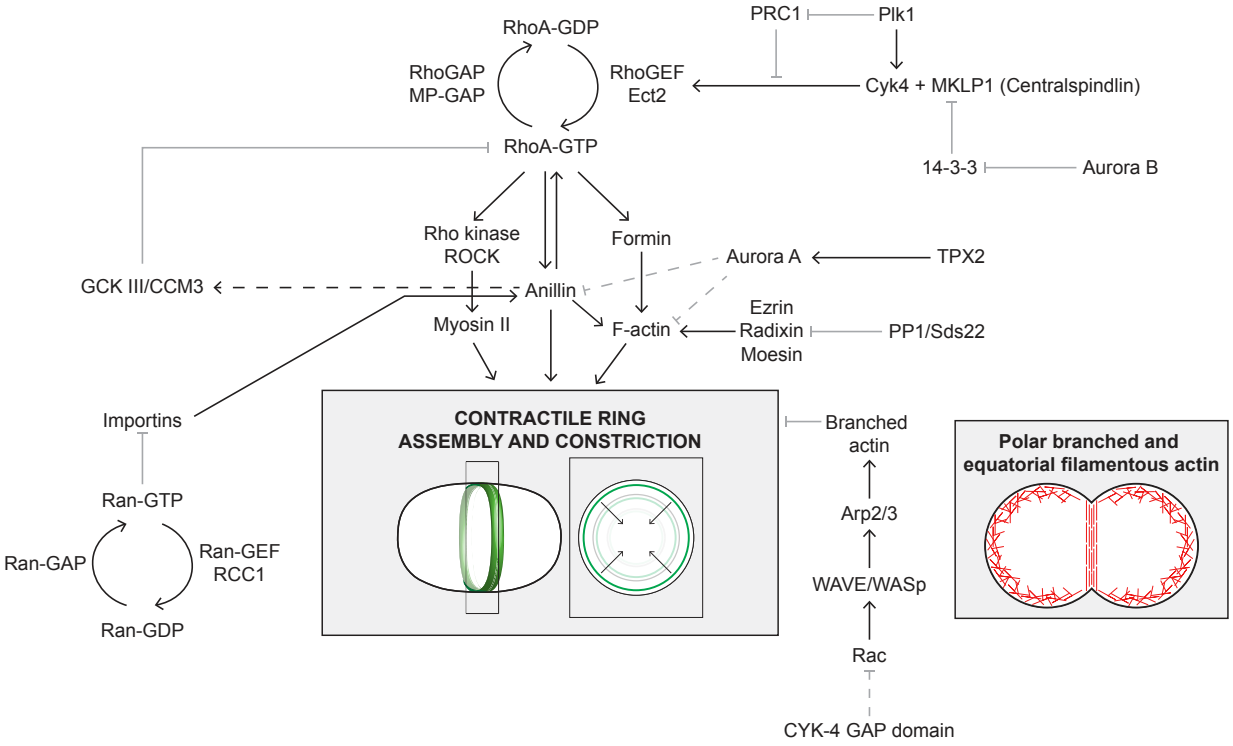
RhoA-GDP
RhoGAP
MP-GAP
RhoGEF
Ect2
RhoA-GTP
PRC1
Plk1
Cyk4 + MKLP1 (Centralspindlin)
14-3-3
Aurora B
Rho kinase
ROCK
Formin
Aurora A
TPX2
GCK III/CCM3
Anillin
Myosin II
F-actin
Ezrin
Radixin
Moesin
PP1/Sds22
Importins
Ran-GTP
Ran-GAP
Ran-GEF
RCC1
Ran-GDP
CONTRACTILE RING
ASSEMBLY AND CONSTRICTION
Branched
actin
Arp2/3
WAVE/WASp
Rac
CYK-4 GAP domain
Polar branched and
equatorial filamentous actin

Figure 2. Multiple pathways regulate cytokinesis. Cytokinesis requires the assembly and ingression of an actomyosin ring (in green) as shown in the schematic. Ring assembly is controlled by multiple pathways acting in concert as shown by the arrows (solid lines are established networks, while dashed lines refer to hypothetical interactions). A schematic shows the location of polar, branched F-actin (red branches) and linear F-actin (red lines) during cytokinesis.

elegans, Pbl in *Drosophila*) (Miki et al., 1993, Tatsumoto et al., 1999, Kimura et al., 2000, Mishima et al., 2002, Piekny et al., 2005, Yuce et al., 2005, Green et al., 2012, Pintard and Bowerman, 2019, Pollard and O'Shaughnessy, 2019). Active RhoA binds to effectors including formins to generate F-actin and RhoA kinase (ROCK) to activate myosin, and together these form force-generating filaments. Another effector that RhoA recruits is anillin. Anillin is a conserved scaffold for the contractile ring that has a number of binding partners including F-actin, myosin, RhoA, phospholipids, microtubules among others (Piekny and Maddox, 2010). Since anillin depletion causes the ring to oscillate and fail cytokinesis in several cell types, it is proposed to crosslink the ring to the overlying membrane to control ring position (Straight et al., 2005, Zhao and Fang, 2005a, Piekny and Glotzer, 2008). Another filament system formed by septins also binds to anillin, and is thought to spatially control the ring during constriction, although this process is not well-understood (Maddox et al., 2007, Carim et al., 2020). The ring then transitions to a midbody after ingression, which functions to control abscission.

The mitotic spindle spatiotemporally controls ring assembly in somatic cells. Early studies by Rappaport in the sand dollar zygote, and subsequently Bement in green urchin blastomeres from 32-cell stage embryos, showed that moving the anaphase spindle repositions the division plane and causes a new ring to assemble in a plane that bisects the spindle (Rappaport, 1961, Bement et al., 2005). The anaphase spindle consists of the astral microtubules, which emanate from the centrosomes to the polar cortex, and the central spindle, which is composed of anti-parallel, bundled microtubules that arise between the segregating chromosomes (**Fig. 3A;** Glotzer, 2005, Piekny et al., 2005, Glotzer, 2009, Glotzer, 2017). The current model is that the astral microtubules and central spindle provide consecutively timed signals to first broadly assemble actomyosin filaments in the equatorial plane that then transition to a narrow ring which constricts

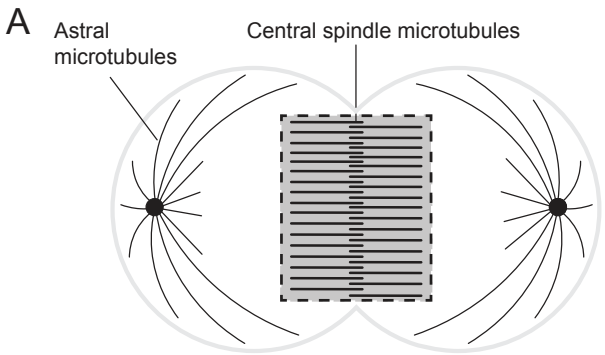

Spindle-dependent structures regulating cytokinesis

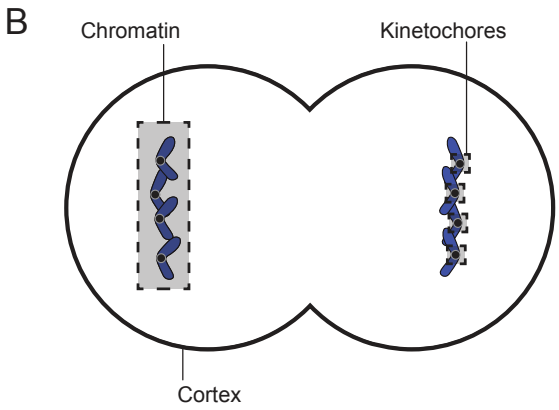

Spindle-independent structures regulating cytokinesis

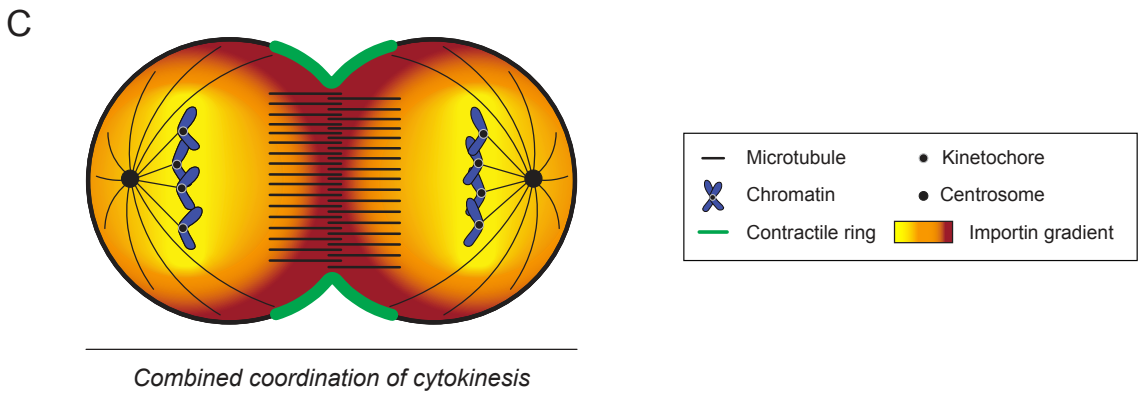

Combined coordination of cytokinesis

Figure 3. An overview of the cell components regulating cytokinesis. A) A cartoon shows the central spindle, which is formed from bundled microtubules in the central plane of the dividing cell, and astral microtubules, which emanate from the centrosomes toward the polar cortex. B) A cartoon shows the locations of chromatin, kinetochores, and cortex. C) A cartoon shows the regulation of cytokinesis through multiple spindle-dependent and -independent pathways. The cues regulating cytokinesis come from distinct components (shown in A and B) that together provide cues for successful cytokinesis.

(Dechant and Glotzer, 2003, Bringmann and Hyman, 2005, Werner et al., 2007, von Dassow et al., 2009, Lewellyn et al., 2010, van Oostende Triplet et al., 2014). Perturbations of the astral or central spindle microtubules cause contractile ring proteins to spread in the equatorial plane, although the relative requirement of the two systems could vary depending on the cell type and organism (Canman et al., 2003, Verbrugghe and White, 2004, Bringmann and Hyman, 2005, Murthy and Wadsworth, 2008, van Oostende Triplet et al., 2014).

Astral microtubules play a particularly important role in the early stages of cytokinesis to define the division plane. These microtubules clear contractile proteins such as anillin and F-actin from the polar cortex through direct or indirect interactions (Tse et al., 2011, van Oostende Triplet et al., 2014, Chen et al., 2021). Studies in *C. elegans* and HeLa cells suggest that anillin binds to astral microtubules in regions of the cell where active RhoA is low, which promotes its removal from the polar cortex (Tse et al., 2011, van Oostende Triplet et al., 2014). Astral microtubules also clear γ-actin from the polar cortex by decreasing the activity of the formin DIAPH1 (Chen et al., 2021). Recent studies in *C. elegans* embryos showed that Aurora A kinase inhibits the accumulation of anillin and F-actin at the polar cortex via TPXL-1 (TPX2 ortholog) (Mangal et al., 2018). However, it is not clear if this regulation is direct or indirect, and if it is conserved in other cell types. After contractile proteins accumulate in the equatorial plane, the central spindle directs ring assembly. The centralspindlin complex is composed of the kinesin-6, MKLP1 (ZEN-4 in *C. elegans*) and Cyk4 (MgcRacGAP; CYK-4 in *C. elegans*), and is required for central spindle assembly (Mishima et al., 2002). Ect2 requires Cyk4-binding for its function, and this complex is tightly controlled. Cdk1 phosphorylation of Ect2 prevents Cyk4-binding prior to mitotic exit, while Plk1 phosphorylation of Cyk4 is required for Ect2-binding (Green et al., 2012, D'Avino et al., 2015). Multiple studies found that the lipid binding domains of Ect2 and Cyk4 are essential for the

generation of active RhoA, while localization to the central spindle itself is not required (Su et al., 2011, Frenette et al., 2012, Basant et al., 2015, Kotynkova et al., 2016). This raises the question of how Cyk4-Ect2 complexes restrict the generation of active RhoA to the division plane. One model is that Plk1 phosphorylation of Cyk4 at the central spindle reduces its affinity for the spindle microtubules by releasing it from PRC1 to the overlying equatorial cortex, where other cortical mechanisms then restrict the active complex to the equatorial plane (Petronczki et al., 2007, Wolfe et al., 2009, Adriaans et al., 2019). One of these mechanisms may involve Aurora B kinase, which functions to promote the oligomerization of centralspindlin complexes at the membrane by inhibiting 14-3-3-binding to MKLP1 (Guse et al., 2005, Douglas et al., 2010, Basant et al., 2015). However, the caveat to these studies is that they were exclusively done in only a few cell types, and there are differences in how these proteins localize both temporally and spatially, suggesting differences in their regulation. Although decades of research have greatly improved our understanding of how cytokinesis takes place, it has also revealed the complexity of cytokinesis regulation.

1.2 DIFFERENCES IN CYTOKINESIS AMONG CELL TYPES

Despite the conservation of core cytokinesis machinery, there are many differences in the regulation of this machinery among different cell types and organisms. For example, although anillin is highly conserved, there are different threshold requirements for anillin among cell types (Piekny and Maddox, 2010). While very low levels of anillin appear to be sufficient for cytokinesis in the early *C. elegans* embryo, higher levels are required in *C. elegans* neuroblasts, *Xenopus* embryos, *Drosophila* S2 and HeLa cells as determined by RNAi studies and measurements of remaining protein levels by western blots (Straight et al., 2005, Hickson and O'Farrell, 2008,

Piekny and Glotzer, 2008, Fotopoulos et al., 2013, Reyes et al., 2014). Surprisingly, a recent study found that Dalmatian dogs carrying an almost complete anillin truncation were born, although they had some developmental defects, suggesting that many cells successfully completed cytokinesis without anillin function (Holopainen et al., 2017). There also could be differences in anillin's role in cytokinesis among cell types. In HeLa cells, anillin depletion causes a decrease in active RhoA and failed ingression in addition to oscillation phenotypes, suggesting that it regulates ring assembly and positioning (Piekny and Glotzer, 2008). However, in S2 cells, anillin depletion causes oscillation phenotypes and abscission failure, suggesting that it is also required to form a stable midbody in these cells (Hickson and O'Farrell, 2008). In the early *C. elegans* embryo, ANI-1 (anillin) depletion does not cause cytokinesis failure, but rather causes minor differences in ring ingression (Maddox et al., 2005, Maddox et al., 2007). Further studies showed that ANI-1 could be part of a negative feedback loop that helps to brake contractility to control constriction. In this model, ANI-1 recruits GCK-1 (human GCK III) and its cofactor CCM-3 to the contractile ring, and GCK-1/CCM-3 then supports RGA-3/4 (RhoGAP; downregulates active RhoA) localization to the cortex, which leads to decreased myosin and anillin levels in the ring (Rehain-Bell et al., 2017, Bell et al., 2020). However, it is not known if a similar negative feedback loop occurs in other cell types.

There are also differences in how cytokinesis proteins localize among cell types. For example, anillin is cytosolic during interphase in *C. elegans* and *Drosophila* embryonic cells, but is nuclear in cultured *Drosophila* and human cells (Piekny and Maddox, 2010). Ect2 (Pbl) localizes to the central spindle or furrow-microtubules and equatorial cortex in HeLa cells and in *Drosophila* embryos (Prokopenko et al., 1999, Tatsumoto et al., 1999, Somers and Saint, 2003, Yuce et al., 2005, Zavortink et al., 2005, Chalamalasetty et al., 2006, Petronczki et al., 2007, Albertson et al.,

2008, Su et al., 2011). However, in the *C. elegans* zygote, ECT-2 is strictly cortical (Gomez-Cavazos et al., 2020). Depending on the cell type, distinct actin and myosin isoforms are differentially enriched at the equatorial versus polar cortex, likely forming different types of filaments required to support different cortical properties. In particular, the ring creates and is under different tension compared to the poles (Maupin et al., 1994, Dugina et al., 2009, Po'uha and Kavallaris, 2015, Chen et al., 2017, Yamamoto et al., 2019). In the early *C. elegans* embryo, myosin and actin are asymmetrically enriched in cells that give rise to daughters with different fates, and this anterior contractility creates flows that could influence ring assembly and/or ingression (also see section 1.3.1.1) (Munro et al., 2004).

Asymmetric ingression also varies among cell types. Asymmetric ingression occurs when part of the membrane ingresses more than other regions causing the midbody to form in an off-center position, and can occur in both symmetrically **(Fig. 4, top right)** and asymmetrically dividing cells **(Fig. 4, bottom right)**. The factors regulating the symmetry of ring closure remain poorly understood, although asymmetric closure presumably occurs due to higher contractility or less tension in part of the ring (also see section 1.3.1.1). Cortical flows could also generate the asymmetric furrowing that is observed in cells with these flows (Maddox et al., 2007, Singh and Pohl, 2014).

There are also differences in the timing of cytokinesis, although the proposed mechanisms controlling this timing are not clear. An early model for cells in *C. elegans* embryos suggested that larger cells have more contractile units in the ring that could drive faster ingression rates compared to cells with fewer units (Carvalho et al., 2009). However, recent studies in *C. elegans* showed that ring closure has distinct phases, each with different kinetics that could have different timing between cell types, and depending on fate, these kinetics may or may not correlate with cell size

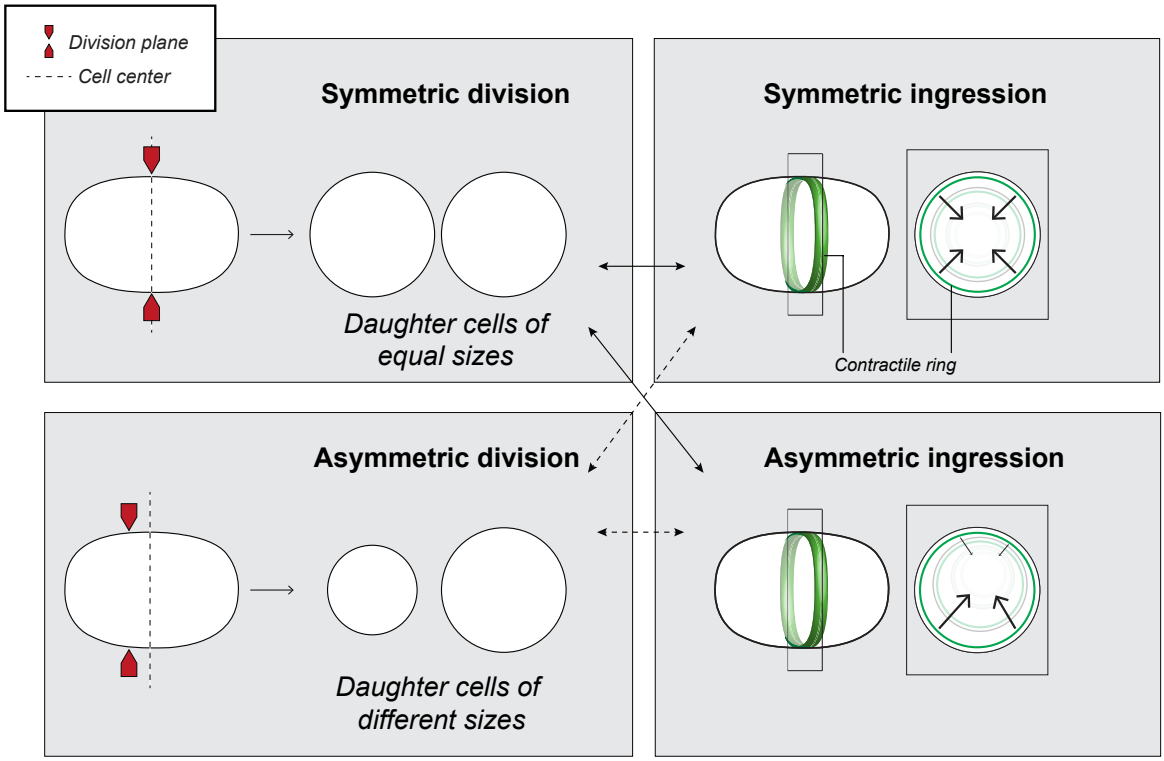
Division plane
Cell center
Symmetric division
Daughter cells of equal sizes
Symmetric ingression
Contractile ring
Asymmetric division
Daughter cells of different sizes
Asymmetric ingression

Figure 4. Division and ingression can occur symmetrically or asymmetrically. Cells can undergo symmetric divisions (top left), where two daughter cells of equal sizes are generated. Alternatively, they can undergo an asymmetric division (bottom left) which results in two cells of different sizes. The spindle is shifted in these cells, so the central axis of the cell is not aligned with the division plane. Either of these divisions can occur through symmetric (top right) or asymmetric (bottom right) closure of the ring. In a symmetrically ingressing cell, the ring closes equally on all sides, whereas an asymmetrically ingressing cell will have greater closure, or 'pull', from one side of the ring.

(Carvalho et al., 2009, Steigemann et al., 2009, Davies et al., 2018, Chan et al., 2019, Osorio et al., 2019). Cortical flows are also thought to improve filament alignment and constriction rates in the ring, and these flows could be influenced by polarity and/or neighbours (Reymann et al., 2016, Khaliullin et al., 2018). The *relative* timing between neighbor cells also influences cell fate and future divisions. The four-cell *C. elegans* embryo demonstrates this. At this stage, the embryo consists of the AB cell daughters (ABa and ABp), and the P_1 cell daughters (P_2 and EMS). The establishment of EMS cell fate in the early *C. elegans* embryo relies on extrinsic signaling with the P_2 cell, and their relative positions are controlled by the coordination of cytokinesis between the AB and P_1 cells of the two-cell embryo (Rose and Gonczy, 2014). A study in the four-cell *C. elegans* embryo demonstrated that certain cell types rely on cell-extrinsic as well as -intrinsic mechanisms to regulate cytokinesis (Davies et al., 2018). Further, studies in *Drosophila* epithelial cells and mammalian embryos showed that cytokinesis regulation can be intrinsic or influenced by neighbours depending on the tissue context (Founounou et al., 2013, Guillot and Lecuit, 2013, Herszterg et al., 2013, Morais-de-Sa and Sunkel, 2013, Paim and FitzHarris, 2022). Research using a broader range of cell types and model organisms is required to improve our understanding of how extrinsic cues are integrated with intrinsic pathways to control cytokinesis. Collectively, this knowledge highlights that although there are conserved components, there is no prototypic way of undergoing cytokinesis.

1.3 SPINDLE-INDEPENDENT REGULATION OF CYTOKINESIS

Multiple spindle-independent mechanisms have been shown to control cytokinesis, and certain cell types could have stronger requirements for these pathways depending on parameters such as geometry, cell fate, ploidy and/or size (**Fig. 3B** shows the structures associated with these

pathways). These pathways would contribute to the cytokinetic diversity that is required by cells with different developmental paths. Together with spindle-dependent mechanisms, these pathways provide a robust system that protects cells from cytokinesis failure **(Fig. 3C)**.

1.3.1 Cortical mechanisms

Several different cortical pathways have been shown to control ring assembly and ingression during cytokinesis. The cortex is a relatively large, encompassing cellular structure with mechanical properties controlled by different types of F-actin (linear vs branched), myosin functions (motor, crosslinking) and/or other filament systems (septins, intermediate filaments). In symmetrically dividing cells (where the two daughter cells are equally sized; **Fig. 4, top left)**, the cortex polarizes to create distinct cortical properties at the poles versus division plane for ring assembly and ingression. These properties are controlled by where active RhoA is generated. For example, RhoA is globally downregulated by MP-GAP (a RhoA GAP) which is overcome by Ect2 activity in the equatorial plane to generate linear actomyosin filaments for ring assembly and constriction (Zanin et al., 2013). Several studies have implicated roles for branched F-actin via Arp2/3 in controlling cortical pliability during cytokinesis, but the role of this pliability, location and the mechanisms controlling it remain unclear. For example, in *C. elegans*, several studies suggest that CYK-4 functions as a GAP for Rac to downregulate Arp2/3-mediated generation of branched F-actin in the equatorial plane, which would make it easier for ring constriction, rather than acting as an activator of Ect2 to generate active RhoA (Canman et al., 2008, Zhuravlev et al., 2017). This was interpreted based on generating a GAP-defective allele of *cyk-4* that displayed ingression defects, which could be rescued by loss of Rac or Rac effectors. Subsequent studies in HeLa cells found that cells expressing GAP-defective Cyk4 were more adherent and had retraction

fibers distributed more uniformly around the cortex compared to non-mutant control cells (Bastos et al., 2012). However, there is overwhelming biochemical and genetic evidence in multiple cell types and organisms showing that Cyk4 is required for Ect2 activation (e.g. Somers and Saint, 2003, Yuce et al., 2005, Nishimura and Yonemura, 2006, Tse et al., 2012, Zhang and Glotzer, 2015). Cyk4 depletion phenocopies Ect2 depletion in HeLa and S2 cells, with no ingression due to failed ring assembly and cytokinesis failure (Somers and Saint, 2003, Yuce et al., 2005, Zhao and Fang, 2005b). In another *C. elegans* study, co-depletion of Rac rescues cytokinesis defects in cells with partial loss of *rho-1* (RhoA) or *ect-2* (Loria et al., 2012). Thus, another explanation is that a general increase in cortical pliability makes it easier for rings with weaker force to ingress, and the findings from the HeLa cell study supports this model (Bastos et al., 2012, Basant and Glotzer, 2017). In this scenario, Rac depletion would decrease cortical stiffness and make the cortex more pliable for constriction of the ring, which would be weaker if Cyk4 – and therefore Ect2 – activity is impeded. Interestingly, in the newly fertilized *C. elegans* embryo, NOP-1 (which is required for contractility during pseudocleavage) functions redundantly with CYK-4 during cytokinesis (Tse et al., 2012). While the molecular function of NOP-1 is not known, one hypothesis is that it could also activate ECT-2, similar to CYK-4. In support of the model where CYK-4 and NOP-1 redundantly activate Ect2, *C. elegans* embryos expressing CYK-4 GAP mutants do not furrow if NOP-1 is also depleted, which phenocopies ECT-2 depletion (Dechant and Glotzer, 2003, Zhang and Glotzer, 2015). Thus, depending on the cell type, there may be other cortical regulators of the core machinery, and/or some of these core components could be differently regulated.

Another role for mechanical regulation of the cortex could be to alleviate pressure for ring positioning. A global increase in cortical stiffness occurs during cell rounding, which presents a challenge because as the contractile ring constricts in the equatorial plane, the polar regions of the

cell would experience increased pressure. High polar tension can result in large changes and instability in cell shape, which in turn could jeopardize cytokinetic success (Sedzinski et al., 2011). This problem of excess intracellular pressure is resolved by decreasing cortical stiffness at the polar regions, which allows for the formation of cortical blebs. Blebs are transient and cause regions of the cortex to extend, which are retracted in a myosin-dependent manner. It is hypothesized that they act as valves to release cortical pressure in the cell and tend to occur with higher frequency when RhoA-mediated contractility is increased in the polar cortex after MP-GAP depletion (Sedzinski et al., 2011, Zanin et al., 2013).

1.3.1.1 Cortical mechanisms in asymmetrically dividing cells

Cortical pathways may play a particularly important role in regulating cytokinesis in asymmetrically dividing cells. Asymmetric divisions give rise to differently sized daughter cells **(Fig. 4, bottom left)**. Cortical polarity regulators are involved in contractile ring positioning, although the mechanism is not clear. In *Drosophila* neuroblasts, which divide asymmetrically to give rise to a smaller basal ganglion mother cell and an apical neuroblast stem cell, the basal enrichment of myosin is controlled by Pins (mammalian LGN, *C. elegans* GPR-1/2; component of the cortical polarity protein complex) and Dlg (Discs large) (Cabernard et al., 2010). In the early *C. elegans* embryo, actomyosin contractility becomes enriched in the anterior cortex via feedback mechanisms that establish and maintain anterior-posterior polarity (Guo and Kemphues, 1996, Munro et al., 2004, Cowan and Hyman, 2007, Rose and Gonczy, 2014). During oogenesis, cortical contractility is uniform, but upon fertilization, active RhoA is decreased in the posterior, causing an anterior shift in contractility (Cowan and Hyman, 2007, Rose and Gonczy, 2014, Lang and Munro, 2017, Delattre and Goehring, 2021). Through a mechanism that is not well understood,

this helps position distinct PAR (*par*titioning defective) proteins to the anterior or posterior cortex. The anterior complex is composed of PAR-3, PAR-6, and PKC-3, while the posterior complex contains PAR-1 and PAR-2 (Rose and Gonczy, 2014, Lang and Munro, 2017, Delattre and Goehring, 2021). They form mutually exclusive boundaries through phosphorylation, where each complex has kinase activity that phosphorylates and negatively regulates the cortical localization of one or more components of the opposite complex (Rose and Gonczy, 2014, Lang and Munro, 2017, Delattre and Goehring, 2021). The major function of this polarity is to asymmetrically position the mitotic spindle to form two asymmetrically sized daughter cells with different fates (Grill et al., 2001, Labbé et al., 2004). To ensure that division occurs asymmetrically, the contractile ring must align with the anterior-posterior boundary (Schenk et al., 2010, Pittman and Skop, 2012). However, it is currently unclear if/how cortical PAR proteins control ring positioning or ingression kinetics. Jordan et al. (2016) proposed that anterior and posterior PAR proteins control ring kinetics by determining the amount of ANI-1 in the ring. The depletion of either an anterior or posterior PAR caused a decrease in the anterior enrichment of anillin, and higher levels of anillin were measured in the ring. This suggests that PAR proteins can influence ingression kinetics in the *C. elegans* zygote (Jordan et al., 2016).

Some of the PAR proteins are conserved in metazoans where they regulate apicobasal polarity. Their role in cytokinesis has not been extensively studied until recently, when PARD6B (PAR-6 homolog) was shown to control ingression through an intrinsic mechanism in cells of the early mouse embryo (Paim and FitzHarris, 2022). Divisions were analyzed until the 64-cell stage embryo, and this model provides an interesting context to study the role of polarity and cell fate, as apical polarity is established at the 8-cell stage, while cell fate begins to be established at the 16-cell stage. This study showed that the localization of anillin and myosin is mutually exclusive

with PARD6B, which is apically enriched. Thus, the contractile ring components are asymmetrically enriched, and the ring ingresses asymmetrically toward the apical cortex. This control of ingression is quite different from studies in *Drosophila* epithelial cells, where extrinsic forces via adherens junctions influence asymmetric ingression (Herszterg et al., 2014, Osswald and Morais-de-Sa, 2019, Buckley and St Johnston, 2022). In this tissue, apicobasal polarity determines the position of adherens junctions which tethers neighbouring cells (Herszterg et al., 2014, Osswald and Morais-de-Sa, 2019, Buckley and St Johnston, 2022). However, since there is no way to separate polarity from junctions in this tissue, it is possible that both intrinsic polarity and extrinsic forces contribute to ring ingression. Further studies are required to understand the polarity-driven mechanisms regulating cytokinesis and understand how this works in different cell types.

1.3.2 Kinetochores

Another spindle-independent mechanism involves kinetochores, which can act as a signaling platform to influence the nearby cortex. Kinetochores are complex structures crucial for forming stable attachments between the chromosomes and the mitotic spindle (Compton, 2000, Walczak and Heald, 2008). Given their proximity to the polar cortex during anaphase, it is not surprising that they also contain signals that affect cortical properties. Ezrin-Radixin-Moesin (ERM) proteins crosslink the actin cytoskeleton to the plasma membrane, and are important for establishing cortical stability, stiffness and contractility (Carreno et al., 2008, Kunda et al., 2008). PP1 phosphatase and its subunit Sds22 were found to localize to the kinetochore in cultured *Drosophila* cells, and have been proposed to mediate cortical relaxation (Roubinet et al., 2011, Kunda et al., 2012, Rodrigues et al., 2015). As chromosomes segregate towards the cell poles in

early-mid anaphase, PP1–Sds22 activity results in moesin and F-actin being cleared from the adjacent polar cortex in *Drosophila* and HeLa cells. Although PP1/Sds22 depletion does not prevent successful cytokinesis, their loss causes cell shape changes which could have a greater impact depending on the cell type (Rodrigues et al., 2015). Reducing moesin also does not cause cytokinesis failure per se, but moesin-depleted cells display extremely erratic membrane protrusions which resolve at the end of cytokinesis (Carreno et al., 2008). More recently, the chloride channel CLIC4 has been implicated in controlling polar cortical stability possibly through interactions that include ezrin, and it is attractive to consider that CLIC4 is also part of this same mechanism (Peterman et al., 2020, Uretmen Kagiali et al., 2020). However, kinetochore-mediated clearance does not appear to function in the early *C. elegans* zygote. This may be because the kinetochores are significantly further from the cortex in the zygote than in the cultured cell lines used by Rodrigues et al. (2015). Also, the astral microtubules in the one-cell *C. elegans* zygote are very large relative to cell size – therefore they may be more effective at clearing the polar cortex than other mechanisms. Thus, the exact mechanism of how phosphoregulatory pathways mediate polar relaxation may depend on cell type; whereas PP1–Sds22 may be effective in cells where the kinetochores are near the cortex during anaphase, astral/Aurora A kinase-dependent mechanisms may be better suited to control polar clearance in cell types where this is not the case. Future studies are required to understand how the mechanisms of polar clearance vary with cell type and explore whether there are other, currently undiscovered mechanisms that mediate polar relaxation.

1.3.3 Chromatin

Chromatin-associated signals can also affect the cortex during cytokinesis. Earlier studies showed that chromosomes can affect the late stages of cytokinesis, likely as a mechanism to

prevent the breakage and/or mis-inheritance of lagging chromosomes that are trapped in the equatorial plane (Steigemann et al., 2009, Kotadia et al., 2012, Montembault et al., 2017). Studies from the Royou lab demonstrated that in *Drosophila* neuroblasts, trailing chromatid arms correlate with broader cortical myosin accumulation, elongation of the cell and delayed completion of cytokinesis (Kotadia et al., 2012). A follow-up study led them to propose that nuclear envelope reassembly is delayed by the presence of trailing chromatid arms, which consequently delays the nuclear sequestration of Pebble (*Drosophila* Ect2), causing persistent active RhoA and accumulated ring components (Montembault et al., 2017).

1.3.3.1 Cortical regulation by the Ran/importin system

Recent studies found that chromatin also controls ring position during early cytokinesis via reciprocal gradients of Ran-GTP and importins (Kiyomitsu and Cheeseman, 2013, Beaudet et al., 2017, Beaudet et al., 2020). Ran is a small GTPase which typically controls nucleocytoplasmic transport and mitotic spindle assembly. Importin-α and -β bind to nuclear localization signals (NLSs) in proteins and Ran-GTP dissociates this complex (Xu and Massague, 2004, Lange et al., 2007, Clarke and Zhang, 2008, Ozugergin and Piekny, 2021). In interphase cells, importin-binding brings NLS-proteins into the nucleus where they are released by active Ran, while in mitosis, importin-binding to spindle assembly factors controls their function (Kalab et al., 2006, Kaláb and Heald, 2008). Ran-GTP is generated in the vicinity of chromatin by histone-tethered RCC1 (RanGEF), while RanGAP negatively regulates Ran in the cytosol. The different localization of these regulators results in inverse gradients of active Ran and importins, where high active Ran releases importins from NLS-proteins in the nucleus or near chromatin, and they remain bound in other regions of the cytosol and cortex **(Fig. 5A)**. Based on studies done in HeLa cells (refer to

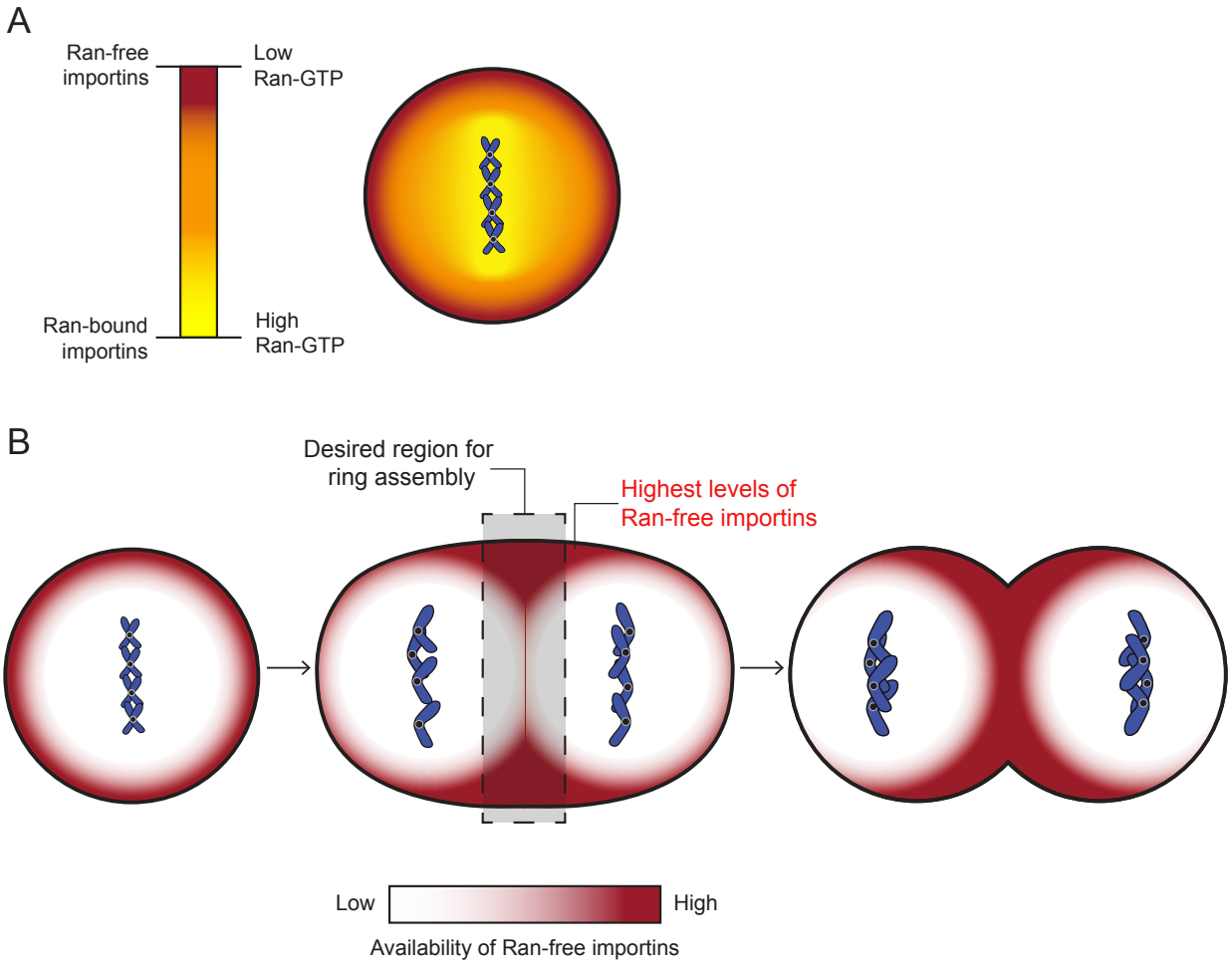
A
Ran-free importins
Low Ran-GTP
Ran-bound importins
High Ran-GTP
B
Desired region for ring assembly
Highest levels of Ran-free importins
Low
High
Availability of Ran-free importins

Figure 5. Ran regulation of cytokinesis. A) During metaphase, Ran-GTP levels are highest near chromatin, and decreases toward the cortex. This results in an inverse gradient of importins that can bind to NLS-containing proteins near the cortex. B) In anaphase, opposing importin-Ran gradients would form around the segregating masses of chromatin, creating a differential gradient of importins in the equatorial plane where the ring would assemble.

section 1.3.3.2), our lab proposes that importins could become enriched in the equatorial plane during anaphase, where they could control the function and localization of cortical NLS-containing proteins in response to chromosome segregation **(Fig. 5B)**.

Seminal studies showed that importin-binding negatively regulates spindle assembly factors, which require 'release' by Ran-GTP to be functional (Kalab et al., 2002, Kalab et al., 2006). However, a very different role for this same pathway was shown to control the cortex during meiosis (Deng et al., 2007). In mouse oocytes Ran-GTP functions as a molecular ruler to control polar body extrusion and coordinate cortical polarity with the position of chromatin (Deng et al., 2007). This study showed that DNA – whether it was meiotic, bacterial or yeast plasmid DNA – elicits a dose- and distance-dependent response of the cortex. Distinct amounts of DNA, or DNA at defined distances to the cortex caused the formation of an ideal sized cortical F-actin cap for polar body extrusion. Although the mechanism is not known, follow-up studies suggested that this pathway functions through Cdc42 and regulation of Arp2/3 (Yi et al., 2011, Dehapiot et al., 2013, Burdyniuk et al., 2018).

Importins were also shown to regulate cellularization of the syncytial *Drosophila* embryo, when membranes form to separate the nuclei. This process is often compared to cytokinesis since some of the same proteins, including anillin and septins, are involved (Mazumdar and Mazumdar, 2002, Lecuit, 2004). Silverman-Gavrila et al. (2008) showed that cellularization was partially inhibited in embryos after overexpression of importin-α, which showed a decrease in anillin and Pnut (Peanut, *Drosophila* septin) localization. The authors proposed a model where anillin recruits Pnut to the ingressing membrane, and this interaction can be outcompeted by importins. The authors proposed that since active Ran outcompetes importin-α and -β, active Ran functions to control the localization of anillin and Pnut to the membrane. Although it is difficult to interpret

these findings as no loss-of-function studies were done, the ability of importins to control the localization of contractile proteins could be conserved in other processes. Indeed, as shown by Beaudet et al. (2017) (discussed in section 1.3.3.2), different threshold levels of importins likely support or inhibit the localization of anillin for cytokinesis.

1.3.3.2 The Ran/importin system during cytokinesis

During the early stages of cytokinesis, chromatin-associated Ran-GTP may control ring assembly and positioning via importins. Early evidence that chromatin position influences cytokinesis came from studies performed in HeLa, Rpe1 (retinal pigment epithelium) and BHK (baby hamster kidney epithelial) cells (Kiyomitsu and Cheeseman, 2013). Kiyomitsu and Cheeseman (2013) showed that cells can correct for a shift in spindle position by asymmetrically elongating the membrane in a Ran-dependent manner. When chromatin shifts closer to one side of the cell, this region of cortex is cleared of anillin and the membrane expands away from the mass of chromatin (Kiyomitsu and Cheeseman, 2013). As an elegant proof-of-concept, the authors showed that tsBN2 cells (BHK cells that express temperature-sensitive RCC1) lacking any microtubules and induced to undergo mitotic exit were able to clear anillin from the cortex near chromatin at the permissive temperature, but not at the restrictive temperature when Ran-GTP levels would be lower (Kiyomitsu and Cheeseman, 2013). Although the mechanism was not explored, this work showed that Ran-GTP controls the cortical localization of anillin during mitotic exit in a microtubule-independent manner.

Studies from our lab found the mechanism by which importins regulate anillin function to control cytokinesis in BHK and HeLa cells (Beaudet et al., 2017, Beaudet et al., 2020). tsBN2 cells upshifted to the restrictive temperature (to reduce RCC1 function and Ran-GTP levels) fail

cytokinesis and have ectopic (non-equatorial) recruitment of anillin and myosin (Beaudet et al., 2017). In addition, targeting constitutively active Ran (Q69L) to the equatorial membrane in HeLa cells caused the displacement of anillin and phenocopied the loss of anillin causing oscillation phenotypes and cytokinesis failure (Beaudet et al., 2017). Subsequent studies found that importin-binding to an NLS in anillin was required for cytokinesis (Beaudet et al., 2017). Anillin has two NLSs; the one in the C-terminus is conserved across homologues and was shown to bind to importin-β, while the other is in the N-terminus and is not required for cytokinesis (Chen et al., 2015). Subsequent studies revealed that RhoA binding relieves autoinhibition of the neighbouring C2 domain containing the NLS to facilitate importin-binding (Beaudet et al., 2017). Thus, our model is that importin binding to the C2 NLS stabilizes the open conformation of anillin for its cortical recruitment (Beaudet et al., 2017, Beaudet et al., 2020). The C2 domain also contains sites for other binding partners such as microtubules and phospholipids, and importin-binding may also impact the localization and function of anillin through these interactions (van Oostende Triplet et al., 2014, Beaudet et al., 2017, Beaudet et al., 2020). Thus, our model also requires that importins bind to anillin with low affinity to permit the hand-off to these other partners. In support of this, anillin is recruited to a narrower region when importin-β is overexpressed, which is similar when the NLS is mutated to prevent importin-binding (Beaudet et al., 2017). Additionally, mutations which strongly disrupt the RBD (Rho binding domain)–C2 interface result in stronger importin-binding, yet anillin does not localize cortically (Beaudet et al., 2020). Thus, we propose importin binds to anillin with low affinity so that it can be outcompeted by other binding partners, such as phospholipids, for its function and localization during cytokinesis. Recent work by Budnar et al. (2019) suggests that the association of anillin with phospholipids is also part of a feedback loop that increases RhoA-effector binding for ring ingression. However, since these studies were done

exclusively in cultured mammalian cells, it was not known if importin-binding regulates cytokinesis in other organisms, or if other cortical proteins could also be regulated by importin-binding.

1.4 THESIS OVERVIEW

Timely and spatially accurate cytokinesis is achieved through a complex network of regulatory pathways. These pathways are categorized as spindle-dependent or -independent. The anaphase spindle determines the division plane for cytokinesis, but the spindle-independent mechanisms controlling cytokinesis are less-well understood; these pathways may simply provide redundancy to protect against cytokinesis failure in some cell types, but they may play a more critical role in asymmetrically dividing cells. It is assumed that cell fate, size or shape contribute to the relative roles of the different pathways, but few studies have explored this idea. In particular, few studies have used the same approaches to compare how cytokinesis takes place among different cell types and in different contexts. This line of investigation is important to obtain a more complete understanding of the conservation of mechanisms controlling cytokinesis and how these mechanisms change during development or disease. Therefore, this thesis explores the diversity in cytokinesis in different cell types within and across a limited number of species. A natural follow-up to these studies would include more cell types from the same organisms, and more expansive comparisons across a greater number of species.

In Chapter 2 of this thesis, we characterize cytokinesis in the two-cell *C. elegans* embryo. The one-cell *C. elegans* zygote has proven to be a useful model for cytokinesis research. *C. elegans* is amenable for genetics and live imaging approaches using fluorescent proteins expressed from fused transgenes or endogenous proteins, and the genome contains homologs for 60-80% of human

genes (Kaletta and Hengartner, 2006). Since divisions in *C. elegans* are highly stereotypical, mild deviations can be quantified, which is particularly helpful in the context of this thesis, since essential cytokinesis proteins cannot be fully depleted. The results described in Chapter 2 provide a first-time characterization of how cytokinesis takes place in the AB and P_1 cells of the two-cell embryo, which are fated to become somatic tissue and germline, respectively. This novel study revealed distinct cytokinesis kinetics between the two cell types, supported by distinct levels, threshold requirements and patterning of myosin. By perturbing cell fate and generating tetraploid strains, we found that cell fate and size/ploidy contribute to distinct kinetics in AB and P_1 cells. Finally, we also found that the Ran pathway functions to regulate ring assembly through distinct pathway components in the two cell types.

Our findings of cytokinetic diversity from studies in Chapter 2 piqued our curiosity of how cytokinesis compares among different cultured human cell types (HeLa, HCT116, HepG2, HEK293) and a canine-line (MDCK). Due to the challenges of studying mammalian cells *in vivo*, in Chapter 3 we took advantage of CRISPR-Cas9 editing to generate tools to study endogenous cytokinesis proteins in cells cultured *in vitro*. Quantitative comparisons revealed that cytokinesis is variable between cell types. We found that the localization of ring proteins and regulators, as well as the duration and symmetry of ingression differed between cell types. These tools and findings highlight that one of the most popular cell lines that has been used for cytokinesis research, HeLa cells, shows intriguing differences from the other cell lines. Thus, this study opens the door to further studies investigating the mechanisms controlling these differences, as well as the generation of similar tools in additional cell types.

In summary, this thesis sheds light on the diversity of cytokinesis in various cell types using both an invertebrate *in vivo* system and several cultured mammalian cell types *in vitro*.

Additionally, we build on existing knowledge of Ran-regulation of cytokinesis by finding that the Ran pathway functions through different targets and possibly through different importins in cells with different fates. The work described here highlights the need for more diverse, comparative studies of cytokinesis among different cell types and developmental contexts.

CHAPTER TWO

Diverse mechanisms regulate contractile ring assembly for cytokinesis in the two-cell *Caenorhabditis elegans* embryo

Manuscript published as: OZUGERGIN, I., MASTRONARDI, K., LAW, C. & PIEKNY, A. 2022. Diverse mechanisms regulate contractile ring assembly for cytokinesis in the two-cell *Caenorhabditis elegans* embryo. *J Cell Sci,* 135.

2.1 PREAMBLE

Cytokinesis studies have relied mainly on the use of the early embryo or cultured HeLa cells, and both systems have proven to be powerful tools in developing our understanding of how cytokinesis takes place. However, one confounding variable in *in vitro* studies is that many of the cultured cell lines are cancerous or transformed, and are no longer in their native tissue context. *In vivo* studies provide the opportunity to better understand how cytokinesis occurs in a healthy, biological context. Combining the knowledge generated in such studies with those *in vitro* will allow us to compare and contrast the mechanisms controlling division in healthy versus pathological contexts.

2.2 ABSTRACT

Cytokinesis occurs at the end of mitosis as a result of the ingression of a contractile ring that cleaves the daughter cells. The core machinery regulating this crucial process is conserved among metazoans. Multiple pathways control ring assembly, but their contribution in different cell types is not known. We found that in the *Caenorhabditis elegans* embryo, AB and P_1 cells fated

to be somatic tissue and germline, respectively, have different cytokinesis kinetics supported by distinct myosin levels and organization. Through perturbation of RhoA or polarity regulators and the generation of tetraploid strains, we found that ring assembly is controlled by multiple fate-dependent factors that include myosin levels, and mechanisms that respond to cell size. Active Ran coordinates ring position with the segregating chromatids in HeLa cells by forming an inverse gradient with importins that control the cortical recruitment of anillin. We found that the Ran pathway regulates anillin in AB cells but functions differently in P_1 cells. We propose that ring assembly delays in P_1 cells caused by low myosin and Ran signaling coordinate the timing of ring closure with their somatic neighbors.

2.3 INTRODUCTION

We have extensive knowledge of the core cytokinesis machinery, but the mechanisms that regulate this machinery are less well understood. Cytokinesis occurs during mitotic exit because of the ingression of a RhoA-dependent contractile ring that assembles in the equatorial plane. The Rho guanine-nucleotide-exchange factor (GEF) Ect2 generates active RhoA in the equatorial plane, which directs the assembly of a contractile ring by recruiting effectors for F-actin polymerization and myosin activation. Consistent with its essential role in this process, Ect2 depletion causes cytokinesis failure in multiple cell types (Piekny et al., 2005, Green et al., 2012, Basant and Glotzer, 2018). In early anaphase, actomyosin filaments assemble as a broad equatorial band, and then transition into a tight ring that pinches in the overlying cortex (Lewellyn et al., 2010, Green et al., 2012, van Oostende Triplet et al., 2014). Various proteins control ring closure kinetics via crosslinking actin or regulating myosin activity. The highly conserved protein anillin is a key regulator of cytokinesis that anchors the contractile ring to the membrane (Piekny and Maddox,

2010, Tse et al., 2011, van Oostende Triplet et al., 2014). In support of this function, anillin depletion causes ring oscillation and cytokinesis failure, or alters the symmetry of ring closure depending on the cell type (e.g. Maddox et al., 2007, Hickson and O'Farrell, 2008, Piekny and Glotzer, 2008).

Numerous spindle-dependent or -independent mechanisms regulate ring assembly. The prevailing dogma in the field is that the anaphase spindle determines the division plane through the spatiotemporal control of Ect2 (Piekny et al., 2005, Green et al., 2012, Basant and Glotzer, 2018). Ect2 activation requires binding to Cyk4 (also known as RACGAP1 and MgcRacGAP), which is part of the centralspindlin complex that builds the central spindle (Mishima et al., 2002, Somers and Saint, 2003, Yuce et al., 2005). The astral microtubules also restrict the localization of active RhoA to the equatorial plane, although the mechanisms regulating this are less clear (Dechant and Glotzer, 2003, Lewellyn et al., 2010, Tse et al., 2011, van Oostende Triplet et al., 2014). Signals from other locations of the cell, including kinetochores and chromatin, have also been shown to regulate cytokinesis (Kiyomitsu and Cheeseman, 2013, Zanin et al., 2013, Rodrigues et al., 2015, Beaudet et al., 2017, Mangal et al., 2018, Beaudet et al., 2020). However, their conservation and relative contribution in different cell types is not well defined, as few studies have been performed in comparable cell types (e.g. cells with different fates in the same organism; Davies et al., 2018, Husser et al., 2021). Spindle-independent pathways might be redundant in symmetrically dividing cells, but could be essential in cells that divide asymmetrically, or that have different ploidy or fate.

Cues associated with chromatin coordinate contractile ring position with segregating chromosomes in HeLa cells, but it is not known if this mechanism functions in other organisms and cell types *in vivo* (Kiyomitsu and Cheeseman, 2013, Beaudet et al., 2017, Beaudet et al., 2020,

Ozugergin and Piekny, 2021). The GTPase Ran is activated by RCC1 (RanGEF) near chromatin and is inactivated by cytosolic RanGAP. Following nuclear envelope breakdown, a gradient of Ran-GTP forms with high levels near chromatin, and low levels near the cortex (Kalab et al., 2002, Kalab et al., 2006, Clarke and Zhang, 2008). Importins can bind to spindle assembly factors with nuclear localization signals (NLSs), which generally impedes their function. The release of importins by Ran-GTP in the vicinity of chromatin permits these factors to become active (e.g. Gruss et al., 2001, Nachury et al., 2001, Wiese et al., 2001, Silljé et al., 2006). However, importin regulation is not 'one size fits all' and the binding of importins could also have positive effects on protein function. Specifically, importin binding is required for anillin function by facilitating its cortical localization and function for cytokinesis (Kiyomitsu and Cheeseman, 2013, Beaudet et al., 2017, Beaudet et al., 2020). In addition, membrane-localized importin-α and -β have been observed by several groups (Beaudet et al., 2017, Brownlee and Heald, 2019). Therefore, we propose that the Ran gradient is an elegant system that can function across the cell, with opposing roles depending on the NLS protein (reviewed in Ozugergin and Piekny, 2021). Our hypothesis is that cortical NLS proteins are regulated by importin binding to ensure that the ring is positioned between the segregating chromosomes to avoid aneuploidy. However, the Ran-dependent regulation of cytokinesis has not been studied in other cell types, particularly *in vivo* where the requirement for this mechanism could vary with parameters such as size and fate.

Cytokinesis has been well characterized in the *Caenorhabditis elegans* P_0 zygote, which is influenced by anterior–posterior polarity. This cell divides asymmetrically to give rise to a larger, anterior AB cell whose descendants form multiple tissues, and a smaller, posterior P_1 cell fated to become the germline (Rose and Gonczy, 2014). Anterior–posterior polarity is controlled by the mutually exclusive distribution of anterior (PAR-3–PAR-6–PKC-3) and posterior (PAR-2–PAR-

1) complexes along the cortex. The establishment of polarity depends on the asymmetric enrichment of actomyosin contractility, which occurs in response to sperm entry (Cowan and Hyman, 2007, Hoege and Hyman, 2013, Rose and Gonczy, 2014, Gan and Motegi, 2020). Polarity is maintained via feedback between the PAR proteins and the actomyosin system at the anterior cortex, although its control switches from regulation by RhoA to Cdc42 (Cowan and Hyman, 2007, Hoege and Hyman, 2013, Rose and Gonczy, 2014, Gan and Motegi, 2020). As the P_0 zygote enters anaphase, actomyosin appears as patches or clusters at the anterior and equatorial cortex (Munro et al., 2004, Tse et al., 2012). Compression-driven flows toward the equatorial cortex may help actomyosin filaments to accumulate and align correctly (Khaliullin et al., 2018).

Three temporal phases of cytokinesis have been defined based on visible cell shape changes: ring assembly, furrow initiation, and ring constriction (e.g. Lewellyn et al., 2010, Price and Rose, 2017, Khaliullin et al., 2018, Chan et al., 2019, Osorio et al., 2019). Multiple factors are likely to influence these phases, although not many studies have explored this. There is a negative correlation between the rate of ring constriction and cell size, which was proposed to help coordinate the timing of cytokinesis among differently sized cells during embryogenesis (Carvalho et al., 2009). Another study showed that cell fate underlies differences in cytokinesis at the four-cell stage, where unique kinetics were observed as a result of different extrinsic and intrinsic pathways that regulate formin-derived F-actin (Davies et al., 2018). However, neither study explored cytokinesis in AB versus P_1 cells, and the mechanisms governing ring assembly in these cell types remain poorly understood.

In this study, we show that AB and P_1 cells have distinct cytokinesis kinetics that are regulated by a combination of myosin levels and different Ran pathway components. We found that although AB cells have a rapid ring assembly phase, it is slower in P_1 cells where myosin

levels are lower and more poorly organized, and assembly negatively correlates with cell size. Based on observations with partial NMY-2 or ECT-2 depletion, we found that slower ring assembly in P_1 cells is not strictly a result of myosin levels. Indeed, disrupting cell fate via depletion of PAR-1 or PAR-3 equalized kinetics. Further, increasing myosin levels were able to override the delay in tetraploid P_1 cells, which retained the ability to control ring assembly in response to size. Next, we found that the Ran pathway governs the differences in the ring assembly phase between AB and P_1 cells, but functions through different components in the two cell types. Our data suggest that the Ran pathway regulates the anillin-like protein ANI-1 for cytokinesis in AB cells similar to HeLa cells, whereas it functions differently in P_1 cells. Having distinct mechanisms that delay ring assembly in germline precursor cells could be important for coordinating ring closure with their somatic neighbors for cell positioning during embryogenesis.

2.4 MATERIALS AND METHODS

2.4.1 Strains

C. elegans strains **(Table S1)** were maintained according to standard protocols (Brenner, 1974) using nematode growth medium (NGM) plates. Control worms were grown on plates seeded with *Escherichia coli* OP50.

2.4.2 RNA interference

RNAi was carried out using feeding vectors for the induction of dsRNA expression in HT115 bacteria to target H39E23.1 (*par-1*), F28B3.8 (*imb-1*), F32E10.4 (*ima-3*), F54E7.3 (*par-3*), T19E10.1 (*ect-2*) and Y49E10.19 (*ani-1*) from the Ahringer library (Kamath et al., 2001). Strains were generously provided by Dr Labbé (IRIC, Université de Montréal) and Dr Roy (McGill

University). Bacterial cultures were grown overnight in Luria broth (LB) with 100 µg/ml ampicillin at 37°C, then diluted 1:100 and grown at 37°C for 7 h. The cultures were pelleted and resuspended in LB (100 µl for *ran-3*, *par-1* and *-3*, 300 µl for *ani-1* and *ima-3*, 400 or 500 µl for *ect-2*, 1700 µl for *imb-1*), and 50–100 µl of each resuspension was seeded onto NGM plates containing 100 µg/ml ampicillin and 1 mM IPTG. After being left to dry, 10–15 L4 hermaphrodites were placed onto each plate for 3 (*imb-1*), 24 (*par-1, par-3, ran-3, ect-2*) or 30 h (*ani-1, ima-3*). Feeding on *imb-1* RNAi plates was kept within a 3–5 h window, as severe DNA defects were observed after longer periods. Data from RNAi conditions were obtained from at least three separate days to control for variability and validate reproducibility of the data. The W02A2.6 clone (*rec-8*) was used to generate tetraploid worms, as described by Clarke et al. (2018). Specifically, L4 stage hermaphrodites of the desired strain were placed on *rec-8* RNAi plates for 8–9 days at 15ºC. Then, 20 L4 stage hermaphrodites were transferred to freshly induced plates. After another 7–9 days, hermaphrodites that appeared longer than control were individually transferred onto OP50 plates and maintained for successive generations by repeatedly selecting long worms. Embryos were confirmed to have higher ploidy by cell size, and staining chromosomes in fixed embryos.

2.4.3 Microscopy

C. elegans embryos were prepared for imaging using a standard stereomicroscope by dissecting gravid hermaphrodites in M9 buffer (40 mM Na_2HPO_4, 22 mM KH_2PO_4, 85 mM NaCl and 2 mM $MgSO_4$) and transferring embryos onto a freshly prepared 2% agarose pad (Evans, 2006). Images of embryos were acquired with the 100×/1.45 NA objective on an inverted Nikon Eclipse Ti microscope fitted with a LiveScan Swept Field scanner (Nikon), Piezo *Z* stage (Prior),

Andor IXON 897 EMCCD camera, and 488 nm and 561 nm lasers, using NIS-Elements (version 4.0, Nikon) software. Central *z*-planes of 0.7 μm for a total *z*-stack of 4 μm were collected at 5 s intervals for kymograph analysis, and 0.5 μm *z*-planes for a total stack of 20 μm were collected at 20 s to measure myosin or actin midplane cortical levels, and ring closure symmetry. All images were saved as ND2 files.

HILO microscopy, a modified form of total internal reflection fluorescence (TIRF) (Tokunaga et al., 2008), was used to image the cortex of the AB and P_1 cells in embryos. Embryos were transferred to agarose pads, as described above. A subcritical incidence angle was used and adjusted until clear images of the cortex were obtained. Images were acquired with a 100×/1.49 NA CFI Apo TIRF objective on an inverted Nikon Eclipse Ti microscope fitted with a TIRF arm, Photometrics Prime BSI (sCMOS) camera and 488 nm laser using NIS Elements (version 4.0, Nikon) software. *Z*-planes of 0.2 μm for a *z*-stack of 0.6 μm were collected at 2 s intervals. Images were saved as ND2 files.

2.4.4 Image analysis

Only cells that successfully completed cytokinesis and had proper DNA segregation with no gross morphological defects were used for analysis, with the exception of a subset of *ect-2*(*RNAi)* AB or P_1 cells that failed cytokinesis as described earlier. All raw data ND2 files were processed and/or analyzed in FIJI (version 2.1, NIH).

To determine the kinetics of ring closure, we used a custom macro written for FIJI to generate kymographs. Time-lapse images were staged to anaphase onset based on chromosome position (mCherry-tagged histone imaged via the 561 laser), and then the change in membrane position (mNeonGreen or GFP-tagged, imaged via the 488 laser) was analyzed over time. To

generate kymographs, the image channels were split and the green (membrane) channel was retained to manually draw a line with a width of 5 pixels over the furrow region at every timepoint until closure. Then, the distance between the two sides of the membrane was measured at each timepoint using the straight-line tool, and measurements were exported to Excel (version 16.40). The distance between the two sides at anaphase onset was set to a maximum value (100%) and used to normalize the distance throughout ingression. In conditions where P_1 membranes visibly shift as a result of the AB cell division, the starting diameter of the P_1 cell was adjusted to the timepoint before any visible indentation of the membrane occurred. All *n* values were averaged for each timepoint, and plotted as a function of time in seconds. As the closure times were variable among cells, measurements were terminated when at least three cells had completed cytokinesis.

Measurements of the accumulation of actin, anillin and myosin at the midplane were performed on *z*-stack sum projections of a similar range of *z* in diploid and tetraploid embryos. A line was manually drawn along the cortex from the anterior to the posterior pole of the membrane at the furrow initiation phase, and both background and bleach corrections were made. To align the scans for each cell, a straight line was drawn in plane with the middle of the furrow region and used to determine the linescan value located in the center of the furrow region. Each linescan within a dataset was then aligned using this datapoint. Average values were calculated for each location, and positions with fewer than 3 *n* were not included. *X*-axis values were multiplied by 0.16 to convert from pixels to microns, and the furrow position was set to 0. The area under the curve calculations were made in GraphPad Prism by setting the baseline to 50% of the peak value for each individual linescan, and including all intensities that fell within the baseline–peak range in the furrow region.

HILO images were falsely colored using the mpl-inferno LUT macro in FIJI to visualize differences in myosin intensity. Cool colors (violet, dark red) reflect weaker levels compared to brighter, warmer colors (orange, yellow). The 'Zoom in Images and Stacks' FIJI macro tool coded by Gilles Carpentier (Université Paris-Est Créteil Val de Marne, France; https://imagej.nih.gov/ij/macros/tools/Zoom_in_Images_and_Stacks.txt) was used to generate images with the zoom inset.

2.4.5 Quantitative data analysis

To measure the duration of the different phases of ring closure, graphs were analyzed using GraphPad Prism (version 8.4.3). A sigmoidal line of best fit was plotted using the averaged data for control AB and P_1 cells, then the second derivative of the best fit line with second order smoothing (four neighbors averaged) was plotted. The minimum and maximum *x* values (in seconds) of this second derivative curve represent the timepoints where there is a change of slope. The *y* value (% change in ring diameter) at the last timepoint of ring assembly, furrow initiation and ring constriction phases was noted for each control cell. These values were used as a cut-off to define phase transitions in individual cells of control and RNAi-treated embryos. Similarly, the second derivative of the sigmoidal line of best fit for averaged tetraploid AB and P_1 cell ingression curves was used to determine the phase transitions in tetraploid cell divisions. The phase duration for individual cells and their average was then plotted using GraphPad Prism.

To determine ring closure symmetry, 20 µm *z*-stacks of embryos expressing GFP::NMY-2 were imaged every 20 s. The position and size of the ring were manually extrapolated for each timepoint of division (from the start of the furrow initiation phase to maximum visible closure of the ring), temporally aligned, averaged and plotted. Briefly, straight lines were drawn in FIJI from

one side of the ring to the other in each timepoint, and then rotated to align the long axis horizontally. A 250×50-pixel box was then drawn around this line. These regions were rotated in Python 3 (version 3.7.6) using SciKit Image (version 0.16.2) to produce an *XZ* view, and a projection was performed in FIJI to produce an image stack of the membrane. The ellipse tool was used to draw ellipses that matched the outline of the cell, and ellipse coordinates were recorded. In Python 3, a best-fit circle was plotted for each timepoint and each embryo. Coordinates were normalized to the first timepoint, where the center of the ring was at 0,0, and the radius at 1. The best-fit circle was averaged across all embryos within a group (*n* values are indicated in the figure panels) and plotted using the Jet colormap. To calculate symmetry, the Pythagorean formula was used to find the displacement of the middle of the ring at the last timepoint (last measurable opening of the ring) compared to the first timepoint (when there is any visible indentation of the membrane). Values greater than 0.2 were defined as asymmetric.

To determine the orientation of myosin filament bundles in a defined region of the furrow of dividing AB and P_1 cells, we used the Directionality plugin for FIJI. A region of the furrow was selected, and the plugin was run using the local gradient orientation method with 90 bins and a histogram from 0° to 90°. The plugin reports the frequency of filament bundles at a given angle, and fits a Gaussian function based on the highest peak in the histogram. The frequency values and Gaussian fit were plotted as a histogram in Excel. To have the center of the Gaussian fit be defined as straight (0°; perpendicular to the furrow region), we subtracted the peak Gaussian value from 0°. The proportion of filament bundles (sum of raw histogram values) that were within the center±two standard deviations of the Gaussian fit (referred to as the 'Amount') was considered to be well aligned. The change in the proportion of well-aligned filament bundles was calculated by subtracting the value from control.

All graphs except those for ring closure were plotted in GraphPad Prism and Excel. Ring closure symmetry graphs were plotted using Python 3 and Matplotlib (version 3.1.3). The full code for the ring closure and membrane accumulation analyses is located at http://github.com/cmci. Graphs showing mean values are displayed with s.e.m. bars (indicated in the figure legends), and all *n* values are reported in the figure labels. All figures were prepared in Adobe Illustrator.

2.4.6 Pull-down assays and western blots

We purified recombinant ANI-1 protein to pull down importin-β from HeLa cell lysates. To do this we cloned the RBD+C2 from ANI-1 (708–1028) into pGEX4T and pMal vectors for protein expression. We also introduced the NLS mutations K938E and K940E or K947A and K949A into the pMal:ANI-1 vector by site-directed mutagenesis. The constructs and control empty vectors were transformed into *E. coli* BL21 cells, grown to an ideal OD and induced with IPTG as per the manufacturer's instructions at 25°C (Sigma Aldrich for pGEX and New England Biolabs for pMal). Cells were resuspended in lysis buffer [2.5 mM $MgCl_2$, 50 mM Tris-HCl, pH 7.5, 150 mM NaCl, 0.5% Triton X-100, 1 mM dithiothreitol (DTT), 1 mM phenylmethanesulfonyl fluoride (PMSF) and 1× protease inhibitors; Roche], then incubated with 1 mg/ml lysozyme on ice for 30 min and sonicated (1 min, 1 s on and 1 s off, 30% amplitude; Sonic Dismembrator Model 500, Fisher Scientific). After sonication and centrifugation, protein was purified by incubating with glutathione agarose (GST; Sigma Aldrich) or amylose resin (MBP; New England Biolabs) for 5 h at 4°C. The protein-bound beads were washed and stored as a 50% slurry at 4°C. Protein concentration was measured by running samples on SDS-PAGE stained with Coomassie Brilliant Blue and measured by densitometry against a standard curve of known BSA concentrations.

HeLa cells were cultured and transfected with a construct expressing Myc-tagged importin-β as previously described in Beaudet et al. (2017). Cells were washed then lysed on ice in lysis buffer (50 mM Tris-HCl, pH 7.6, 150 mM NaCl, 5 mM $MgCl_2$, 0.5% Triton X-100, 1 mM DTT and 1 mM PMSF). To pull down Myc–importin-β, cell lysate was incubated at 4°C with 5–10 µg of purified GST or MBP-tagged ANI-1 protein bound to glutathione or amylose beads. The beads were washed several times with wash buffer (50 mM Tris-HCl, pH 7.6, 150 mM NaCl and 5 mM $MgCl_2$), after which sample buffer was added. Samples were run by SDS-PAGE, then wet-transferred to nitrocellulose for western blotting. Transfer efficiency was visualized by Ponceau S staining. Membranes were incubated with mouse anti-Myc antibodies (clone 9E10; Developmental Studies Hybridoma Bank; 1:250) for 2 h, and then washed and incubated with anti-mouse horseradish peroxidase (HRP)-conjugated secondary antibodies (Cedarlane Labs; 1:10,000) for 1–2 h. After washing, signal was detected using ECL western blotting detection reagents (GE Healthcare) and a GE Amersham Imager 6000, and the resulting images were converted to 8-bit using FIJI. Figures were prepared using Adobe Photoshop and Adobe Illustrator.

2.4.7 Statistical analysis

Statistical significance was determined using GraphPad Prism using unpaired Welch's *t*-test with corrections for multiple comparisons made using the Holm–Šídák method **(Figs 7F and 8C)**, or a two-way ANOVA with Šídák's corrections for multiple comparisons **(Figs 6C, 7C, 9C, 10C,H)**. Statistical significance was defined as: $P \geq 0.05$ not significant (ns); *$P \leq 0.05$, **$P \leq 0.01$, ***$P \leq 0.001$, ****$P \leq 0.0001$.

2.5 RESULTS

2.5.1 Cytokinesis occurs differently in AB and P_1 cells

Cytokinesis is likely to be differently regulated depending on the cell type. In particular, the mechanisms regulating contractile ring assembly likely vary with parameters including cell fate, ploidy and/or size. We studied cytokinesis of AB and P_1 cells in the early *C. elegans* embryo, which have different fates and sizes. Since cytokinesis has not been studied extensively in these cells before, we first characterized the different phases of cytokinesis. To do this, we imaged embryos co-expressing GFP::PLCδ^{PH} or mNeonGreen::PLCδ^{PH} (hereafter referred to as GFP::PH and mNeonGreen::PH, respectively) and mCherry::HIS-58 to visualize the membrane and chromatin, respectively, from anaphase onset until furrow closure with high temporal resolution **(Fig. 6A; Fig. S1A)**. Kymographs produced from the images were used to measure the change in cell diameter until the end of ingression **(Fig. S2A)**. Cytokinesis was not linear in AB or P_1 cells **(Fig. 6B)**, and the inflection points of each averaged ingression curve were calculated to mathematically delineate three distinct temporal phases **(Fig. 6C)**. The phases, which were previously defined, include (1) ring assembly as the time from anaphase onset until shallow indentation of the equatorial cortex, (2) furrow initiation as the time from shallow indentation until the membrane appears to be back-to-back, and (3) ring constriction as closure of the membrane (Osorio et al., 2019). We imaged GFP::NMY-2 to further support that the membrane can report for the different phases based on myosin localization (**Fig. S2B;** Green et al., 2012, Osorio et al., 2019). We also tested for variation between AB and P_1 cells in different ('unpaired') versus the same ('paired') embryos, by repeating our analysis using only sister pairs **(Fig. S2C)**. We found that the average ingression curves generated from only paired cells were not considerably different from the dataset ('Control') that included both unpaired and paired cells. Paired AB cells showed

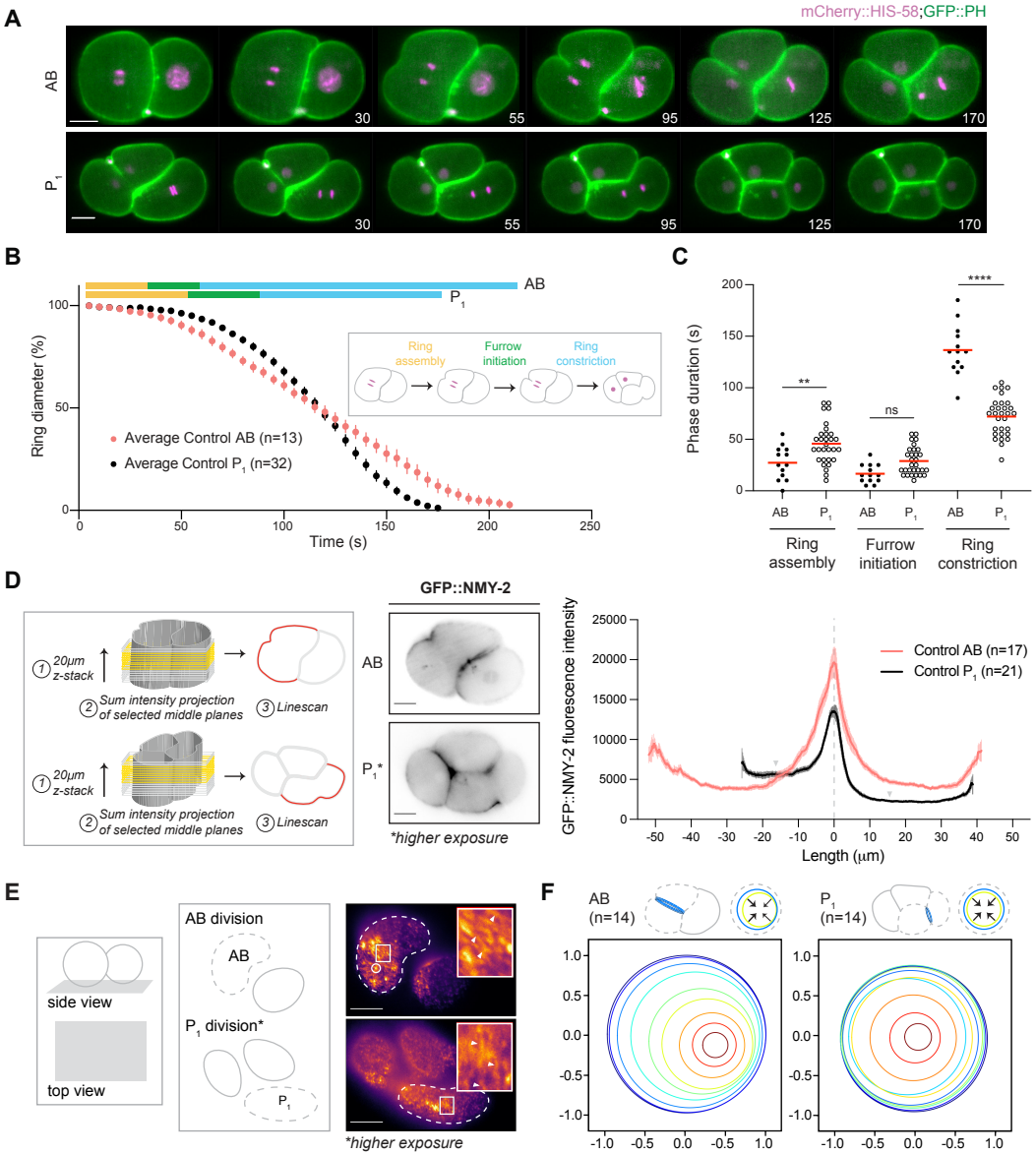
A
mCherry::HIS-58;GFP::PH
AB
P1
30
55
95
125
170
B
AB
P1
Ring diameter (%)
Time (s)
Ring assembly
Furrow initiation
Ring constriction
Average Control AB (n=13)
Average Control P1 (n=32)
C
Phase duration (s)
**
ns
****
Ring assembly
Furrow initiation
Ring constriction
D
GFP::NMY-2
20µm z-stack
Sum intensity projection of selected middle planes
Linescan
*higher exposure
GFP::NMY-2 fluorescence intensity
Control AB (n=17)
Control P1 (n=21)
Length (µm)
E
side view
top view
AB division
P1 division*
*higher exposure
F
AB (n=14)
P1 (n=14)

Figure 6. AB and P_1 cells have unique cytokinesis kinetics. A) Timelapse images show furrow ingression in AB and P_1 cells in embryos expressing mCherry::HIS-58 (magenta) and GFP::PH (green). B) Cartoon schematics and a graph show the phases of ring closure in AB and P_1 cells. Bars show the duration of ring assembly, furrow initiation and ring constriction. C) A plot shows ring closure phases in individual cells (mean, red lines; $^{**}P \leq 0.01$; $^{****}P \leq 0.0001$; ns, not significant; two-way ANOVA). D) Left: schematics show how GFP::NMY-2 levels were measured at the midplane cortex. Middle: inverted images show myosin localization in AB and P_1 cells at furrow initiation. Right: graph showing GFP::NMY-2 accumulation in AB and P_1 cells [furrow, dashed gray line; gray arrowheads indicate anterior (left) and posterior (right) cortex]. E) Left and middle: cartoon schematics show the planes visualized by HILO imaging (cells outlined by dashed lines). Right: Pseudocolored HILO images show GFP::NMY-2 in AB (top) and P_1 (bottom) cells. The circle outlines a myosin cluster. Arrowheads in the zoomed images (boxes) point to myosin filament bundles. F) Cartoons show end-on ring closure. Ring closure is shown over time, with each timepoint as a different color. *X*- and *y*-axes indicate ratios of the distance from the starting position (0). Scale bars: 10 μm. Data in B and D are expressed as mean±s.e.m.

a greater difference during the constriction phase, which might indicate that these cells inherently show more variability.

Our results showed that AB cells had shorter ring assembly compared to P_1 cells, while the ring constriction phase took longer **(Fig. 6B,C)**. To determine whether the difference in ring assembly kinetics is related to the levels of cortical myosin or actin, we imaged AB and P_1 cells expressing GFP::NMY-2 or LifeAct::mKate2. We measured myosin or actin levels along the midplane cortex at furrow initiation, where the membrane is visibly pulled in and forms a 'V' **(Fig. 6D, left)**. This is when actomyosin filaments would have 'maximally' assembled and begun to generate force. Myosin and actin localized with a bell-like distribution in AB cells, with higher peak levels in the furrow region compared to P_1 cells (**Fig. 6D; Fig. S3A;** Pimpale et al., 2020). In P_1 cells, myosin and actin levels were higher along the anterior cortex compared to the posterior **(Fig. 6D; Fig. S3A)**. Thus, myosin and actin levels are unique to each cell type. Repeating this analysis with only sister pairs showed that there was no significant difference compared to our measurements from different embryos **(Fig. S3B)**.

To determine if the differences in myosin levels contribute to the differences in cytokinesis between AB and P_1 cells, we partially depleted NMY-2 **(Fig. S3C)**. Delays in ring closure were observed in both cell types after partial RNAi as expected, but the relative differences in their kinetics was not altered **(Fig. S3C)**. For example, the ring assembly phase still took longer relative to constriction in P_1 compared to AB cells. This suggests that differences in cytokinesis kinetics are not simply caused by myosin levels.

We also compared how myosin filament bundles are organized, as this could influence ring kinetics. We used highly inclined and laminated optical sheet (HILO) microscopy to visualize GFP::NMY-2 at the cortex in AB and P_1 cells **(Fig. 6E)**. As reported previously, we observed an

asymmetric, rotational wave of myosin in AB cells (**Fig. 6E, Movie 1;** Singh and Pohl, 2014). We also saw clusters of myosin flowing towards the equatorial zone, resembling those seen during pseudocleavage (Munro et al., 2004, Tse et al., 2012). In contrast, there were no clusters or cortical flow in P_1 cells **(Fig. 6E; Movie 2)**, as observed by Pimpale et al. (2020).

Next, we measured the symmetry of ring closure. To measure symmetry, we compared the position of the ring before ingression to where it closes. Rings that closed in the middle were considered to be symmetric (<0.2) compared to those that closed near the periphery (>0.2; **Fig. S3D)**. As reported by Bai et al. (2020), we found that ring closure was more asymmetric in AB versus P_1 cells, where ingression occurred toward the AB–P_1 cell boundary **(Fig. 6F; Fig. S3D)**. To determine whether dividing AB cells can affect the symmetry of ring closure in P_1 cells, we also separately analyzed 'influenced' P_1 cells, where the division plane shifted because of the dividing AB cell. We did not observe any differences in symmetry for influenced compared to influence-free P_1 cells **(Fig. S4A)**.

2.5.2 Contractility controls the rate of ring assembly

Although the relative differences in cytokinesis kinetics was maintained in AB and P_1 cells after partial depletion of NMY-2, upstream regulators of actomyosin could contribute to different kinetics by controlling F-actin levels or actomyosin organization. Active RhoA is required for actin polymerization and myosin bipolar filament assembly, and is regulated by the GEF ECT-2 (**Fig. 7A;** Green et al., 2012). We partially depleted ECT-2 to avoid phenotypes in the germline or P_0 zygote, and only considered embryos at the threshold required to support furrowing in AB and P_1 cells. Cytokinesis kinetics were strikingly similar to the partially depleted NMY-2 embryos, where ring closure was delayed, but relative differences were retained between AB and P_1 cells **(Fig.**

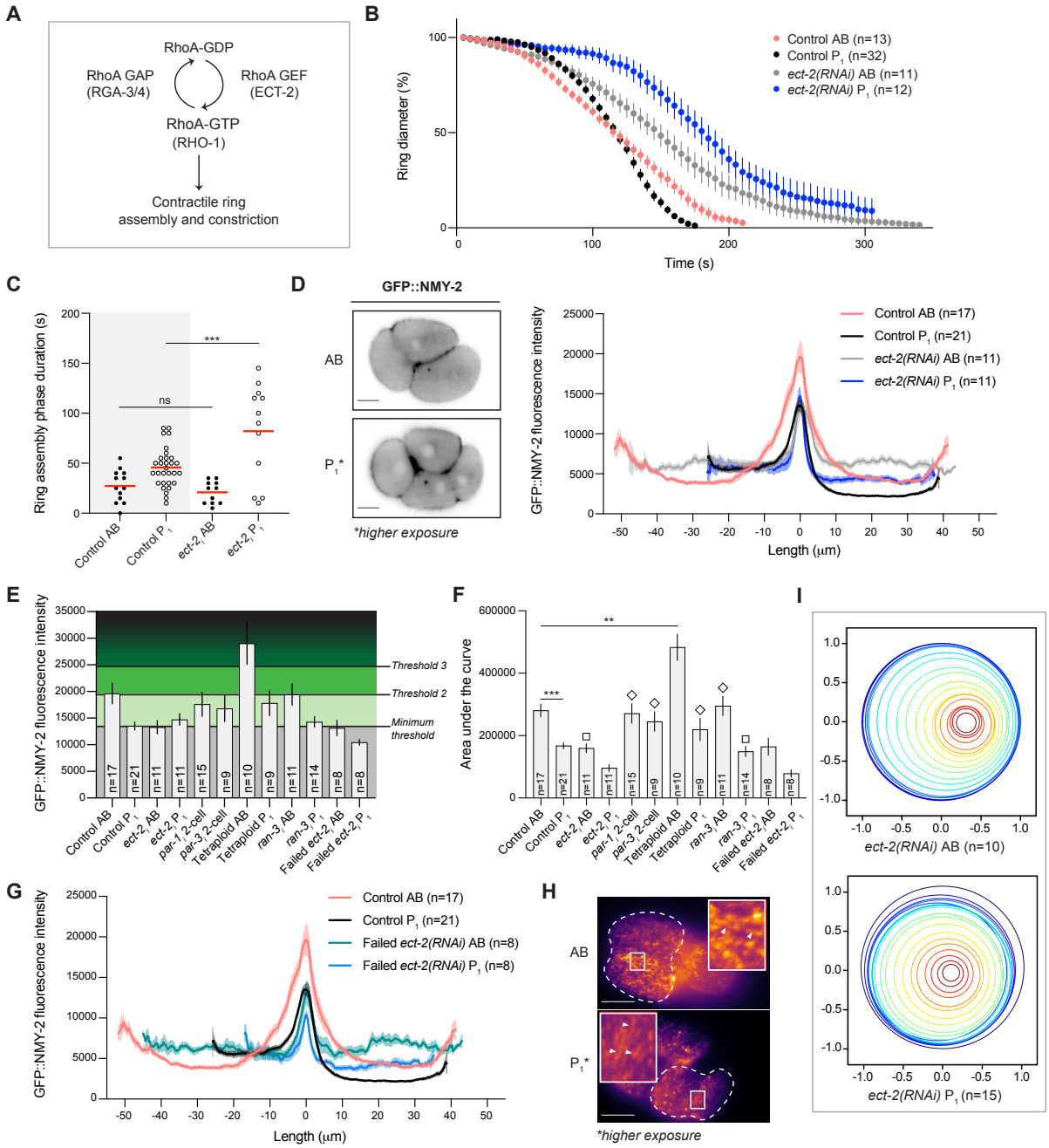
A
RhoA-GDP
RhoA GAP (RGA-3/4)
RhoA GEF (ECT-2)
RhoA-GTP (RHO-1)
Contractile ring assembly and constriction
B
Ring diameter (%)
Time (s)
Control AB (n=13)
Control P1 (n=32)
ect-2(RNAi) AB (n=11)
ect-2(RNAi) P1 (n=12)
C
Ring assembly phase duration (s)
***
ns
Control AB
Control P1
ect-2 AB
ect-2 P1
D
GFP::NMY-2
AB
P1*
*higher exposure
GFP::NMY-2 fluorescence intensity
Length (μm)
Control AB (n=17)
Control P1 (n=21)
ect-2(RNAi) AB (n=11)
ect-2(RNAi) P1 (n=11)
E
GFP::NMY-2 fluorescence intensity
Threshold 3
Threshold 2
Minimum threshold
F
Area under the curve
**
***
I
ect-2(RNAi) AB (n=10)
ect-2(RNAi) P1 (n=15)
G
GFP::NMY-2 fluorescence intensity
Length (μm)
Control AB (n=17)
Control P1 (n=21)
Failed ect-2(RNAi) AB (n=8)
Failed ect-2(RNAi) P1 (n=8)
H
AB
P1*
*higher exposure

Figure 7. Cytokinesis still occurs uniquely in AB and P_1 cells after perturbing actomyosin contractility. A) The RhoA pathway for contractile ring assembly is shown. B) A graph shows ring closure in *ect-2(RNAi)* AB and P_1 cells compared to control cells. C) A plot shows the duration of ring assembly for individual cells (mean, red lines; ns, not significant; ***P<0.001; two-way ANOVA). D) Left: inverted images show GFP::NMY-2 localization in *ect-2(RNAi)* AB and P_1 cells. Right: GFP::NMY-2 levels at the midplane cortex are shown for control and *ect-2(RNAi)* AB and P_1 cells that complete cytokinesis. E) A graph shows the maximum GFP::NMY-2 intensity values in the furrow of cells under different conditions. The distinct myosin threshold levels for ring assembly are indicated by different shades of green. F) Accumulated myosin based on area under the peak region of the curve from cells in E (**P<0.01; ***P<0.001; diamonds, not significant versus control AB; squares, not significant versus control P_1; Welch's t-test). G) GFP::NMY-2 intensity in *ect-2(RNAi)* AB and P_1 cells that fail cytokinesis is shown as in D. H) Pseudocolored HILO images show GFP::NMY-2 in a dividing *ect-2(RNAi)* AB and P_1 cell (outlined by dashed line). Arrowheads in the zoomed images (boxes) point to myosin filament bundles. I) End-on views of ring closure are shown over time, with each timepoint as a different color. X- and y-axes indicate ratios of the distance from the starting position (0). Scale bars: 10 μm. Data in B and D–G are expressed as mean±s.e.m.

7B,C; Fig. S1B). This finding suggests that ECT-2-independent factors control the ring assembly phase differently in AB versus P_1 cells.

To correlate changes in myosin localization with cytokinesis phenotypes, we measured myosin levels along the midplane of *ect-2(RNAi)* embryos. There were narrower peaks of myosin in both AB and P_1 cells compared to their control counterparts, and it was no longer asymmetrically distributed in P_1 cells **(Fig. 7D)**. The average peak value of myosin in AB cells was 68% of control levels, but similar between control and *ect-2(RNAi)* P_1 cells **(Fig. 7E)**. Additionally, we measured total accumulated myosin levels in the furrow region by calculating the area under the peak **(Fig. 7F)**. The total accumulated myosin levels in *ect-2(RNAi)* AB and P_1 cells were 57% and 58% compared to their control counterparts, and total levels in *ect-2(RNAi)* AB cells dropped to those in control P_1 cells **(Fig. 7F)**. These data suggest that the levels of myosin in the furrow region are well above the threshold needed to support cytokinesis in AB cells, whereas P_1 cells operate closer to this threshold. To validate this, we repeated our analysis in *ect-2(RNAi)* embryos where cells formed a furrow, but ultimately failed cytokinesis **(Fig. 7G; Fig. S5A, Movie 3)**. Indeed, myosin levels in AB cells that failed cytokinesis were similar to P_1 cells that succeeded, whereas the levels in P_1 cells that failed cytokinesis dropped even lower **(Fig. 7G)**.

To assess how ECT-2 depletion changes myosin organization, we performed HILO imaging of myosin in *ect-2(RNAi)* AB and P_1 cells **(Fig. 7H; Movie 4)**. There was a dramatic loss in clusters and decreased rotational flow in AB cells compared to control cells (**Fig. 7H;** Pimpale et al., 2020). We also observed that myosin had a more punctate pattern with fewer filament bundles compared to control cells **(Fig. 7H)**. Since flows are predicted to align myosin filaments in the ring, we determined the frequency of filament bundles in a defined region of the furrow where 0° reflects full alignment and considered the proportion within two standard deviations of

the central peak **(Fig. S5B)**. Although there was a high frequency of aligned filament bundles in both control AB and P_1 cells, there was a higher proportion within two standard deviations in AB cells compared to P_1 cells ('amount'; **Fig. S5B**). In *ect-2(RNAi)* AB and P_1 cells, we observed an increase in the frequency of filament bundles with angles that deviate from 0°, and a decrease in the amount of aligned filaments (compare **Fig. 7H** and **Fig. S5C** with **Fig. 6E** and **Fig. S5B**). We observed even poorer filament organization in *ect-2(RNAi)* AB and P_1 cells that failed cytokinesis **(Fig. S5D,E)**. Thus, the poor alignment of filament bundles in *ect-2(RNAi)* AB cells could reflect a loss of cortical flows, and the loss of alignment in both cells would support the delayed kinetics. Despite a change in kinetics, we found that ring closure remained symmetric in *ect-2(RNAi)* P_1 cells, and asymmetric in AB cells **(Fig. 7I; Figs S3D and S4B)**.

2.5.3 Cell fate determines the rate of ring assembly

Our findings suggest that several parameters contribute to ring assembly that extend beyond actomyosin levels. To determine whether these parameters are fate dependent, we assessed cytokinesis in *par-1(RNAi)* and *par-3(RNAi)* embryos. As described earlier, the P_0 zygote divides asymmetrically to give rise to AB and P_1 cells, which is controlled by anterior and posterior complexes containing PAR-3 and PAR-1, respectively (Cowan and Hyman, 2007, Hoege and Hyman, 2013, Rose and Gonczy, 2014, Gan and Motegi, 2020). The loss of either PAR complex should equalize cell fate, but depletion of posterior PAR-1 should cause higher cortical contractility and AB-like kinetics, whereas the loss of anterior PAR-3 should cause lower contractility and P_1-like kinetics (Munro et al., 2004, Cowan and Hyman, 2007). *Par-3(RNAi)* and *par-1(RNAi)* P_0 daughter cells were equal in size and divided synchronously (**Fig. 8A; Fig. S1C;**

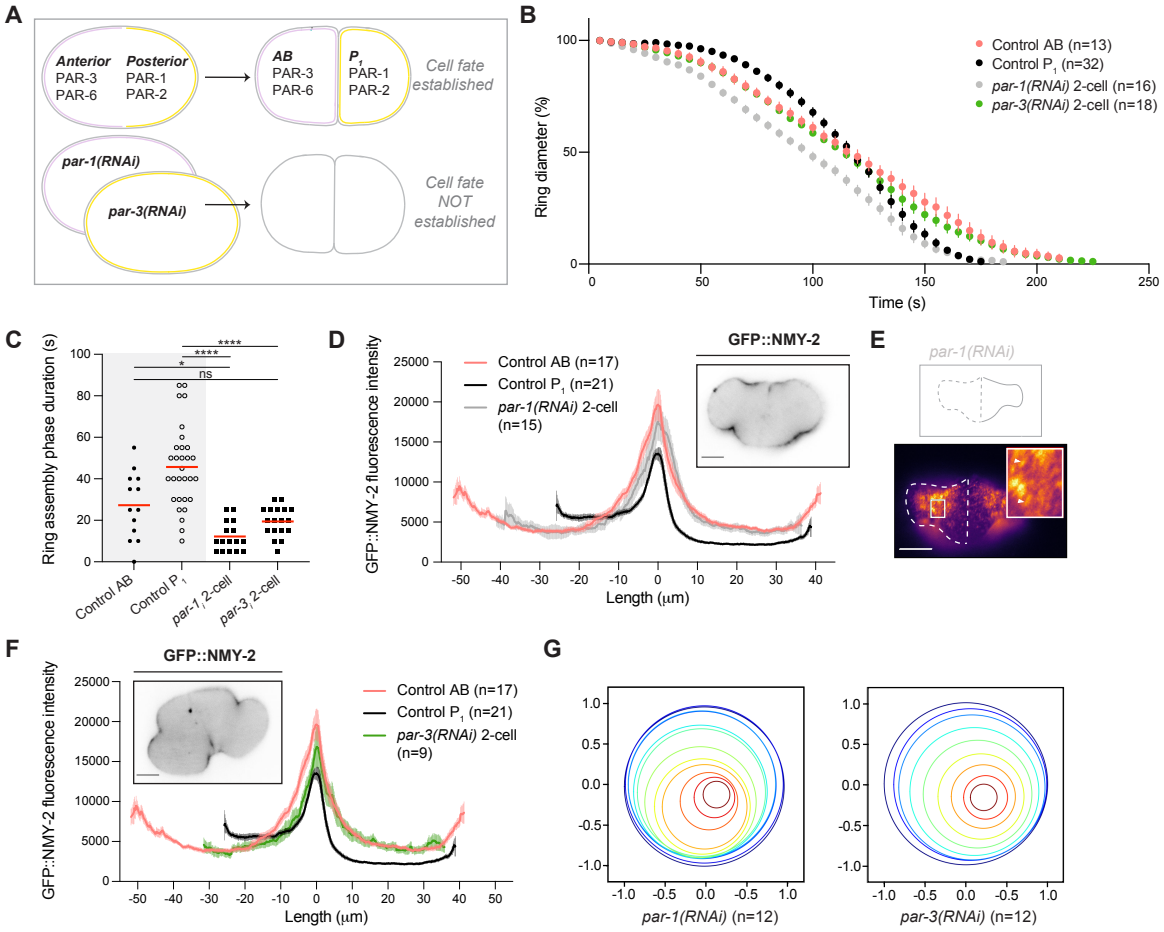
A
Anterior
PAR-3
PAR-6
Posterior
PAR-1
PAR-2
AB
PAR-3
PAR-6
P1
PAR-1
PAR-2
Cell fate established
par-1(RNAi)
par-3(RNAi)
Cell fate NOT established
B
Control AB (n=13)
Control P1 (n=32)
par-1(RNAi) 2-cell (n=16)
par-3(RNAi) 2-cell (n=18)
Ring diameter (%)
Time (s)
C
Ring assembly phase duration (s)
****
****
*
ns
Control AB
Control P1
par-1 2-cell
par-3 2-cell
D
GFP::NMY-2
Control AB (n=17)
Control P1 (n=21)
par-1(RNAi) 2-cell (n=15)
GFP::NMY-2 fluorescence intensity
Length (μm)
E
par-1(RNAi)
F
GFP::NMY-2
Control AB (n=17)
Control P1 (n=21)
par-3(RNAi) 2-cell (n=9)
GFP::NMY-2 fluorescence intensity
Length (μm)
G
par-1(RNAi) (n=12)
par-3(RNAi) (n=12)

Figure 8. Differences in ring assembly between AB and P_1 cells are fate dependent. A) Cartoons show the distribution of PAR proteins in the P_0 zygote, and how their depletion disrupts cell fate. B) A graph shows ring closure in *par-1(RNAi)* and *par-3(RNAi)* P_0 daughters compared to control. C) A plot shows the duration of ring assembly for individual cells (mean, red lines; *$P \leq 0.05$; ****$P \leq 0.0001$; ns, not significant; Welch's *t*-test). D) GFP::NMY-2 levels at the midplane cortex are shown for *par-1(RNAi)* P_0 daughter cells compared to control. GFP::NMY-2 localization is shown in the inset. E) Pseudocolored HILO images show GFP::NMY-2 in a dividing *par-1(RNAi)* P_0 daughter cell (dashed outline). Arrowheads in the zoomed image (box) point to myosin filament bundles. F) GFP::NMY2 levels are shown as in D for *par-3(RNAi)* P_0 daughter cells. G) End-on views of ring closure are shown over time, where each timepoint is a different color. *X*- and *y*-axes indicate ratios of the distance from the starting position (0). Scale bars: 10 μm. Data in B,D and F are expressed as mean±s.e.m.

Kemphues et al., 1988). However, *par-3(RNAi)* and *par-1(RNAi)* cells had kinetics that were similar to AB cells **(Fig. 8B,C)**.

Next, we determined whether myosin levels and/or the organization of myosin filaments support the rapid kinetics in the PAR-depleted cells. Indeed, peak myosin levels were between those of control AB and P_1 cells [90% versus AB for *par-1(RNAi)* and 86% versus AB for *par-3(RNAi)*], and total accumulated levels in PAR-depleted cells were comparable to control AB cells **(Figs 7E,F and 8D,F)**. Furthermore, HILO imaging revealed strong cortical flows and broad swaths of densely packed filament bundles that appeared to be well-aligned in the furrow region of *par-1(RNAi)* cells **(Fig. 8E; Movie 5)**. Strong cortical flows could facilitate the localization and alignment of myosin filament bundles to support their enhanced kinetics. Interestingly, ring closure occurred asymmetrically in *par-3(RNAi)* and *par-1(RNAi)* P_0 daughter cells, similar to AB cells **(Fig. 8G; Figs S3D, S4C,D)**. These data show that the differences in actomyosin between AB and P_1 cells are fate dependent.

2.5.4 Cell size and ploidy influence the rate of ring assembly

We also determined how ring assembly was affected by changing cell size and ploidy. We generated tetraploid (4n) mNeonGreen::PH; mCherry::HIS-58 embryos, which have a 1.3-fold and 1.5-fold increase in AB (27–35 μm) and P_1 (18.1–27.2 μm) cell size, respectively **(Table 1, Fig. 9A; Fig. S1D)**. The average size of tetraploid P_1 cells is nearly identical to diploid AB cells, and the cells retain their appropriate fates. The ring assembly phase was similar in tetraploid P_1 and diploid AB cells **(Fig. 9B,C)**, but took much longer in tetraploid AB cells compared to diploid AB or P_1 cells **(Fig. 9B,C)**.

Table 1. Mean size of cells in the two-cell embryo across different conditions.

	Mean size (μm)	s.e.m.
Control AB	26.97	0.59
Control P_1	18.14	0.33
ect-2(RNAi) AB	26.66	0.38
ect-2(RNAi) P_1	21.72	0.77
par-1(RNAi)	23.53	0.62
par-3(RNAi)	28.58	0.39
Tetraploid AB	35.00	0.51
Tetraploid P_1	27.21	0.78
ran-3(RNAi) AB	22.53	0.98
ran-3(RNAi) P_1	21.82	0.45

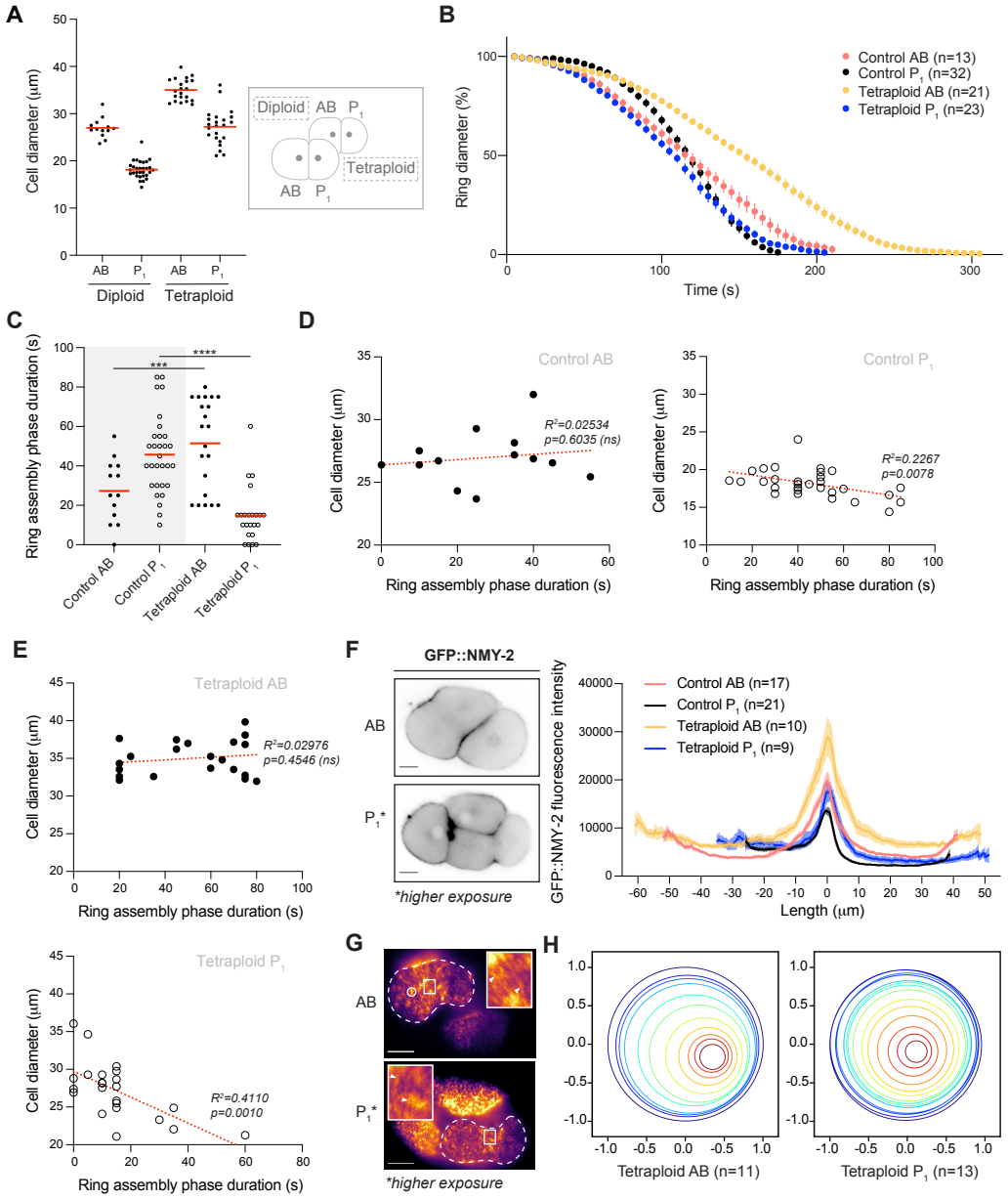
A
Cell diameter (µm)
AB
P1
Diploid
Tetraploid
B
Ring diameter (%)
Time (s)
Control AB (n=13)
Control P1 (n=32)
Tetraploid AB (n=21)
Tetraploid P1 (n=23)
C
Ring assembly phase duration (s)
***
****
Control AB
Control P1
Tetraploid AB
Tetraploid P1
D
Control AB
R²=0.02534
p=0.6035 (ns)
Control P1
R²=0.2267
p=0.0078
Cell diameter (µm)
Ring assembly phase duration (s)
E
Tetraploid AB
R²=0.02976
p=0.4546 (ns)
Tetraploid P1
R²=0.4110
p=0.0010
F
GFP::NMY-2
*higher exposure
GFP::NMY-2 fluorescence intensity
Length (µm)
Control AB (n=17)
Control P1 (n=21)
Tetraploid AB (n=10)
Tetraploid P1 (n=9)
G
*higher exposure
H
Tetraploid AB (n=11)
Tetraploid P1 (n=13)

Figure 9. Cell size and ploidy contribute to differences in ring assembly between AB and P_1 cells. A) Left: a plot shows the size of diploid and tetraploid AB and P_1 cells (mean, red lines). Right: cartoons highlight their relative sizes. B) A graph shows ring closure in tetraploid AB and P_1 cells compared to control; *n* values include 21 sister pairs. C) A plot shows the duration of ring assembly for individual cells (mean, red lines; ***$P \leq 0.001$; ****$P \leq 0.0001$; two-way ANOVA). D,E) Graphs show the correlation between ring assembly and cell diameter for control AB and P_1 cells (D) and for tetraploid AB and P_1 cells (E). Red dotted lines show simple linear regression (R^2 and *P* are shown; ns, not significant). F) Left: inverted images show GFP:: NMY-2 localization in tetraploid AB and P_1 cells. Right: GFP::NMY-2 levels at the midplane cortex of tetraploid AB and P_1 cells are shown compared to control. G) Pseudocolored HILO images show GFP::NMY-2 in a tetraploid AB and P_1 cell (dashed line). The circle shows a myosin cluster. Arrowheads in the zoomed image (box) point to myosin filament bundles. H) Ring closure is shown over time, with each timepoint as a different color. *X*- and *y*-axes indicate ratios of the distance from the starting position (0). Scale bars: 10 μm. Data in B and F are expressed as mean±s.e.m.

The unexpected delay in ring assembly in tetraploid AB cells prompted us to determine whether there is a relationship between ring assembly and cell size in AB and P_1 cells. First, we compared the duration of each phase with cell size in control diploid cells. We used simple linear regression and found that there was no correlation between ring assembly and cell size in diploid AB cells, whereas P_1 cells had a negative correlation regardless of the sample size, suggesting that rings take longer to assemble in the smaller P_1 cells **(Fig. 9D; Fig. S6A)**. We observed different trends during the other phases when actomyosin filaments transition to force generation. Whereas furrow initiation showed a positive correlation with size in P_1 cells and no correlation in AB cells, both cell types had a positive correlation with size during ring closure **(Fig. S6B)**. We were surprised to see that larger cells took longer to constrict, which is contradictory to a previously published study showing that constriction rates positively correlate with size. However, the previous study explored cells with greater differences in size compared to this study, where cells are closer in range and could reflect differences within versus between different size scales. Next, we determined whether there was a correlation with cell size and duration of ring assembly after depletion of ECT-2, PAR-1 or PAR-3 **(Fig. S6C,D)**. There was no correlation in AB cells as expected, but the correlation was lost in P_1 cells in all treatments, suggesting that this depends on actomyosin levels and cell fate **(Fig. S6C,D)**. In support of this, there was no correlation between ring assembly and size in tetraploid AB cells, whereas a stronger negative correlation was observed in tetraploid P_1 cells **(Fig. 9E)**. The strong negative correlation in tetraploid P_1 cells supports the hypothesis that the factors controlling ring assembly in response to size are fate dependent. As tetraploid cells have higher ploidy, it is possible that these factors include Ran signaling, which relies on inverse Ran-GTP and importin gradients formed by chromatin (Hasegawa et al., 2013).

To determine whether the different ring assembly kinetics in tetraploid AB and P_1 cells correlates with myosin levels and/or organization, we generated tetraploid embryos expressing GFP::NMY-2. Peak myosin levels in tetraploid AB cells were 48% higher and more broadly distributed compared to diploid AB cells **(Figs 7E and 9F)**. There was also a 32% increase in peak myosin levels in tetraploid P_1 cells such that they were comparable to control AB cells **(Figs 7E and 9F)**. The same results were obtained regardless of whether AB or P_1 cells from the same or different embryos were analyzed **(Fig. S3E)**. Accumulated myosin in the furrow region was also higher in tetraploid AB cells, and tetraploid P_1 cells were comparable to diploid AB cells **(Fig. 7F)**. HILO imaging revealed a high number of myosin clusters in tetraploid AB cells, with densely packed, well-aligned filament bundles throughout the cortex **(Fig. 9G; Movie 6)**. Tetraploid P_1 cells also appeared to have a greater density of myosin compared to diploid P_1 cells **(Fig. 9G; Movie 6)**. The slower kinetics in tetraploid AB cells could be due to excessive force generation outside the furrow region. Surprisingly, we also found that rings closed asymmetrically in tetraploid P_1 cells, similar to diploid AB cells **(Fig. 9H; Fig. S3D)**. Our results suggest that distinct thresholds of myosin support different kinetics, and high levels can hinder ring assembly. These data also suggest that ideal levels of myosin can override the factors that delay ring assembly in P_1 cells.

2.5.5 The Ran pathway regulates cytokinesis differently in AB and P_1 cells

Our data show that multiple mechanisms regulate contractile ring assembly. We recently found that the Ran pathway controls ring position in response to chromatin in HeLa cells, and our model is that importin binding to NLS-containing cortical proteins positively regulates their

recruitment and/or function at the equatorial cortex (Beaudet et al., 2017, Beaudet et al., 2020). The Ran pathway has not been studied in many cell types and its requirement could vary with cell size, ploidy and fate. First, we determined whether Ran regulates cytokinesis in AB and P_1 cells. We partially depleted RAN-3 (RCC1) to decrease the levels of Ran-GTP and increase the pool of importins that can bind to NLS-containing proteins **(Fig. 10A)**. We observed equalized kinetics in *ran-3(RNAi)* AB and P_1 cells, which both had shorter ring assembly phases compared to control cells **(Fig. 10B,C; Fig. S1E)**. A comparison of other phase durations showed that furrow initiation was not altered in *ran-3(RNAi)* AB and P_1 cells, whereas constriction was faster for AB cells and slower for P_1 cells **(Fig. S7A)**. Interestingly, we also saw no correlation between cell size and the duration of ring assembly in *ran-3(RNAi)* AB or P_1 cells **(Fig. S6E)**. In addition to changes in cytokinesis, we observed a prophase delay in *ran-3(RNAi)* P_1 cells, which increased the heterochronicity between AB and P_1 divisions. We used this delay as a visible marker to follow the efficiency of *ran-3(RNAi)* knockdown. We also observed that AB and P_1 cells were similar in size **(Table 1)**. To ensure that the *ran-3(RNAi)* phenotypes were not caused by a change in polarity, we imaged embryos co-expressing GFP::PH with PGL-1::RFP, which is a marker of P granules **(Fig. S7B)**. We saw that P granules segregated asymmetrically to P_1 and P_2 cells in embryos after *ran-3(RNAi),* similar to control embryos (Strome and Wood, 1982). We also considered that *ran-3(RNAi)* could cause spindle defects, because changes in Ran-GTP levels can affect spindle assembly (e.g. Schatz et al., 2003). However, as we only measured cytokinesis in *ran-3(RNAi)* cells where chromosomes segregated, we did not think that our RNAi treatment was severe enough to cause spindle defects. We verified this by imaging embryos co-expressing mCherry::HIS-58, GFP::PH and GFP::TBB-2 to visualize microtubules, and indeed spindle length was similar between control and *ran-3(RNAi)* AB and P_1 cells **(Fig. S7C).**

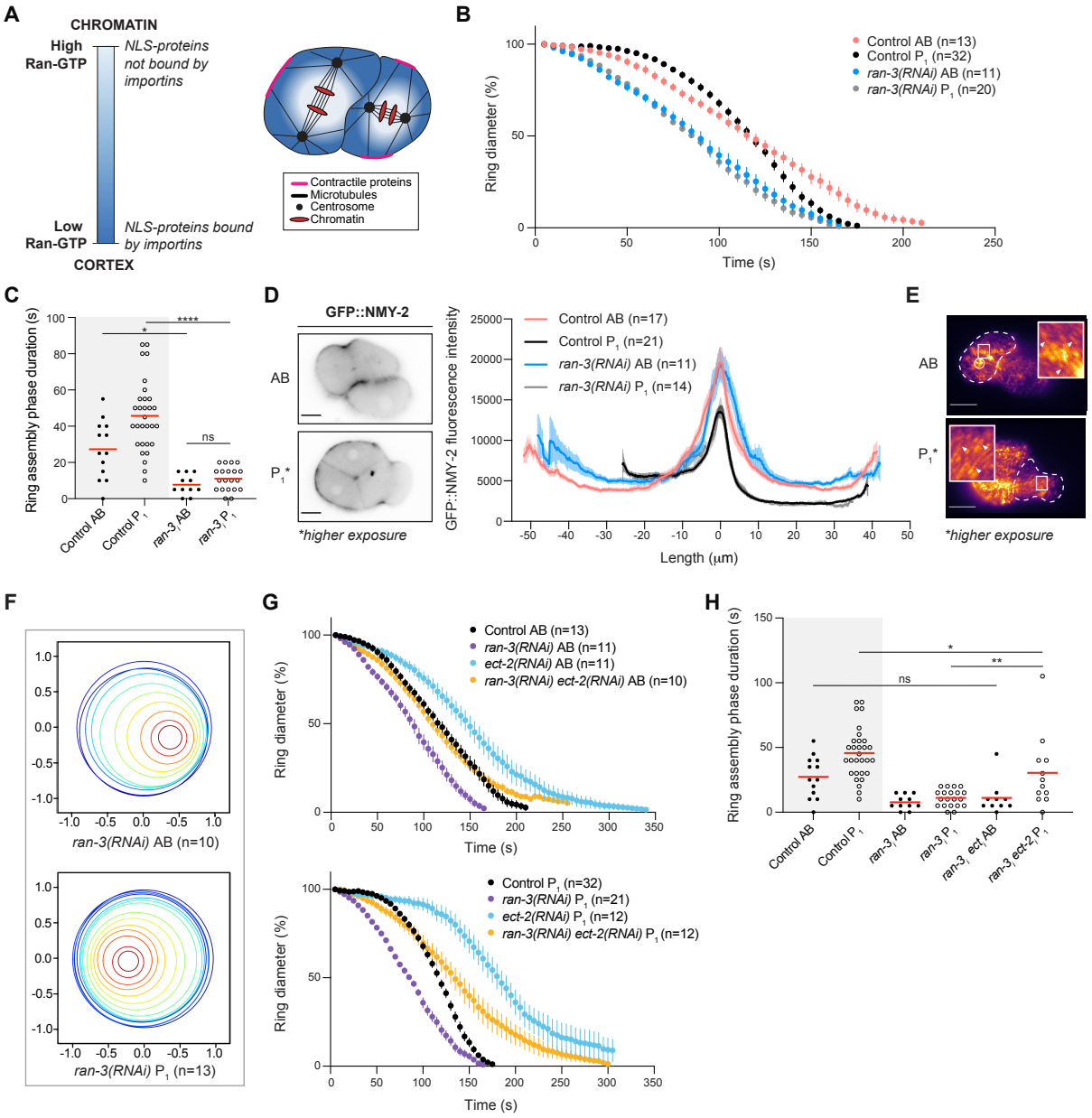
A
CHROMATIN
High Ran-GTP
NLS-proteins not bound by importins
Low Ran-GTP
NLS-proteins bound by importins
CORTEX
Contractile proteins
Microtubules
Centrosome
Chromatin
B
Control AB (n=13)
Control P1 (n=32)
ran-3(RNAi) AB (n=11)
ran-3(RNAi) P1 (n=20)
Ring diameter (%)
Time (s)
C
Ring assembly phase duration (s)
Control AB
Control P1
ran-3 AB
ran-3 P1
ns
D
GFP::NMY-2
AB
P1*
*higher exposure
Control AB (n=17)
Control P1 (n=21)
ran-3(RNAi) AB (n=11)
ran-3(RNAi) P1 (n=14)
GFP::NMY-2 fluorescence intensity
Length (μm)
E
AB
P1*
*higher exposure
F
ran-3(RNAi) AB (n=10)
ran-3(RNAi) P1 (n=13)
G
Control AB (n=13)
ran-3(RNAi) AB (n=11)
ect-2(RNAi) AB (n=11)
ran-3(RNAi) ect-2(RNAi) AB (n=10)
Control P1 (n=32)
ran-3(RNAi) P1 (n=21)
ect-2(RNAi) P1 (n=12)
ran-3(RNAi) ect-2(RNAi) P1 (n=12)
Ring diameter (%)
Time (s)
H
Ring assembly phase duration (s)
Control AB
Control P1
ran-3 AB
ran-3 P1
ran-3 ect AB
ran-3 ect-2 P1

Figure 10. Ran regulates ring assembly in AB and P_1 cell cytokinesis. A) A cartoon shows the importin gradient in the two-cell embryo. Ran-GTP is high near chromatin and low near the cortex where importins are free to bind to NLS-containing cortical proteins. B) A graph shows ring closure in *ran-3(RNAi)* AB and P_1 cells compared to control. C) A plot shows the duration of ring assembly for individual cells (mean, red lines). D) Left: inverted images show GFP::NMY-2 localization in *ran-3(RNAi)* AB and P_1 cells. Right: GFP::NMY-2 levels at the midplane cortex of *ran-3(RNAi)* AB and P_1 cells are shown compared to control. E) Pseudocolored HILO images show GFP::NMY-2 in a dividing *ran-3(RNAi)* AB and P_1 cell (outlined by dashed line). The circle shows a myosin cluster. Arrowheads in the zoomed image (box) point to myosin filament bundles. F) Ring closure is shown over time, with each timepoint as a different color. *X*- and *y*-axes indicate ratios of the distance from the starting position (0). G) Graphs show ring closure in AB and P_1 *ran-3(RNAi)*, *ect-2(RNAi)* and *ran-3(RNAi) ect-2(RNAi)* cells compared to control. H) A plot shows the duration of ring assembly for individual cells (mean, red lines). Scale bars: 10 μm. Data in B,D,G are expressed as mean±s.e.m. For C and H, **P*≤0.05, ***P*≤0.01; *****P*≤0.0001; ns, not significant; two-way ANOVA.

Next, we determined whether the rapid ring assembly kinetics in *ran-3(RNAi)* cells was caused by an increase in myosin levels and/or organization. Peak myosin levels and total accumulation of myosin in the furrow region of *ran-3(RNAi)* AB or P_1 cells showed no significant change **(Figs 7E,F and 10D)**. As myosin levels are not sufficient to support the faster kinetics in P_1 cells, we also characterized the appearance of the filaments. HILO imaging revealed that both AB and P_1 cells had densely packed filamentous myosin, and AB cells had strong cortical flows **(Fig. 10E; Movies 7 and 8)**. In support of their rapid kinetics, the myosin filament bundles appeared to be well aligned in both AB and P_1 *ran-3(RNAi)* cells, but particularly in P_1 cells compared to control. These results suggest that decreasing the levels of Ran-GTP enhances the organization of actomyosin filaments. Interestingly, we also observed that rings closed asymmetrically in both AB and P_1 cells after RAN-3 depletion **(Fig. 10F; Fig. S3D)**.

Next, we determined whether the faster kinetics in *ran-3(RNAi)* AB and P_1 cells are a result of RhoA-mediated contractility. Partial depletion of ECT-2 partially suppressed the rapid ring assembly kinetics caused by RAN-3 depletion in AB and P_1 cells **(Fig. 10G,H)**, with the caveat that the ring assembly phase is more challenging to define in *ect-2(RNAi)* cells. Therefore, decreasing active RhoA and contractility could counter the increase in contractility caused by decreasing Ran-GTP.

2.5.6 Ran regulation occurs through different components in AB and P_1 cells

Next, we determined whether Ran influences ring assembly by regulating importins. To do this, we depleted IMA-3 (importin-α) or IMB-1 (importin-β). *C. elegans* has three importin-α homologs (IMA-1, -2 and -3), but IMA-1 depletion has no obvious phenotype, and IMA-2 is

essential for spindle assembly precluding its use in this study (Geles and Adam, 2001, Askjaer et al., 2002). Interestingly, whereas *ima-3(RNAi)* caused faster ring assembly in both AB and P_1 cells, *imb-1(RNAi)* caused faster assembly only in P_1 cells **(Fig. 11A)**. *ima-3(RNAi)* also causes embryos to be smaller in size, which allowed us to follow knockdown efficiency. Co-depletion of IMB-1 suppressed the rapid ring assembly caused by IMA-3 in AB cells, but only partially suppressed assembly in P_1 cells **(Fig. S7D)**. This differential response suggests that there are different threshold requirements for the different importins in AB and P_1 cells, with the caveat that this could reflect differences in RNAi efficiency. One interpretation is that IMB-1 influences ring assembly in AB cells, but not IMA-3, whereas in P_1 cells IMA-3, IMB-1 and/or the heterodimer can influence ring assembly.

We then determined whether ANI-1 (anillin) is a target of the Ran pathway in AB and P_1 cells. Currently, anillin is the only cytokinesis protein known to be regulated by importin-β-binding for its cortical function in human cells. ANI-1 shares homology with human anillin **(Fig. 11B, top)**, and the NLS in the C2 domain is somewhat conserved **(Fig. 11B, bottom left)**. Indeed, GST-tagged ANI-1 [RhoA-GTP binding domain (RBD)+C2] pulled down Myc-tagged human importin-β from cell lysates **(Fig. 11B, bottom right)**. This binding was reduced by point mutations in the NLS **(Fig. S7E)**. As further support for the importin regulation of ANI-1, we observed a decrease in the midplane levels of mNeonGreen-tagged ANI-1 in the furrow region of P_0 cells in *imb-1(RNAi)* embryos **(Fig. 11C)**. Collectively, these data suggest that ANI-1 could be regulated by importin binding and the Ran pathway in *C. elegans*. To determine whether lowering Ran-GTP levels causes rapid ring assembly by facilitating ANI-1 function, we co-depleted RAN-3 and ANI-1. In *ani-1(RNAi)* embryos, the early phases of cytokinesis were similar or slightly delayed compared to control AB and P_1 cells **(Fig. 11D,E)**. Interestingly, ANI-1 depletion suppressed the

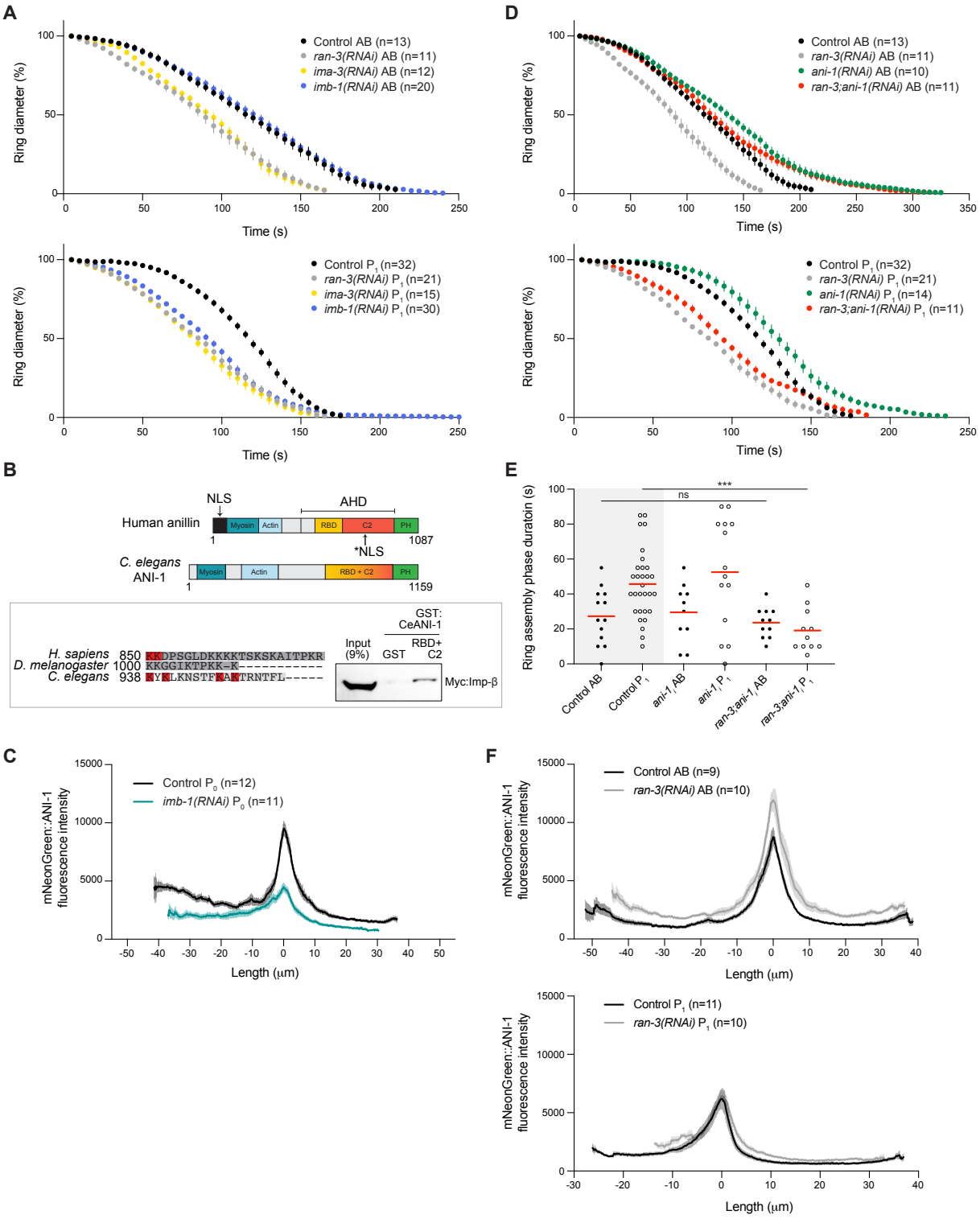
A
Ring diameter (%)
Time (s)
Control AB (n=13)
ran-3(RNAi) AB (n=11)
ima-3(RNAi) AB (n=12)
imb-1(RNAi) AB (n=20)
Control P1 (n=32)
ran-3(RNAi) P1 (n=21)
ima-3(RNAi) P1 (n=15)
imb-1(RNAi) P1 (n=30)
D
Control AB (n=13)
ran-3(RNAi) AB (n=11)
ani-1(RNAi) AB (n=10)
ran-3;ani-1(RNAi) AB (n=11)
Control P1 (n=32)
ran-3(RNAi) P1 (n=21)
ani-1(RNAi) P1 (n=14)
ran-3;ani-1(RNAi) P1 (n=11)
B
NLS
AHD
Human anillin
Myosin
Actin
RBD
C2
PH
1
1087
*NLS
C. elegans ANI-1
1159
H. sapiens 850 KKDPSGLDKKKKTSKSKAITPKR
D. melanogaster 1000 KKGGIKTPKK-K----------
C. elegans 938 KYKLKNSTFKAKTRNTFL-----
GST: CeANI-1
Input (9%)
GST
RBD+ C2
Myc:Imp-β
E
Ring assembly phase duratoin (s)
***
ns
Control AB
Control P1
ani-1 AB
ani-1 P1
ran-3;ani-1 AB
ran-3;ani-1 P1
C
mNeonGreen::ANI-1 fluorescence intensity
Length (μm)
Control P0 (n=12)
imb-1(RNAi) P0 (n=11)
F
Control AB (n=9)
ran-3(RNAi) AB (n=10)
Control P1 (n=11)
ran-3(RNAi) P1 (n=10)

Figure 11. Ran differently regulates ring assembly in AB and P_1 cells. A) Graphs show ring closure in AB and P_1 *ran-3(RNAi)*, *ima-3(RNAi)* and *imb-1(RNAi)* cells compared to control. B) Top: schematics show the structures of human anillin and *C. elegans* ANI-1 (Myosin, myosin binding domain; Actin, F-actin binding domain; RBD, RhoA-GTP binding domain; C2, C2 domain; PH, pleckstrin homology domain; AHD, anillin homology domain). NLS sites are shown in human anillin; the asterisk indicates the site required for cytokinesis. Bottom left: the C-terminal NLS is shown for anillin homologs; residues required for importin binding are in red. Bottom right: a western blot shows Myc-tagged importin-β from HeLa cell lysates (input) and after pull down with recombinant, purified GST or GST-tagged ANI-1 (RBD+C2). Blot shown is representative of three experiments. C) mNeonGreen::ANI-1 levels at the midplane cortex are shown for *imb-1(RNAi)* P_0 cells compared to control. D) Graphs show ring closure in AB and P_1 *ran-3(RNAi)*, *ani-1(RNAi)* and *ran-3(RNAi); ani-1(RNAi)* cells compared to control. E) A plot shows the duration of ring assembly for individual cells (mean, red lines; ***$P \leq 0.001$; ns, not significant; two-way ANOVA). F) mNeonGreen::ANI-1 levels at the midplane cortex are shown for control and *ran-3(RNAi)* AB and P_1 cells. Data in A,C,D and F are expressed as mean±s.e.m.

rapid assembly kinetics caused by RAN-3 depletion in AB, but not P_1, cells **(Fig. 11D,E)**. To ensure that ANI-1 was sufficiently depleted, we followed the large polar body phenotype, and measured ANI-1 levels in single and double knockdown embryos **(Fig. S7F)**. To determine whether ANI-1 could be regulated by RAN-3 in AB cells, we measured changes in ANI-1 localization in *ran-3(RNAi)* embryos. Indeed, although peak ANI-1 levels increased in *ran-3(RNAi)* AB cells relative to control, they remained unchanged in P_1 cells **(Fig. 11F)**. These data support that the Ran pathway regulates the cortical recruitment of ANI-1 for the equatorial organization of actomyosin filaments in AB cells. However, the pathway functions differently in the germline precursor P_1 cells and involves different targets.

2.6 DISCUSSION

2.6.1 AB and P_1 cells have distinct cytokinesis kinetics

We demonstrate that AB and P_1 cells in the *C. elegans* embryo have unique ring assembly kinetics, which reflect differences in actomyosin levels and mechanisms affecting their organization. We found that the ring assembly phase is faster in AB cells compared to P_1 cells, which correlates with higher levels of equatorial myosin and aligned filament bundles that appear to flow into the contractile ring **(Fig. 6)**. This is consistent with previous studies suggesting that long-range flows promote ring assembly (Singh and Pohl, 2014, Reymann et al., 2016, Khaliullin et al., 2018, Illukkumbura et al., 2020). Additionally, the clusters that form in the AB cortex could facilitate the alignment and organization of actomyosin and/or compression (Reymann et al., 2016, Khaliullin et al., 2018). We also observed asymmetric closure of the ring in AB cells towards the AB–P_1 cell boundary, in line with previous reports (Maddox et al., 2007; Bai et al., 2020). This

closure is required to position the midbody to align the spindle in the P_1 cell. However, the mechanisms driving asymmetric closure of AB cells are not well understood. In contrast, actomyosin takes longer to accumulate in P_1 cells, which lack cortical flows and have less cortical myosin, and ring constriction occurs with less hindrance due to lower cortical tension that antagonizes furrowing (Silva et al., 2016). These data indicate that the levels of myosin and their organization correlate with the observed kinetics in the two cell types **(Figs 7E, F and 12A)**. Partial depletion of ECT-2, which generates active RhoA for actomyosin filament assembly (Green et al., 2012), revealed that AB cells are sensitized to cytokinesis failure when myosin levels drop closer to those typically found in control P_1 cells, which operate closer to the minimum threshold **(Fig. 7D**–**F)**. Rings still closed asymmetrically in *ect-2(RNAi)* AB cells, although they were more symmetrical compared to control, suggesting the contribution of multiple factors. Another surprising finding was that the rate of ring assembly remained AB-like in AB cells after partial depletion of NMY-2 or ECT-2 **(Fig. 7B; Fig. S3C)**. This result shows that multiple factors control ring assembly, which could be differently partitioned between AB and P_1 cells.

2.6.2 Differences in AB and P_1 ring assembly are fate dependent

Disrupting cell fate by depleting PAR-1 or PAR-3 equalized ring closure kinetics between the daughter cells, which had short ring assembly phases similar to control AB cells **(Fig. 8)**. PAR-1 and PAR-3 are part of posterior and anterior complexes, respectively, which reinforce anterior-enriched cortical contractility (Cowan and Hyman, 2007, Hoege and Hyman, 2013, Rose and Gonczy, 2014, Gan and Motegi, 2020). We expected different kinetics after depletion of PAR-1 or PAR-3; however, the loss of either PAR caused cells to be more AB-like, with myosin levels

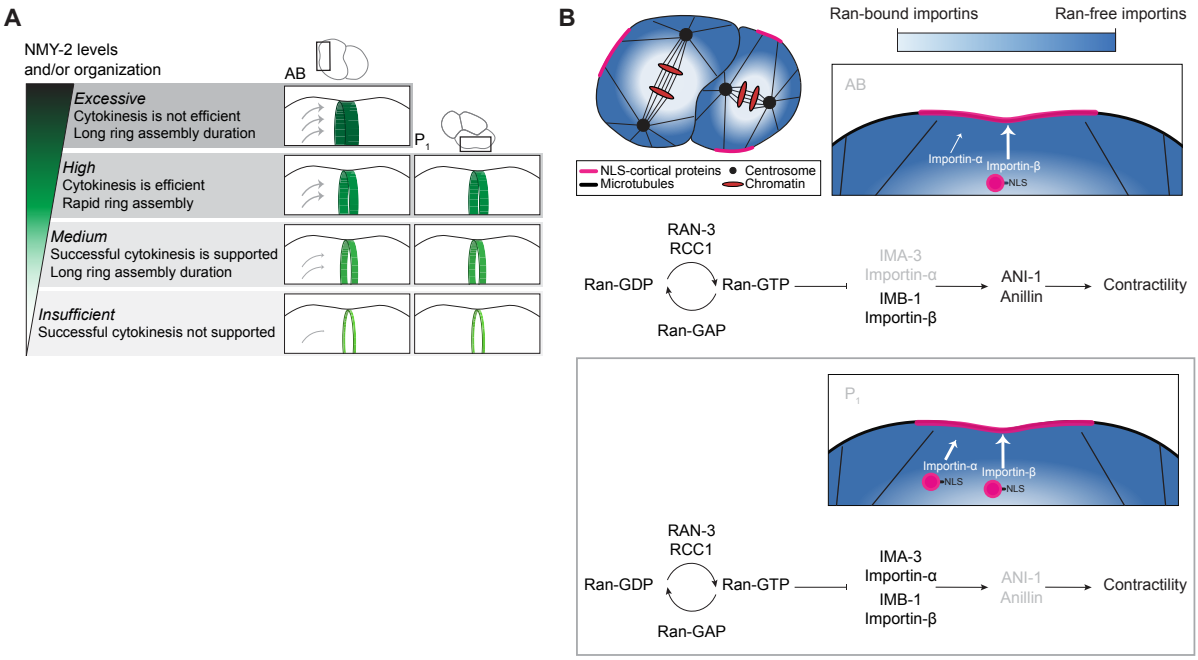
A
NMY-2 levels
and/or organization
AB
P1
Excessive
Cytokinesis is not efficient
Long ring assembly duration
High
Cytokinesis is efficient
Rapid ring assembly
Medium
Successful cytokinesis is supported
Long ring assembly duration
Insufficient
Successful cytokinesis not supported
B
Ran-bound importins
Ran-free importins
AB
Importin-α
Importin-β
NLS
NLS-cortical proteins
Centrosome
Microtubules
Chromatin
RAN-3
RCC1
Ran-GDP
Ran-GTP
Ran-GAP
IMA-3
Importin-α
IMB-1
Importin-β
ANI-1
Anillin
Contractility
P1

Figure 12. Myosin levels and organization in addition to the pathways of regulation contribute to differences in cytokinesis. A) A schematic shows the correlation between the thresholds of myosin, ring assembly and cytokinesis efficiency. The contractile ring is in green, myosin levels are in shades of green, and arrows indicate flows. B) Cartoons show different requirements for the Ran pathway in AB and P_1 cells (black font, high; gray font, low). The gradient of importins free to bind to NLS-containing cortical proteins (NLS-cortical proteins) is shown relative to chromatin.

between AB and P_1 cells, and swaths of well-aligned filament bundles **(Figs 7E,F, 8E and 12A)**. It is not clear why PAR-3 depletion caused AB-like kinetics. Multiple factors regulate global cortical contractility in oocytes, which is inhibited at the posterior cortex by PAR-1–PAR-2, and expansion of this complex may be insufficient to entirely suppress these factors (Cowan and Hyman, 2007, Hoege and Hyman, 2013, Rose and Gonczy, 2014, Gan and Motegi, 2020). Also, this early pool of contractile myosin would be distributed equally to the daughters.

2.6.3 Size and ploidy govern differences in AB and P_1 ring closure kinetics

Cell size also influences the duration of ring assembly in P_1, but not AB, cells. We observed a negative correlation between size and the duration of ring assembly in P_1 cells **(Fig. 9D)**, meaning that rings assemble more quickly in larger cells. One hypothesis is that the Ran-GTP gradient extends closer to the cortex in smaller cells, where it could inhibit contractile ring assembly. This hypothesis is supported by the loss of correlation between cell size and ring assembly in *ran-3(RNAi)* embryos **(Fig. S6E)**. In this model, higher levels of importins free to bind to cortical NLS-containing proteins would promote ring assembly in larger cells, whereas lower levels prevent efficient assembly in smaller cells. A non-mutually exclusive hypothesis is that a larger P_1 cell could reflect a larger inheritance of actomyosin compared to a smaller P_1 cell because of a more symmetric P_0 division. Since P_1 cells already operate at thresholds of myosin close to what is required to support division, even minor increases in myosin or its regulators could facilitate ring assembly more easily, despite their increase in size. Both models could apply to tetraploid P_1 cells, which displayed a shorter ring assembly phase similar to control AB cells, yet still showed a negative correlation between ring assembly and size **(Fig. 9C,E)**. We observed higher levels of

myosin in tetraploid P_1 cells compared to control P_1 cells, which could more readily facilitate ring assembly **(Fig. 9F)**. This finding supports that increasing actomyosin can override the delays in ring assembly in P_1 cells, but the mechanisms controlling ring assembly in P_1 cells, such as the Ran pathway, can still respond to size differences. The negative correlation with ring assembly and size was lost in *ect-2(RNAi), par-1(RNAi)* and *par-3(RNAi)* embryos **(Fig. S6C,D)**. Although myosin levels could be too low to support a correlation in *ect-2(RNAi)* cells, the loss of cell identity after PAR depletion would remove any cell-specific correlations. After ring assembly, we observed positive correlations with size and furrow initiation and constriction phases in P_1 cells, and with constriction in AB cells **(Fig. S6B)**. These results indicate a switch where larger cells take longer to furrow or ingress, suggesting that it is harder to generate the force needed to overcome tension in the larger cells. Although our findings appear to be somewhat contradictory to what was previously published, this prior study explored vastly different cell sizes, and the idea that rings have structural memory to coordinate division during development could still apply in a broader context (Carvalho et al., 2009).

2.6.4 The Ran pathway regulates cytokinesis differently in AB and P_1 cells

We found that the Ran pathway controls ring assembly and functions differently in AB and P_1 cells **(Fig. 12B)**. Our studies of cytokinesis in HeLa cells showed that Ran-GTP coordinates the position of the contractile ring with segregating chromosomes, and we propose that the requirement for this mechanism could vary with cell size, ploidy or fate (Beaudet et al., 2017, Beaudet et al., 2020). A gradient of active Ran associated with chromatin forms inverse to a gradient of importins free to bind to NLS-containing proteins (Ozugergin and Piekny, 2021).

Although importin binding negatively regulates spindle assembly factors, we propose that it positively regulates cortical proteins for cytokinesis, such that the same gradient has reciprocal functions near chromatin versus near the cortex (Ozugergin and Piekny, 2021). Importantly, the Ran-importin gradient was shown to vary with size and ploidy in various cell types and contexts (Deng et al., 2007, Hasegawa et al., 2013). Human anillin contains an NLS that binds to importin-β and is required for its localization and function during cytokinesis (Beaudet et al., 2017, Beaudet et al., 2020). This NLS is conserved in ANI-1, and binding to importin-β could similarly facilitate its cortical recruitment during cytokinesis **(Fig. 11B,C; Fig. S7E)**. Lowering Ran-GTP levels equalized kinetics in AB and P_1 cells, which had a faster ring assembly phase compared to control cells **(Fig. 10)**. This change in kinetics was not a result of changes in myosin levels, but rather improved myosin organization, which could generate stronger forces for filament alignment **(Fig. 10D–F)**. Additionally, we found that ANI-1 is a target of the Ran pathway in AB but not P_1 cells **(Figs 11D–F and 12B)**, and we are currently identifying NLS proteins that are regulated by this pathway.

We also found that different components of the Ran pathway have different threshold requirements in AB and P_1 cells. Ring assembly was faster in both cells after IMA-3 depletion, but only in P_1 cells after IMB-1 depletion **(Fig. 11A)**. The dogma is that importin-α binds to the NLS of proteins and acts as an adaptor protein for importin-β (Xu and Massague, 2004, Ozugergin and Piekny, 2021). However, data from multiple labs suggest that importins can bind independently or as a heterodimer (e.g. Chan and Jans, 1999, Gruss et al., 2001, Schatz et al., 2003, Silljé et al., 2006, Giesecke and Stewart, 2010, Ozugergin and Piekny, 2021). As the depletion of either importin led to faster kinetics in P_1 cells, we propose that either IMA-3 or IMB-1 can regulate cortical proteins for cytokinesis in these cells **(Fig. 12B)**. However, our data support that IMB-1

might play a stronger role in AB cell ring assembly, as IMA-3 depletion could release more IMB-1 to bind to ANI-1 and facilitate faster kinetics.

Our findings build on studies of cytokinesis in the four-cell *C. elegans* embryo demonstrating that cells have different levels of F-actin regulated by intrinsic or extrinsic mechanisms (Davies et al., 2018). These differences in F-actin reflect the differences in myosin that we observed in AB and P_1 cells, suggesting that they arise at the previous division. We also expand on this knowledge by demonstrating that filament organization correlates with ring assembly kinetics, and that the Ran pathway differently regulates ring assembly in AB versus P_1 cells. Why would AB and P_1 cells have different mechanisms that control ring assembly? AB cells are fated to give rise to multiple somatic tissues, whereas P_1 cells are fated to form the germline. Ring assembly may occur similarly in AB cells and somatic cells in other organisms. P cells might differ because they undergo several asymmetric divisions before daughters are born that fail cytokinesis and ultimately form the germline syncytium (Amini et al., 2014, Goupil et al., 2017, Bauer et al., 2021). Having less actomyosin and factors that control the timing of ring assembly in P cells could temporally coordinate the completion of cytokinesis with their neighboring somatic cell, which could be crucial for proper cell fate determination during embryogenesis.

CHAPTER THREE

Cytokinetic diversity among cultured mammalian cells

Adapted from: HUSSER, M.C., OZUGERGIN, I., RESTA, T., MARTIN, V.J.J., PIEKNY, A.J. 2022. Imaging tools generated by CRISPR/Cas9 tagging reveal cytokinetic diversity in mammalian cells. *bioRxiv*.

3.1 PREAMBLE

In vitro studies are a very powerful tool for studying cytokinesis and enable the exploration of cytokinesis in a variety of cell types. There is likely to be more compatibility in the expertise and infrastructure required to perform comparative studies across multiple cell lines *in vitro* versus using model organisms which require years of specialized expertise. However, the bulk of *in vitro* studies of cytokinesis have relied on methods such as fixation, which cannot provide information on dynamics, or overexpression, which can be challenging to control. Endogenously tagged cell lines are ideal tools for qualitative and comparative studies, but there is a lack of cell lines with endogenously tagged cytokinesis proteins. Another issue is that most *in vitro* studies of human cytokinesis have been done using HeLa cells. While these cells have been preferred due to factors such as transfection efficiency and amenability to imaging, not all findings using this cancerous cell type may be applicable to healthy cells in a developmental or tissue context. The work described here compares cytokinesis among different cultured mammalian cell lines, which were endogenously tagged using CRISPR-Cas9 editing to fuse fluorophores to several cytokinesis proteins. Since the generation of these tools was done by Mathieu Husser and is separable from

the characterization and analysis described in this chapter, portions of the manuscript describing the generation of the endogenously tagged cell lines were omitted from this thesis.

3.2 ABSTRACT

Cytokinesis is required to physically separate the daughter cells at the end of mitosis. This process occurs via the assembly and ingression of a membrane-tethered actomyosin ring. Mechanistic studies have uncovered different pathways that regulate ring assembly and position in mammalian cells, but the majority of these studies were done using overexpressed transgenes in HeLa cells, and the relative requirement for these mechanisms in different cell types is not known. Here, we used CRISPR/Cas9 gene editing to endogenously tag cytokinesis components (RhoA, Ect2 and anillin) with a fluorescent protein. These tools enabled live imaging and quantitative studies of these key contractile ring regulators during cytokinesis. Further, tagging anillin in multiple cell types revealed extensive cytokinetic diversity, which will be useful to study how the mechanisms controlling cytokinesis vary in different cell types.

3.3 INTRODUCTION

Cytokinesis is the physical separation of a cell into two daughter cells that occurs at the end of mitosis. This process must be tightly and spatiotemporally controlled as failure can cause changes in cell fate and developmental defects or diseases (Lacroix and Maddox, 2012, D'Avino et al., 2015). Cytokinesis occurs via the assembly and ingression of a RhoA-dependent contractile ring that constricts to pull in the overlying plasma membrane. Multiple pathways have been shown to regulate ring assembly in cultured cells and model organisms (Green et al., 2012, Pollard and O'Shaughnessy, 2019, Husser et al., 2021, Ozugergin and Piekny, 2021). These pathways ensure

that active RhoA is enriched in the equatorial plane to assemble the ring. Ect2 is the guanine nucleotide exchange factor (GEF) that activates RhoA during cytokinesis, and requires binding to phospholipids and the central spindle protein Cyk4 (MgcRacGAP) for its activity (**Fig. 13A;** Yuce et al., 2005, Wolfe et al., 2009, Gomez-Cavazos et al., 2020). The depletion of Cyk4 or Ect2 in HeLa cells prevents the accumulation of active RhoA at the equatorial cortex and leads to cytokinesis failure (Kim et al., 2005, Yuce et al., 2005, Zhao and Fang, 2005b, Kamijo et al., 2006, Nishimura and Yonemura, 2006). Active RhoA (RhoA-GTP) recruits and activates effectors, including formin and RhoA kinase (ROCK), to generate actomyosin filaments and assemble the ring (**Fig. 13A;** Piekny et al., 2005, Pollard and O'Shaughnessy, 2019). Anillin is also recruited by active RhoA and acts as a scaffold protein that tethers the ring to the plasma membrane (Piekny and Glotzer, 2008, Piekny and Maddox, 2010, Green et al., 2012, Sun et al., 2015). In support of its crosslinking function, the depletion of anillin in HeLa or S2 cells leads to ring oscillations and cytokinesis failure (Hickson and O'Farrell, 2008, Piekny and Glotzer, 2008, Piekny and Maddox, 2010). Anillin may also be involved in the retention of active RhoA at the equatorial cortex, as well as its removal during constriction (El Amine et al., 2013, Budnar et al., 2019, Carim et al., 2020). Multiple mechanisms have been shown to control this core cytokinesis machinery in different model systems, but little is known about how their requirement varies in different cell types in metazoans (Husser et al., 2021).

Spindle-dependent and -independent pathways regulate cytokinesis. The central spindle recruits and activates Ect2 in proximity to the equatorial cortex where it generates active RhoA (Mishima et al., 2002, Mishima et al., 2004, Yuce et al., 2005, Petronczki et al., 2007, Burkard et al., 2009, Wolfe et al., 2009, Su et al., 2011, Frenette et al., 2012, Lekomtsev et al., 2012, Basant et al., 2015, Kotynkova et al., 2016, Adriaans et al., 2019). Astral microtubules also define the

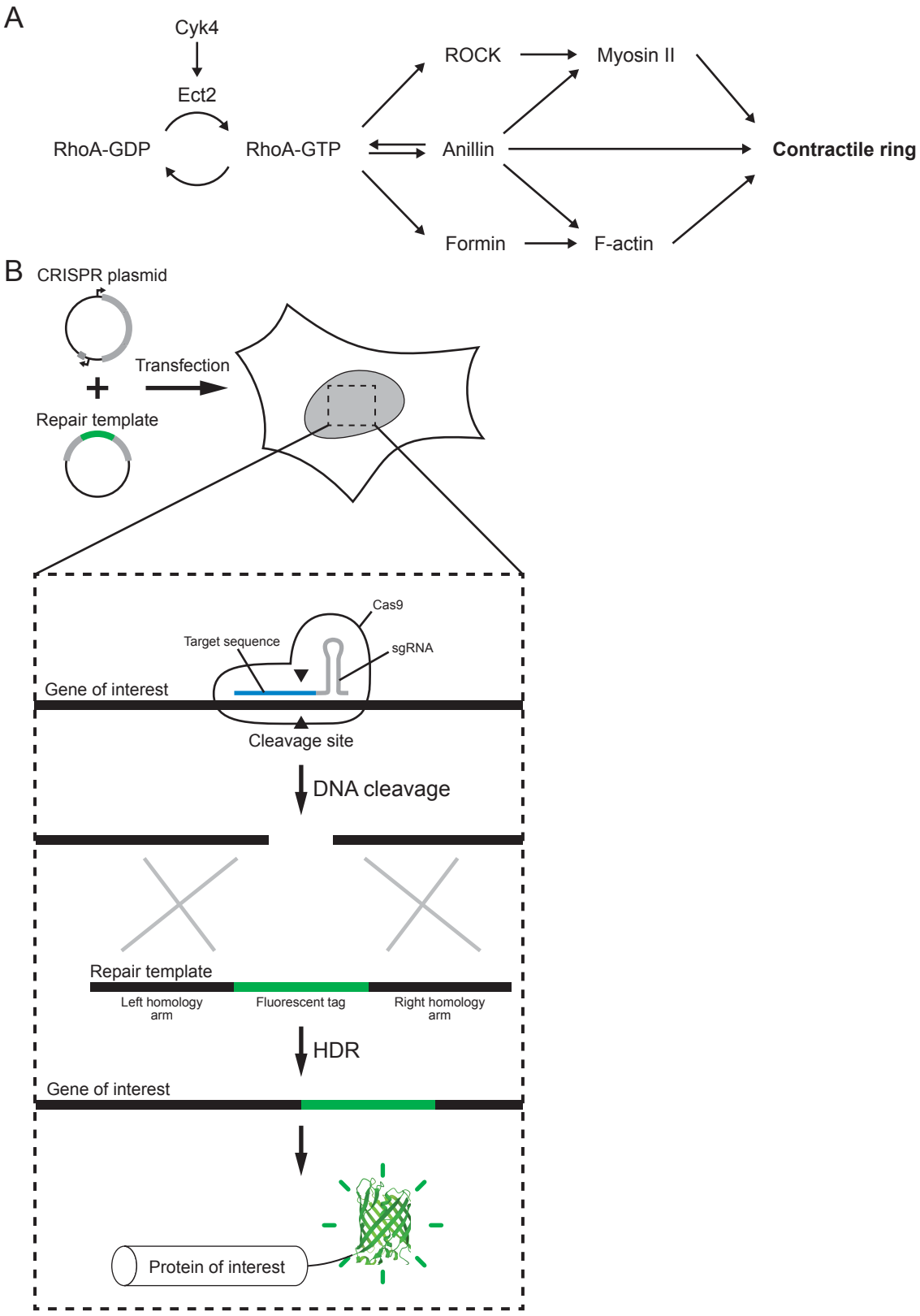
A
Cyk4
Ect2
RhoA-GDP
RhoA-GTP
ROCK
Myosin II
Anillin
Contractile ring
Formin
F-actin
B
CRISPR plasmid
Transfection
Repair template
Cas9
Target sequence
sgRNA
Gene of interest
Cleavage site
DNA cleavage
Repair template
Left homology arm
Fluorescent tag
Right homology arm
HDR
Gene of interest
Protein of interest

Figure 13. Endogenous tagging of cytokinesis using CRISPR/Cas9. A) A diagram shows the core pathway regulating contractile ring assembly during cytokinesis. The generation of active RhoA (RhoA-GTP) by its GEF Ect2 at the equatorial cortex is required for ring assembly. Active RhoA recruits and/or activates effectors (anillin, formin and ROCK proteins) to assemble actomyosin filaments into the contractile ring. B) A diagram shows the mechanism of endogenous tagging by CRISPR/Cas9. A gene-specific sgRNA directs DNA cleavage by Cas9 at the target site. The double-stranded break (DSB) generated by Cas9 can be repaired by homology directed repair (HDR) using the provided repair template and integrate a fluorescent marker at the target site. This will result in the expression of the fluorescent marker fused to the target protein.

cleavage plane by directly or indirectly removing cortical regulators from the poles (Lewellyn et al., 2010, Tse et al., 2011, Zanin et al., 2013, van Oostende Triplet et al., 2014, Mangal et al., 2018, Chen et al., 2021). Spindle-independent pathways polarize the cortex via signals associated with chromatin, centrosomes and kinetochores (Canman et al., 2000, Canman et al., 2003, von Dassow et al., 2009, Cabernard et al., 2010, Kiyomitsu and Cheeseman, 2013, Zanin et al., 2013, Rodrigues et al., 2015, Beaudet et al., 2017, Beaudet et al., 2020, Ozugergin and Piekny, 2021, Ozugergin et al., 2022). A kinetochore-derived pathway induces relaxation of the polar cortex in HeLa and *Drosophila* S2 cells via the dephosphorylation of ERM proteins by a kinetochore-tethered protein phosphatase 1 (PP1; Rodrigues et al., 2015). Several studies also revealed a role for chromatin-associated active Ran (Ran-GTP; Ras-related nuclear protein) in coordinating the position of cortical regulators with segregating chromosomes (Kiyomitsu and Cheeseman, 2013, Beaudet et al., 2017, Beaudet et al., 2020, Ozugergin and Piekny, 2021, Ozugergin et al., 2022). These pathways also act in concert with the negative regulator of RhoA, MP-GAP (M-phase GTPase-activating protein), which is globally localized (Zanin et al., 2013). Having multiple mechanisms to control the function of cortical regulators ensures robust cytokinesis, but their requirement may differ with cell type.

The mechanisms regulating cytokinesis vary widely depending on the organism and tissue (Cabernard et al., 2010, Lewellyn et al., 2010, Fotopoulos et al., 2013, van Oostende Triplet et al., 2014, Rodrigues et al., 2015, Davies et al., 2018, Mangal et al., 2018, Ozugergin et al., 2022, Paim and FitzHarris, 2022). For example, anillin is essential for cytokinesis in cultured cells (HeLa and *Drosophila* S2 cells), but not in the early *Caenorhabditis elegans* zygote, and Dalmatian dogs carrying an anillin truncation mutant did not have obvious cell division defects (Maddox et al., 2005, Hickson and O'Farrell, 2008, Piekny and Glotzer, 2008, Holopainen et al., 2017). However,

later in *C. elegans* development, neuronal precursor cells require anillin for cytokinesis (Fotopoulos et al., 2013, Wernike et al., 2016). Thus, the mechanisms regulating cytokinesis vary with cell fate, but also with other parameters including size, shape, and ploidy. In the two-cell *C. elegans* embryo, the somatic AB and germline P_1 cells have different ring assembly and ingression kinetics with different levels of myosin in the ring (Ozugergin et al., 2022). In the four-cell *C. elegans* embryo, the ABa and ABp cells have stronger requirements for formin-derived F-actin compared to EMS or P_2 cells, which are regulated by cell-extrinsic and intrinsic factors, respectively (Davies et al., 2018). These studies highlight the need to investigate cytokinetic diversity and understand how the mechanisms regulating cytokinesis vary among cell types.

Gene editing tools provide an opportunity to study proteins in diverse cell types (Drubin and Hyman, 2017, Husser et al., 2021). In human cells, cytokinesis has mostly been studied using overexpressed transgenes fused to fluorescent tags for visualization and/or affinity tags for biochemical assays. In HeLa cells, the localization of endogenous anillin fixed and stained with antibodies is similar to anillin overexpression. However, Ect2 and RhoA show inconsistent localization patterns and/or cause cytokinesis phenotypes when over-expressed (Yuce et al., 2005, Chalamalasetty et al., 2006, Piekny and Glotzer, 2008). TCA-fixation-based immunofluorescence microscopy is still one of the most reliable methods to visualize the enrichment of RhoA at the equatorial cortex (Yonemura et al., 2004, Yuce et al., 2005, Koh et al., 2021, Schneid et al., 2021), and Ect2 overexpression can lead to cytokinesis failure (Chalamalasetty et al., 2006). In addition, measurements can be confounded by the variability in transgene expression between transfected cells, whereas endogenous probes enable more quantitative measurements (Husser et al., 2021). Several studies have shown that proteins tagged endogenously with fluorescent proteins report more accurately and cause fewer phenotypes than using overexpressed transgenes (Doyon et al.,

2011, Mahen et al., 2014). Moreover, the same tools can be used to introduce genetic edits into different cell lines derived from the same organism.

The most popular tool for gene editing is CRISPR/Cas9 (clustered regularly interspaced short palindromic repeats/CRISPR-associated protein 9), which is comprised of a Cas9 nuclease and a sgRNA (single guide RNA), which contains a 20-nucleotide target sequence that corresponds to a genomic target site (**Fig. 13B;** Cong et al., 2013, Mali et al., 2013, Wang et al., 2016, Pickar-Oliver and Gersbach, 2019). Cas9 is targeted to this site by the sgRNA and cleaves the DNA to introduce a double-stranded break (DSB). Human cells typically repair DSBs by non-homologous end joining (NHEJ), but can also use the homology-directed repair (HDR) pathway, which makes use of a homologous repair template to fill in the gap where the DSB was introduced (Wright et al., 2018, Scully et al., 2019). To introduce a fluorescent marker at a precise location in the genome of human cells, CRISPR/Cas9 can be used along with a synthetic repair template designed to carry the fluorescent marker flanked with homology arms for HDR (**Fig. 13B;** Verma et al., 2017). When introduced in frame with a gene, the fluorescent marker will be expressed as a fusion with the protein of interest. Efforts to share validated tools for endogenous tagging (sgRNA sequence and repair template) have made these tags more readily accessible and easy to use (Pinder et al., 2015, Savic et al., 2015, Sakuma et al., 2016, Roberts et al., 2017, Iyer et al., 2019, de Man et al., 2021, Sun et al., 2021; Allencell.org; Addgene.org). However, despite these shared resources and the advantages to using endogenous tags, few cytokinesis proteins have been tagged endogenously in human cells (Mahen et al., 2014, Mann and Wadsworth, 2018, Peterman et al., 2020).

In this work, we studied various cell lines that expressed endogenously tagged anillin, Ect2 and RhoA to compare their spatiotemporal distribution during cytokinesis. Specifically, we found differences in the breadth, enrichment and timing of the cortical localization of anillin among the

cell types. By making these tools available to the cell biology community and characterizing the similarities and differences in cytokinesis in commonly studied cell lines, we hope to fuel new studies of the mechanisms regulating cytokinesis in diverse cell types.

3.4 MATERIALS AND METHODS

3.4.1 Cell culture

HEK293, HeLa and MDCK cells were cultured in Dulbecco's modified Eagle medium (DMEM; Wisent) media supplemented with 10% Cosmic calf serum (CCS; Cytoviva). HCT116 cells were cultured in McCoy's media (Wisent) supplemented with 10% CCS. HepG2 cells were cultured in Eagle's minimum essential medium (EMEM; Wisent) supplemented with 10% Fetal bovine serum (FBS; Cytoviva). The cells were maintained in 10 cm dishes in incubators at 37°C with 5% CO_2 as per standard protocols (Beaudet et al., 2017, Beaudet et al., 2020). For long-term storage, cells were washed and resuspended in freezing media (50% FBS, 40% DMEM or EMEM media and 10% DMSO) and stored in liquid nitrogen.

3.4.2 Transfection

For transient transgene expression, vectors [pGG-mNG-Anillin, pGG-mNG-Ect2, pGG-mScar-Ect2(C-term) and GFP-RhoA] were transfected into HeLa cells plated on coverslips to 60% confluency using Lipofectamine 3000 and P3000 reagent (Thermo Fisher Scientific) as per manufacturer's instructions.

3.4.3 Microscopy

To collect images of the endogenous tags and overexpressed transgenes, the coverslips were transferred to a magnetic chamber with 1 ml of media one day after transfection, and imaged on a Leica DMI6000B inverted epifluorescence microscope with filters for the appropriate wavelengths, a 10×/0.25 NA objective, an Orca R2 CCD camera (Hamamatsu) and Volocity software (PerkinElmer).

To image cells during cytokinesis, tagged HeLa, HCT116, HepG2 and MDCK cell lines were seeded onto acid-etched round coverslips (25mm, No. 1.5) in 6-well plates and grown to 70% confluency. The coverslips were transferred to a magnetic chamber (Quorum) with 1 ml media before imaging. Tagged HEK293 cells were seeded directly onto 4-well μ-slides (Ibidi) for imaging. To visualize chromatin, Hoechst 33342 (Invitrogen) was added to the cells at a final concentration of 0.4 μM for 30 minutes prior to imaging. Imaging was performed using an inverted Nikon Eclipse Ti microscope (Nikon) equipped with a Livescan Sweptfield scanner (Nikon), Piezo Z stage (Prior), IXON 879 EMCCD camera (Andor), and 405, 488 and 561 nm lasers (100 mW, Agilent) using the 100×/1.45 NA objective. The cells were kept at 37°C and 5% CO_2 during imaging in an INU-TiZ-F1 chamber (MadCityLabs). Z-stacks of 1 μm thickness were acquired every 1–2 minutes using NIS Elements software (Nikon, version 4.0).

3.4.4 Image analysis

Linescans were performed and measured for the different tagged cell lines using FIJI. All images acquired using NIS Elements (Nikon) were opened in FIJI (Version 2.3, NIH) and analyzed using a macro modified from Ozugergin et al. (2022). Briefly, the macro first isolated the green channel from the movie file, subtracted background signal, and then performed a bleach correction.

The desired timepoint and *z* slices were entered manually, and the macro generated an average *z*-stack projection. A 5-pixel wide line was then traced along the cortex of the cell, from one pole of the cell to the other, along with a straight line intersecting the furrow. The macro then measured the fluorescence intensity of each pixel along the length of the linescan, and positioned the pixels relative to the furrow. The average intensity projection of two central *z* slices were used for cortical linescans, while six central slices were used to measure the central spindle in Ect2-tagged cells. All data measured by the macro was exported for use in Excel (Microsoft) and Prism (Version 9.3, GraphPad) for further analysis. Pixel intensity values were normalized by subtracting the average baseline intensity (the average intensity of the first or last 50 pixels of the linescan) from the maximum intensity value. To obtain breadth measurements, the number of pixels > 50% or 75% of the peak value were counted and converted to microns. Intensities >50% were used to compare the breadth of RhoA to Ect2 and anillin **(Fig. 14; Fig. S9)** to account for low peak intensity levels for RhoA, and intensities >75% were used to compare anillin across cell lines **(Fig. 15; Figs S9, S10)**. Enrichment at the equatorial versus polar cortex was calculated as a ratio between the average pixel intensity in the furrow (pixels >50 or >75% of the peak value) and the average intensity of pixels in the poles (the first or last 50 pixels in the linescan). To measure the ratio of cortical to cytosolic anillin in metaphase cells, the average intensity of signal at the cortex was measured by a linescan drawn around the cortex using the macro as described above, while the average intensity of the cytosol was measured by drawing a region of interest.

Ring closure was measured as described in Ozugergin et al. (2022). In short, a 250×50-pixel area containing the ring was rotated using SciKit Image (version 0.16.2) to generate an end-on view of the ring. Best-fit ellipses were manually drawn on the cell outline in FIJI, and their coordinates were noted. Best-fit circles for each ellipse were then graphed using Python 3 and the

Jet colormap. The radius and center of the ring in the first timepoint were set to 1 and 0,0 respectively, and ellipse coordinates in the subsequent timepoints were normalized to this timepoint. Symmetry values were obtained by using the Pythagorean theorem to calculate the distance between the center of the cell in the first timepoint and the center of the ring in the last measured timepoint. Cells with symmetry values <0.2 were defined as having symmetric ring closure, and cells with symmetry values >0.2 and >0.6 were defined as having asymmetric and very asymmetric ring closure, respectively.

3.4.5 Statistical analysis

Box and whiskers plots were generated using Prism (Version 9.3, GraphPad) to show median values (central line), quartiles (box edges) and minimum and maximum values (whiskers). Statistical significance was tested using a Brown-Forsythe and Welch's ANOVA, followed by multiple comparisons using Dunnett's T3 test, or by Welch's *t*-test (GraphPad Prism version 9.3). Significance levels were defined as: $P>0.5$ non-significant (ns), $*P\leq0.05$; $**P\leq0.01$; $***P\leq0.001$; $****P\leq0.0001$.

3.5 RESULTS

3.5.1 Visualization of endogenously tagged cytokinesis proteins

We characterized the localization of endogenous mNeonGreen-tagged anillin, Ect2 and RhoA in HeLa cells by fluorescence microscopy. First, we compared the expression of the endogenous tags to transiently transfected transgenes. When comparing fields of view of the endogenously tagged cells to the transfected cells, there was a striking difference in levels and variability across the cell populations **(Fig. S8)**. The endogenously tagged proteins were expressed at much lower and more consistent levels across the cell population compared to the overexpressed transgenes. In the endogenously tagged cell lines, anillin and Ect2 were nuclear in interphase cells as expected, whereas RhoA was cytosolic **(Fig. S8A)**. While there was some variability in anillin and Ect2 expression in the endogenously tagged cell lines, this was likely due to their cell cycle-dependent turnover and was far less than what was observed for the overexpressed transgenes **(Fig. S8)**. Thus, these probes can be used to accurately measure endogenous protein expression and localization.

We then imaged cells during cytokinesis to follow the localization of endogenously tagged anillin, Ect2 and RhoA **(Fig. 14A–C)**. As expected, anillin was enriched at the equatorial cortex shortly after anaphase onset and remained in the furrow throughout ingression, after which it localized to the midbody **(Fig. 14A)**. We measured this enrichment by drawing linescans to plot the intensity of mNeonGreen-anillin along the cortex of cells at furrow initiation (~9-14 min; **Fig. 14D and E, left**). To measure localization over time, we repeated this analysis every two minutes, starting two minutes before anaphase onset and until furrowing appeared to be completed **(Fig. 14F and G, left)**. We observed an increase in the enrichment and a gradual decrease in the breadth of anillin at the equatorial cortex over time, with the enrichment being first visible 4-6 minutes

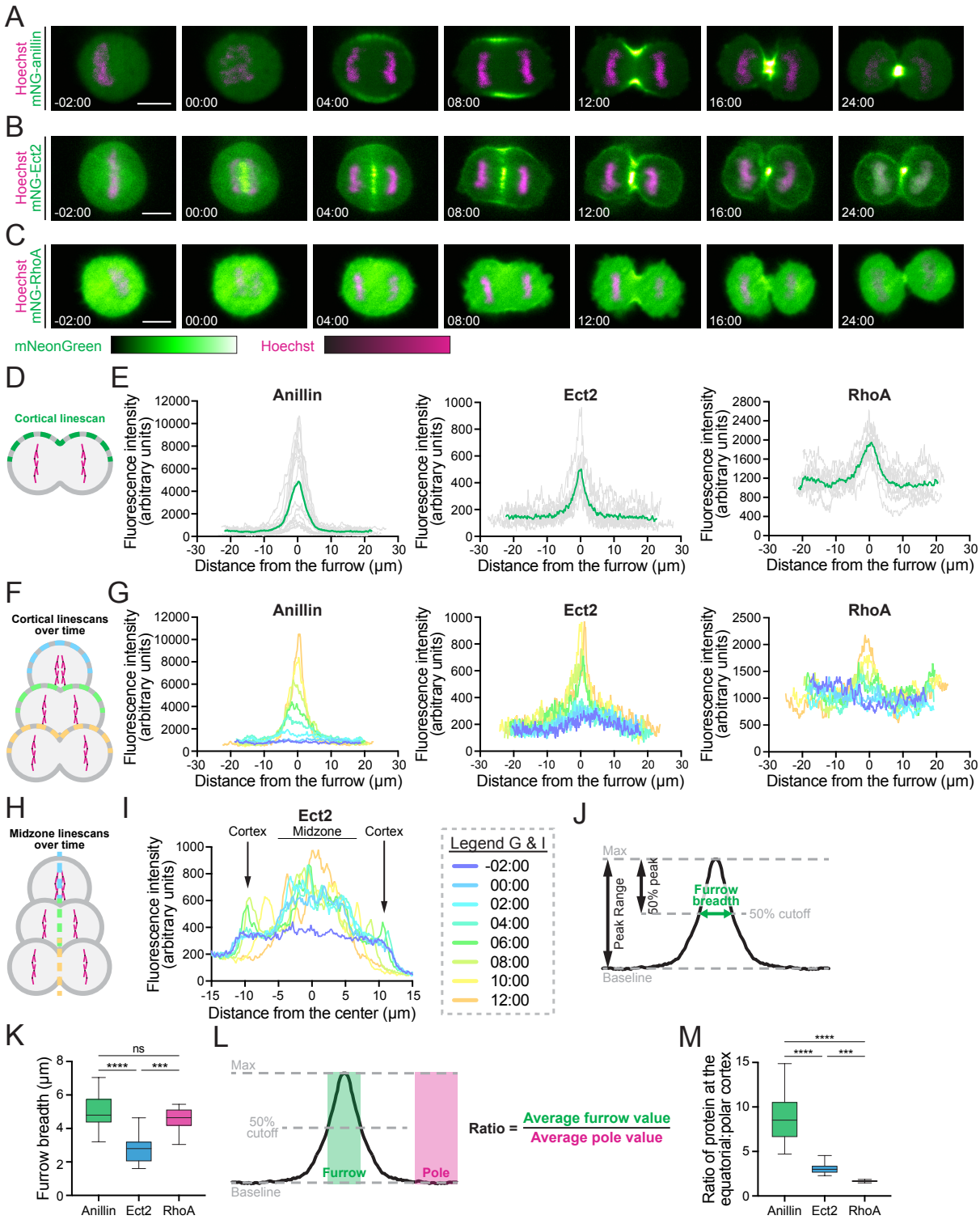
A
Hoechst
mNG-anillin
-02:00
00:00
04:00
08:00
12:00
16:00
24:00
B
Hoechst
mNG-Ect2
C
Hoechst
mNG-RhoA
mNeonGreen
Hoechst
D
Cortical linescan
E
Anillin
Ect2
RhoA
Fluorescence intensity (arbitrary units)
Distance from the furrow (µm)
F
Cortical linescans over time
G
H
Midzone linescans over time
I
Ect2
Cortex
Midzone
Cortex
Distance from the center (µm)
Legend G & I
-02:00
00:00
02:00
04:00
06:00
08:00
10:00
12:00
J
Max
Peak Range
50% peak
Furrow breadth
50% cutoff
Baseline
K
Furrow breadth (µm)
ns
****
***
Anillin
Ect2
RhoA
L
Max
50% cutoff
Furrow
Pole
Baseline
Ratio = Average furrow value / Average pole value
M
Ratio of protein at the equatorial:polar cortex
****
****
***
Anillin
Ect2
RhoA

Figure 14. Comparison of endogenous anillin, Ect2 and RhoA localization in HeLa cells during cytokinesis. A-C) Timelapse images show cells expressing endogenous mNeonGreen-anillin (A), mNeonGreen-Ect2 (B) and mNeonGreen-RhoA (C) during cytokinesis. mNeonGreen is shown in green and DNA (stained with Hoechst) in magenta. Times are shown relative to anaphase onset. The scale bar is 10 μm. Relative intensity for mNeonGreen and Hoechst is shown in the corresponding scales. D) Schematic of the linescans used to plot the fluorescence intensity along the cell cortex during the furrow initiation phase in E. E) Graphs show fluorescence intensity along the cortex of HeLa cells expressing endogenously tagged anillin (left, *n*=16), Ect2 (middle, *n*=10) and RhoA (right, *n*=10). Individual replicates are shown in gray, and the average is shown in green. F) Schematic of the linescans used to plot the fluorescence intensity along the cell cortex over time in G. G) Graphs show fluorescence intensity along the cortex of a single HeLa cell expressing endogenously tagged anillin (left), Ect2 (middle) and RhoA (right) at multiple timepoints starting at two minutes before anaphase onset, shown in different colors as indicated in the scale below. H) Schematic of the linescans used to plot the fluorescence intensity along the cell equator over time in I. I) A graph shows fluorescence intensity along the equator of a single HeLa cell expressing endogenously tagged Ect2 at multiple timepoints starting two minutes before anaphase onset, shown in the same colors as G. J) A schematic shows how the breadth at the equatorial cortex was calculated for K. K) Box plots show the breadth of anillin (*n*=16), Ect2 (*n*=10) and RhoA (*n*=10) in HeLa cells. L) A schematic shows how the ratio of protein at the equatorial cortex relative to the polar cortex was calculated for M. M) Box plots show the enrichment of anillin (*n*=16), Ect2 (*n*=10) and RhoA (*n*=10) at the equatorial cortex in HeLa cells. Box plots in K and M show the median line, quartile box edges and minimum and maximum value whiskers.

Statistical significance was determined by one-way ANOVA (ns, not significant; *$P \leq 0.05$; **$P \leq 0.01$; ***$P \leq 0.001$; ****$P \leq 0.0001$).

after anaphase onset **(Fig. 14G, left)**. Ect2 initially localized to the central spindle, then was also visible at the equatorial cortex and remained in both locations during ingression, followed by its localization to the midbody **(Fig. 14B)**. We used linescans to measure the intensity of mNeonGreen-Ect2 along the cortex at furrow initiation **(Fig. 14E, middle)**, and along the cortex and central spindle over time **(Fig. 14G, middle and H, I)**. The localization of Ect2 to the central spindle preceded the equatorial cortex, which was first visible ~6 minutes after anaphase onset and was narrower compared to anillin. Lastly, we found that RhoA was also enriched at the equatorial cortex at the onset of ingression **(Fig. 14C and E, right)**. Linescans revealed that this enrichment was visible ~6-8 minutes after anaphase onset **(Fig. 14C and G, right)**. This enrichment appeared weak compared to Ect2 and anillin, likely because of the large pool of cytoplasmic RhoA. We also showed that mNeonGreen-RhoA could be activated by the overexpression of the GEF region from Ect2, which caused an increase in cortical localization as expected (data not shown).

Next, we compared the localization of RhoA, Ect2 and anillin in HeLa cells to establish a comparison of these key cytokinesis regulators using the same cell type. We measured the breadth of localization of each endogenously tagged protein, along with the ratio of enrichment at the equatorial cortex relative to the polar cortex at furrow initiation **(Fig. 14J–M)**. To measure breadth, we used the linescans to determine the number of pixels above 50% of the normalized peak intensity **(Fig. 14J)**. Interestingly, the breadth of RhoA and anillin was similar, while the breadth of Ect2 was more restricted **(Fig. 14K)**. Similar results were obtained when measuring breadth in proportion to cortex length **(Fig. S9A)**. To measure the accumulation of proteins in the furrow, we calculated the ratio of the average pixel intensity in the furrow to the average pixel intensity at the polar cortex **(Fig. 14L)**. As expected from the levels of expression and breadth, anillin was most

enriched in the furrow, with 8.9 ± 2.9-fold (*n*=16) more protein in the furrow than at the poles compared to Ect2 (3.1 ± 0.7-fold, *n*=10) and RhoA (1.7 ± 0.1-fold, *n*=10; **Fig. 14M**).

3.5.2 Cytokinetic diversity across mammalian cell lines

Next, we characterized cytokinesis between different cell types by measuring mNeonGreen-tagged anillin localization in HEK293, HCT116, HepG2 and MDCK in addition to HeLa cells **(Figs 14A, 15A–D)**. First, we observed that mNeonGreen-anillin is localized at the cortex in HEK293, HCT116 and MDCK cells during metaphase, but not in HeLa and HepG2 cells, where it is strictly cytosolic (**Figs 14A, 15A–D**; -02:00 timepoint). This difference was most striking in HCT116 cells compared to HepG2 cells **(Fig. 15B,C)**. To quantify this difference, we measured the ratio of cortical to cytosolic mNeonGreen-anillin in HCT116 and HepG2 cells one timepoint before anaphase onset **(Fig. S9B,C)**. As expected, anillin was significantly enriched at the cortex during metaphase in HCT116 cells (1.6 ± 0.3-fold), but not in HepG2 cells (0.6 ± 0.1-fold; **Fig. S9C**). During cytokinesis, mNeonGreen-anillin was visible at the equatorial cortex ~4-8 minutes after anaphase onset in all cell lines, and remained in the furrow throughout ingression, after which it localized to the midbody **(Figs 14A, 15A-D)**. This was also shown by linescans, which were used to measure mNeonGreen-anillin along the cortex at furrow initiation **(Fig. 14E, left and 15E-H)**, and every two minutes starting two minutes before anaphase and until furrowing appeared to be completed **(Figs 14G, left and 15I-L)**. We also measured the duration of furrow ingression in these cell lines **(Fig. 15M,N)**. We found that the duration of ingression was similar in HeLa (20.4 ± 1.7 min, n=11), HEK293 (22.3 ± 5.2 min, n=7) and MDCK cells (17.7 ± 5.0 min, *n*=6; **Fig. 15N**). HepG2 cells took longer to ingress (31.0 ± 7.0 min, *n*=11), while HCT116 cells took the least amount of time to ingress (12.3 ± 1.4 min, *n*=8).

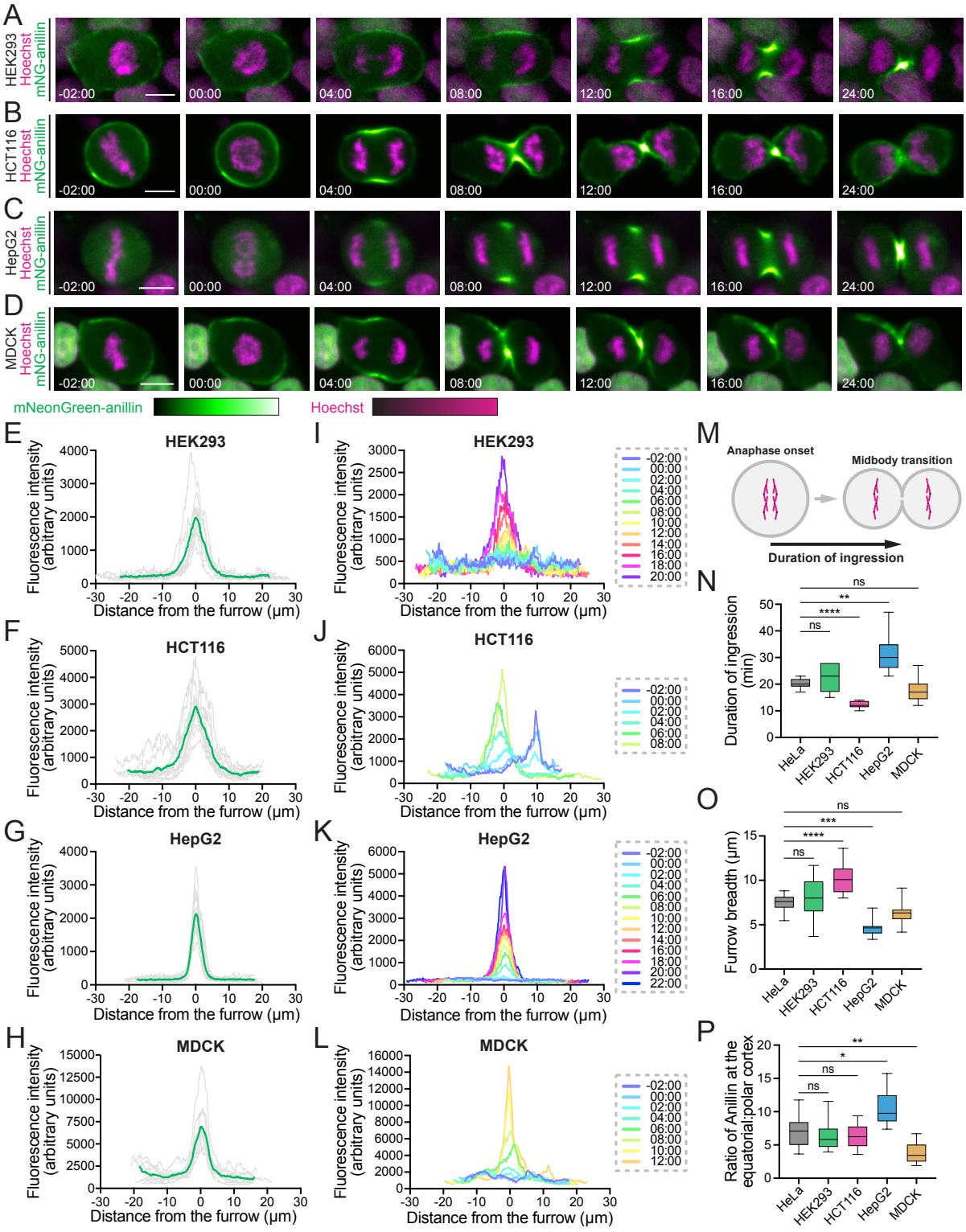
A
HEK293
Hoechst
mNG-anillin
B
HCT116
C
HepG2
D
MDCK
-02:00
00:00
04:00
08:00
12:00
16:00
24:00
mNeonGreen-anillin
Hoechst
E
HEK293
F
HCT116
G
HepG2
H
MDCK
I
J
K
L
Fluorescence intensity (arbitrary units)
Distance from the furrow (μm)
M
Anaphase onset
Midbody transition
Duration of ingression
N
Duration of ingression (min)
O
Furrow breadth (μm)
P
Ratio of Anillin at the equatorial:polar cortex
HeLa
HEK293
HCT116
HepG2
MDCK
ns
**
****
***
*

Figure 15. Endogenous tagging of anillin reveals cytokinetic differences between different cell lines. A-D) Timelapse images show endogenous mNeonGreen-anillin in HEK293 (A), HCT116 (B), HepG2 (C), and MDCK (D) cells during cytokinesis. mNeonGreen is shown in green and DNA (stained with Hoechst) is in magenta. Times are shown relative to anaphase onset. The scale bar is 10 μm. Relative intensity for mNeonGreen-anillin and Hoechst is shown in the corresponding scales. E-H) Graphs show fluorescence intensity of mNeonGreen-anillin along the cortex of HEK293 (E, n=9), HCT116 (F, n=11), HepG2 (G, n=13), and MDCK (H, n=10) cells at furrow initiation. I-L) Graphs show fluorescence intensity of mNeonGreen-anillin along the cortex of a single HEK293 (I), HCT116 (J), HepG2 (K), and MDCK (L) cell at multiple timepoints starting at two minutes before anaphase onset, shown in different colors as indicated by the scale. M) A schematic shows how ingression time was measured in N. N) A box plot shows the duration of ingression in HeLa (n=11), HEK293 (n=7), HCT116 (n=8), HepG2 (n=11) and MDCK (n=6) cells. O) A box plot shows the breadth of mNeonGreen-anillin localization at the equatorial cortex at furrow initiation in HeLa (n=16), HEK293 (n=9), HCT116 (n=11), HepG2 (n=13) and MDCK (n=10) cells. P) A box plot shows the ratio of anillin at the equatorial cortex compared to the polar cortex in HeLa (n=16), HEK293 (n=9), HCT116 (n=11), HepG2 (n=13), and MDCK (n=10) cells. Box plots in N-P show the median line, quartile box edges and minimum and maximum value whiskers. Statistical significance was determined by one-way ANOVA (ns, not significant; *P≤0.05; **P≤0.01; ***P≤0.001; ****P≤0.0001).

We found that the breadth and intensity of mNeonGreen-anillin in the furrow varied between the cell lines, with a broader peak in HCT116 cells and a narrower peak in HepG2 cells **(Figs 14E, left and 15E-H)**. We also observed differences in the localization of mNeonGreen-anillin over time in the different cell lines. In HCT116, HEK293 and MDCK cells, the cortical pools of mNeonGreen-anillin present in metaphase were removed or shifted to the equatorial cortex by 4-8 minutes after anaphase onset **(Fig. 15I,J,L)**. In most of the cell lines, we observed an increase in the enrichment and a gradual decrease in the breadth of mNeonGreen-anillin at the equatorial cortex over time **(Figs 14G, left and 15I-L)**. However, the breadth of mNeonGreen-anillin was consistently narrow in HepG2 cells **(Fig. 15K)**. Measurements of breadth and equatorial cortical enrichment supported our observations **(Fig. 15O, P)**. Since anillin localized to the furrow as a well-defined peak across all cell lines **(Figs 14E, left and 15E-H)**, we considered pixels within >75% of the intensity of the maximum peak value to capture more of the furrow and compare anillin breadth and intensity measurements between the cell lines. The mNeonGreen-anillin furrow was the broadest in HCT116 cells, narrowest in HepG2 cells, and was similar between HeLa, HEK293 and MDCK cells **(Fig. 15O)**. Interestingly, the breadth of mNeonGreen-anillin appeared to be inversely proportional to the duration of ingression, with HCT116 cells ingressing the fastest and HepG2 ingressing the slowest **(Fig. 15N-O)**. Surprisingly, mNeonGreen-anillin was similarly enriched in the equatorial cortex of HeLa, HEK293 and HCT116 cells (7.1 ± 2.4, 6.3 ± 2.3 and 6.3 ± 1.9-fold enrichment, respectively), while HepG2 cells had a significantly stronger enrichment (10.4 ± 2.6-fold), and MDCK cells had a weaker enrichment (3.8 ± 1.5-fold; **Fig. 15P**). Similar results were obtained when measuring breadth as a percentage of cortex length, showing that these differences are independent of cell size **(Fig. S9D)**. These data suggest that the breadth of anillin localization rather than accumulated levels influence the rate of ingression. This

is further supported by our observation that within our homozygously tagged mNeonGreen-anillin HeLa cell line, two populations of cells were present with higher and lower mNeonGreen-anillin levels **(Fig. 14E, left)**. HeLa cells are cancerous with high aneuploidy, and this difference in anillin levels is likely due to heterogeneity amongst the cells causing changes in gene expression. We plotted these two populations of anillin-tagged HeLa cells side-by-side and compared the same parameters **(Fig. S10)**. We found no difference in the duration of ingression and in the breadth of the furrow between the two populations **(Fig. S10B-F)**. However, the total levels accumulated in the peak were higher in one population compared to the other **(Fig. S10G-H)**.

We also noted some variability in the symmetry of how MDCK cells ingress, which we did not observe in the other cell lines. MDCK cells acquire apicobasal polarity when grown to confluency in culture, although we did not grow our cells to confluency prior to imaging (Balcarova-Stander et al., 1984). By measuring closure using end-on-views of the ring, we found that MDCK cells ingressed asymmetrically, although this was more pronounced in some cells compared to others **(Fig. 16A,B)**. We plotted ring closure starting from the last timepoint in metaphase until the end of ring closure, and indeed, our data show that ingression occurred more asymmetrically in some cells compared to others **(Fig. 16C,D)**. We also calculated the distance between the center of the cell in the first measured timepoint and the center of the ring in the final timepoint before closure. We observed that there was a range for the degree of asymmetry; ring closure occurred asymmetrically or highly asymmetrically in most cells (symmetry value between 0.2 and 0.6, n=13; and value >0.6, n=7), and the ring closed symmetrically in only one out of 21 cells (symmetry value<0.2) **(Fig. 16E,F)**. Since MDCK cells were not confluent during imaging, these variabilities could reflect intrinsic regulation of cytokinesis and/or extrinsic influences from neighboring cells before polarization (Herszterg et al., 2014).

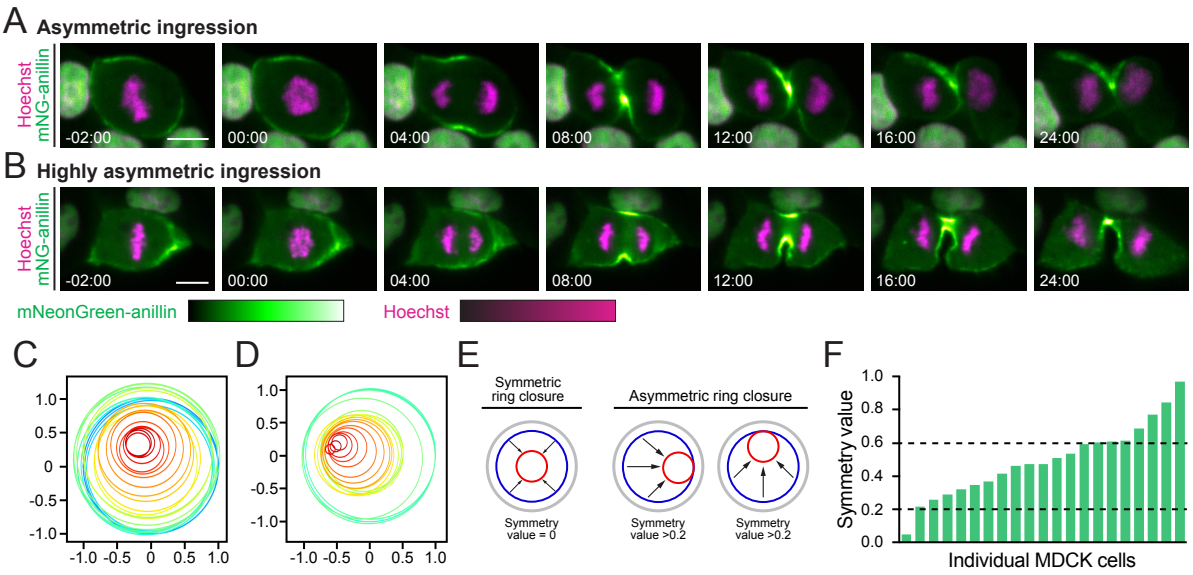
A
Asymmetric ingression
Hoechst
mNG-anillin
-02:00
00:00
04:00
08:00
12:00
16:00
24:00
B
Highly asymmetric ingression
Hoechst
mNG-anillin
-02:00
00:00
04:00
08:00
12:00
16:00
24:00
mNeonGreen-anillin
Hoechst
C
D
1.0
0.5
0
-0.5
-1.0
-1.0 -0.5 0 0.5 1.0
E
Symmetric ring closure
Asymmetric ring closure
Symmetry value = 0
Symmetry value >0.2
Symmetry value >0.2
F
Symmetry value
1.0
0.8
0.6
0.4
0.2
0.0
Individual MDCK cells

Figure 16. Ingression occurs with variable symmetry in MDCK cells. Timelapse images show endogenous mNeonGreen-anillin localization in different MDCK cells during cytokinesis where ingression appeared to be asymmetric (A), or highly asymmetric (B). mNeonGreen is shown in green and DNA (stained by Hoechst) is in magenta. Relative intensity for mNeonGreen-anillin and Hoechst is shown in the corresponding scales. Times are from anaphase onset. The scale bars are 10 μm. C) A graph depicts ring closure in a cell that undergoes asymmetric ingression. D) A graph shows ring closure in a cell that undergoes highly asymmetric ingression. E) A schematic shows the relative end position of the ring compared to the first timepoint to determine if it closes symmetrically or asymmetrically. F) A graph shows the symmetry values for ring closure in 21 cells. Values <0.2 were defined as symmetric (n=1), between 0.2 and 0.6 as asymmetric (n=13), and >0.6 as highly asymmetric (n=7).

3.6 DISCUSSION

Here, we use new tools to explore cytokinesis diversity among mammalian cell types, building on our current understanding of cytokinesis and opening new avenues of research to identify the mechanisms contributing to this diversity. By endogenously tagging RhoA, Ect2 and anillin with a fluorescent protein, we were able to perform robust comparative studies of the localization of these key cytokinesis regulators for the first time in HeLa cells. To date, most cytokinesis proteins have been studied using overexpressed transgenes in HeLa cells, which may influence the interpretation of their function, while probes to visualize RhoA (reviewed in Koh et al., 2021) or its GEF Ect2 have been notoriously difficult to use (Tatsumoto et al., 1999, Yuce et al., 2005, Chalamalasetty et al., 2006, Petronczki et al., 2007, Su et al., 2011, Kotynkova et al., 2016, Schneid et al., 2021). Comparing the spatiotemporal localization of endogenous RhoA, Ect2 and anillin revealed that their enrichment at the equatorial cortex occurs at similar times and aligns with the timing of ring assembly and ingression. However, while anillin and RhoA broadly localize along the equatorial cortex, Ect2 localizes to a much narrower region, suggesting differences in how the cortical localization of Ect2 is controlled compared to anillin and RhoA. Importantly, these core cytokinesis regulators have not been studied extensively in other mammalian cell types, where mechanisms regulating cytokinesis likely vary. Indeed, we revealed distinct differences in cytokinesis in different cell types by comparing the spatiotemporal localization of endogenously tagged anillin in mammalian cells including several where cytokinesis has not been well-studied (HEK293, MDCK) or has never been studied before (HepG2, HCT116). We observed differences in both the timing and breadth of anillin's cortical localization. Anillin is cortically localized before anaphase onset in HEK293, HCT116, and MDCK cells, but not in HeLa and HepG2 cells. Previous studies reported that anillin is cortically localized during metaphase in BHK-21 and *Drosophila*

S2 cells, but this was not investigated further (Field and Alberts, 1995, Oegema et al., 2000, El Amine et al., 2013). It would be interesting to determine why anillin is cortical in some metaphase cells but not others, and whether this reflects differences in the machineries required for anillin's cortical recruitment among cell types. Based on recent studies showing that importin-binding regulates anillin's cortical localization, one hypothesis is that ploidy or chromatin position create distinct cortical pools of importins (Beaudet et al., 2017, Beaudet et al., 2020, Ozugergin et al., 2022). Importins bind to nuclear localization signals (NLS) in proteins, which are competed off by Ran-GTP (Xu and Massague, 2004, Clarke and Zhang, 2008). Since the RanGEF (RCC1) is tethered to chromatin, Ran-GTP is typically enriched around chromatin and creates an inverse gradient of importins that are free to bind to NLS-containing proteins in the cytosol and cortex (Xu and Massague, 2004, Clarke and Zhang, 2008). Our working hypothesis is that cells with higher ploidy (e.g. HeLa, HepG2) have less Ran-free importins at the cortex which only meets threshold in the equatorial plane during anaphase, while cells with lower ploidy (e.g. HCT116) would have uniformly enriched importins earlier in mitosis, and cells where chromatin is asymmetrically positioned would form asymmetric gradients (e.g. MDCK) (Beaudet et al., 2017, Beaudet et al., 2020, Husser et al., 2021, Ozugergin and Piekny, 2021).

Interestingly, we also observed that the ring closes asymmetrically in MDCK cells. Although these cells establish apicobasal polarity in culture when grown to confluency (Balcarova-Stander et al., 1984), we performed our studies when they were well below confluency, suggesting that intrinsic mechanisms influence ring ingression. Few studies have explored the symmetry of ring closure and its mechanism is not well-understood. The ring may close at least partially asymmetrically in many cell types, and the extent of asymmetry could reflect differences in cell size and fate, as well as adhesion to neighboring cells (Bourdages et al., 2014). The ring system

may lend itself to asymmetric closure – as the ring pulls in part of the membrane, this induces curvature and flows which further promote actomyosin filament alignment, which gains energy-efficiency to ingress faster in that location (Dorn et al., 2016). The biological significance of asymmetric closure is not clear, although one hypothesis is that it may help prevent aneuploidy. For example, in the two-cell *C. elegans* embryo, ring closure occurs asymmetrically in the larger AB daughter cell fated to be somatic tissue, but not the smaller P_1 fated to become germline (Ozugergin et al., 2022). However, inducing size changes or perturbing the Ran pathway changes the symmetry of ring closure in P_1 cells, suggesting that multiple factors control this process (Ozugergin et al., 2022).

We also observed that the breadth of cortical anillin is different among the cell types. Anillin is distributed more broadly along the equatorial cortex in HCT116 cells, while it is narrower in HepG2 cells compared to the other cell types. Interestingly, this distribution correlates with the duration of ingression, where the ring ingresses more quickly in cells with broader cortical anillin and vice versa. We were also surprised to see that the duration of ring ingression did not correlate with the total levels of anillin in the ring. Anillin can form distinct complexes that could have different roles during cytokinesis. A recent hypothesis paper suggested that an anillin-septin complex controls the removal of membrane microdomains away from the ring to relieve tension during ring closure (Carim et al., 2020). Therefore, a broader distribution of anillin outside the ring in HCT116 cells could promote more efficient ring closure by providing a greater surface area for this "outflow" and removal of microdomains (Carim et al., 2020).

In addition to producing novel tools and knowledge of cytokinesis, our work provides some methods that could be used for analyzing cytokinesis in more uniform ways. Especially for studies in mammalian cells, there is inconsistency in how the parameters of cytokinesis are measured and

reported, and/or a general lack of analysis depending on the cell type and context. Previous studies in *C. elegans* provide a strong foundation for tools that could be universally applied to other cell types, and include macros used in this study which are publicly available. Additionally, the reagents used to generate our endogenously tagged cell lines are available from Addgene for other researchers. Our hope is that by combining the use of endogenous tags with quantitative measurements, we can capture the diversity in cytokinesis across a broader range of cell types, which can then be used to study differences in the mechanisms controlling different aspects of cytokinesis.

Overall, this study provides quantitative measurements of cytokinesis proteins to reveal cytokinetic diversity across commonly used human and mammalian cell lines. This work also emphasizes the benefits of generating and using endogenously tagged cells for cytokinesis studies, as well as the need for comparative studies between different cell types and organisms. Since most prior studies of human cytokinesis have been performed using HeLa cells, this work lays the foundation for future studies to investigate how the mechanisms regulating cytokinesis vary with cell type. It will be crucial to extend cytokinesis studies beyond HeLa cells, by studying more diverse cell lines, human or mouse stem cells and their differentiated counterparts, or different cell types *in vivo* (Hyman and Simons, 2011, Drubin and Hyman, 2017, Davies et al., 2018, Chaigne et al., 2021, Husser et al., 2021, McNeely and Dwyer, 2021, Ozugergin et al., 2022, Paim and FitzHarris, 2022).

CHAPTER FOUR

Conclusion and Future Directions

4.1 OVERVIEW

In many cell types, cytokinesis typically occurs as the last step in mitosis to separate a cell into two daughter cells. The successful completion of this event is orchestrated through several pathways working together. As discussed in Chapter 1, these pathways function at different times and places in the cell, resulting in a robust system capable of tolerating some errors. These pathways collectively ensure the assembly and ingression of a well-positioned actomyosin contractile ring to prevent aneuploidy or cell fate changes, which would be detrimental to the cell or organism.

The field is at an exciting turning point where we are beginning to change the way we approach studies of cytokinesis. Until recently, most of our knowledge of cytokinesis was derived using a small number of model systems, making it challenging to interpret variability in the core machinery and regulatory mechanisms. It is presumed that mechanisms controlling cytokinesis will vary with cell type, shape, and size, among other parameters, but few researchers have studied these parameters in a truly comparative way. Several recent publications revealing cytokinetic diversity among distinct cell types in the same model system are paving the way for similar studies in other model systems and cell types, which is explored in Chapters 2 and 3 of this thesis.

4.2 CYTOKINESIS KINETICS DIFFER BETWEEN AB AND P_1 CELLS IN *C. ELEGANS* EMBRYOS

Chapter 2 compares cytokinesis kinetics in the differently fated AB and P_1 cells of the two-cell *C. elegans* embryo, and reveals parameters contributing to cytokinetic diversity *in vivo*. Finding diversity at the earliest possible stage of development – at the two-cell stage – emphasizes how a 'one size fits all' approach to cytokinesis is not appropriate. The core machinery shows differences in localization and patterning and is controlled by different parameters in the two cell types. Part of this difference appears to be a result of the asymmetric division of the P_0 cell; actin and myosin are enriched in the anterior cortex of the P_0 cell such that the AB daughter inherits higher levels of actin and myosin compared to the P_1 daughter (Munro et al., 2004). We found that this difference correlates with different ring closure kinetics in AB and P_1 cells, and equalizing their fate through PAR depletion **(Fig. 8)** equalizes their cytokinesis kinetics and actomyosin levels. Interestingly, a recent study of cytokinesis in mouse embryos also suggests that cytokinesis kinetics are influenced by polarity (Paim and FitzHarris, 2022). In this system, apical polarity arises at the 8-cell stage, such that the outer cells of the 16-cell stage embryo are polarized with an apical domain that is enriched in F-actin and PAR proteins, while the inner cells lack polarity (Chazaud and Yamanaka, 2016, Paim and FitzHarris, 2022). Paim and FitzHarris (2022) show that the apical domain intrinsically inhibits the localization of anillin and myosin from that side of the contractile ring in the outer cells. Although the mechanism of inhibition is not clear, this results in asymmetric furrowing where ingression is slower on the apical side. Collectively, the mouse and *C. elegans* studies both support a role for polarity in regulating cytokinesis kinetics, but further work is required to reveal the mechanisms.

Our results also demonstrate that myosin is more organized in the furrow of AB cells compared to P_1 cells, suggesting that different regulatory mechanisms control contractility in the two cell types. Indeed, increasing the size and ploidy of P_1 cells by generating tetraploid embryos caused them to have myosin levels and ring assembly kinetics similar to diploid AB cells **(Fig. 9)**. Presumably, the higher levels of myosin and/or having more organized myosin contributes to an increase in cortical flows in diploid AB cells and tetraploid P_1 cells that were not seen in diploid P_1 cells. It is not clear whether these flows contribute to ring assembly kinetics or ring closure symmetry. Since flows unidirectionally bring myosin and actin to the equatorial furrow, it is possible that the increased cortical flows in AB cells contribute to the asymmetric ring closure we observed in these cells **(Fig. 6)**. However, ring closure still occurred asymmetrically in AB cells where myosin organization and contractility were hindered by the loss of active RhoA, and it is not clear if there are other fate determinants or positioning cues that contribute to ring closure **(Fig. 7)**. Interestingly, reducing active RhoA also revealed distinct thresholds in myosin requirements in AB and P_1 cells, where higher levels are required in AB cells, and P_1 cells operate close to their threshold **(Figs 7 and 12)**. Overall, our findings demonstrate that cell fate, size and/or ploidy are factors that contribute to the unique cytokinesis kinetics observed in the two-cell *C. elegans* embryo.

The differences in cytokinesis between AB and P_1 cells may have physiological relevance in the context of the developing embryo. First, it is interesting to note that the kinetics and pathway requirements in AB cells appear to be more similar to somatic cells from other organisms, while the germline-fated P_1 cells are distinct. Also, despite the AB and P_1 cells having very different levels of actomyosin and kinetics, they both end cytokinesis at the same time, which could be essential for correctly establishing cell fate in subsequent divisions. It is not clear why these cell

types would have adopted such different kinetics, which are essentially the opposite: while ring assembly occurs rapidly in AB compared to P_1 cells, constriction is slower. The differences in actomyosin levels at least partially support these differences – in P_1 it takes longer to assemble the lower actomyosin levels into functional rings, but then they constrict faster due to lower competing cortical forces. The longer assembly phase occurs during anaphase, which would give chromosomes more time to segregate, while the rapid constriction in telophase could prevent lagging chromosomes from 'moving' back into the other daughter. This would ensure that the genome stays intact and is correctly partitioned for future offspring. Interestingly, males are generated by aneuploidy caused by loss of one of the X chromosomes, which occurs with higher temperatures. Temperature could impact rates of microtubule dynamics and kinetochore attachments, but it would be interesting to determine if temperature also affects actomyosin activity. On the other hand, ring assembly occurs more rapidly in the larger AB cells and has a more linear rate of constriction. The AB cells may not require a 'safeguard' to prevent aneuploidy due to their larger size. However, it is interesting to note that we observed that chromosome congression and segregation appears to be less 'clean' in AB cells, and so this cell type may require the ring to constrict more slowly to give the chromosomes more time to segregate by the time the ring reaches the middle of the cell. With the pace of cytokinesis being more constant in the AB cell, P_1-specific mechanisms may be more likely to dictate the relative timing and geometry between these cells to influence developmental success. It remains to be seen how P_1 cells avoid cytokinesis failure due to operating at threshold levels of actin and myosin, and it will be exciting to determine if some mechanisms of cytokinesis regulation are more robust in the P_1 cell to make up for the lower levels of ring proteins, or if there are P_1-specific mechanisms that operate only in this lineage.

4.3 THE ROLE OF THE CHROMATIN PATHWAY DIFFERS IN AB AND P_1 CELLS IN *C. ELEGANS* EMBRYOS

Chapter 2 of this thesis also reveals differences in how cytokinesis is regulated between AB and P_1 cells. After uncovering differences in cytokinesis between these two cell types, we also revealed how a novel pathway could control these differences. Our lab recently discovered that active Ran acts as a chromatin-sensing cue that controls where the ring assembles for cytokinesis. This regulation occurs through the recruitment of anillin to the equatorial cortex by importin-binding in early anaphase (Beaudet et al., 2017, Beaudet et al., 2020). This work was performed in cultured HeLa cells, and we wanted to know if this pathway could also control cytokinesis of cell types in other model systems. Taking advantage of the early *C. elegans* embryo where we can perform studies in comparable cell types, we investigated whether Ran controls cytokinesis kinetics in AB and P_1 cells, and if the pathway functions similarly in both cell types. Indeed, we found that Ran signaling controls cytokinesis kinetics in AB and P_1 cells, but unexpectedly, found that this pathway functions differently in each cell type. While the pathway functions in AB cells similar to HeLa cells, with importin-β regulating the cortical localization of ANI-1, the pathway functions through multiple importins and targets other than ANI-1 in P_1 cells (Ozugergin et al., 2022). These exciting findings suggest that there are alternate targets of the chromatin pathway, which vary with cell type. Further, these findings also show that cells fated to be somatic may rely on conserved mechanisms versus cells fated to be germline.

We also found that the Ran pathway plays a stronger role in controlling cytokinesis kinetics in P_1 cells compared to AB cells. Specifically, reducing Ran-GTP levels through depletion of RAN-3 (RCC1) caused more extreme differences in ring assembly in P_1 compared to AB cells. Since the P_1 cell divides asymmetrically, one hypothesis is that the Ran pathway could play an

important role in asymmetric division. During asymmetric division, the spindle is shifted closer to one pole, and having a signal associated with chromatin could ensure that the ring is positioned correctly between the segregating chromosomes to avoid aneuploidy. Another possibility is that since the P_1 cell is smaller than the AB cell, the chromatin could more strongly influence importins at the cortex compared to the larger AB cell. The current model is that the levels of importins that can bind to and control the localization of NLS-containing anillin or other contractile proteins is controlled by the distance of chromatin relative to the cortex (Silverman-Gavrila et al., 2008, Kiyomitsu and Cheeseman, 2013, Beaudet et al., 2017). This model is supported by our finding that tetraploid P_1 cells which have the same size as diploid AB cells also have similar cytokinesis kinetics. In addition, a previous study showed that different cancer cell types with increased ploidy had higher levels of RCC1 and steeper Ran-GTP gradients compared to cells with lower ploidy (Hasegawa et al., 2013). Thus, our various Ran pathway perturbations and use of tetraploid embryos support the model where size and/or ploidy play an important role in determining how the Ran pathway modulates cytokinesis in a particular cell type.

Based on the findings presented in this thesis, we elaborate on our initial model **(Fig. 5)** to consider differences in how Ran signaling works in different cell types **(Fig. 17)**. We propose that the chromatin sensing pathway may function as a sliding scale to differently control cortical properties depending on the cell type and context. In cells with higher ploidy, or when chromatin is closer to the cortex (e.g., in a small cell), the high levels of Ran-GTP would create a reciprocal gradient of importins which are enriched to sufficient thresholds only in the plane between the segregating chromosomes **(Fig. 17A)**. However, in other cells, the importins at the cortex would be more uniformly enriched because chromatin and associated Ran-GTP is too far away. In these cells, cortical properties would be more uniform, and chromatin would not play a dominant role in

A

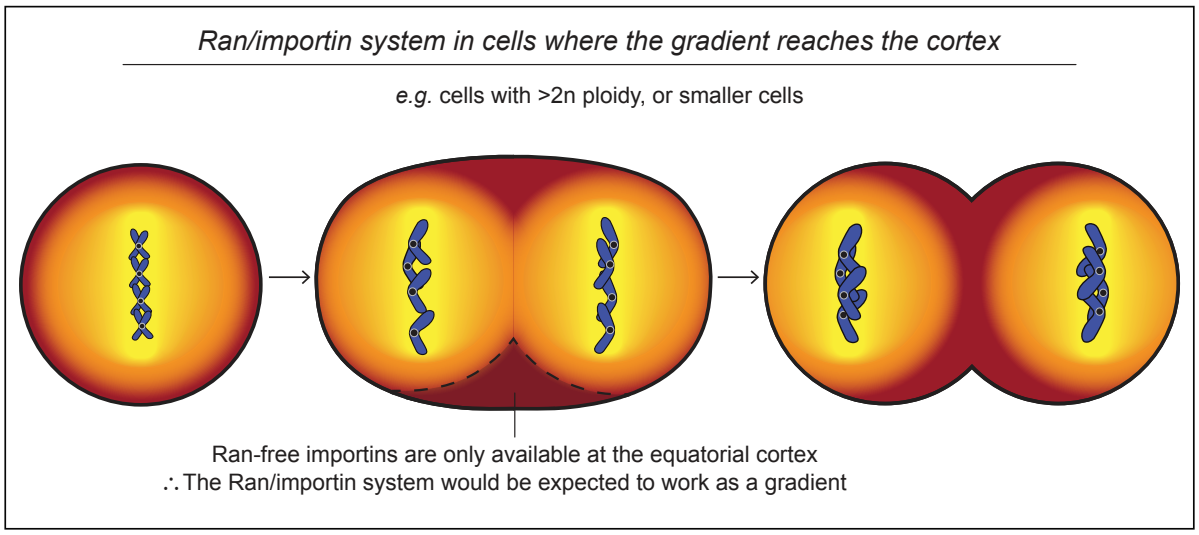
Ran/importin system in cells where the gradient reaches the cortex
e.g. cells with >2n ploidy, or smaller cells
Ran-free importins are only available at the equatorial cortex
∴ The Ran/importin system would be expected to work as a gradient

B

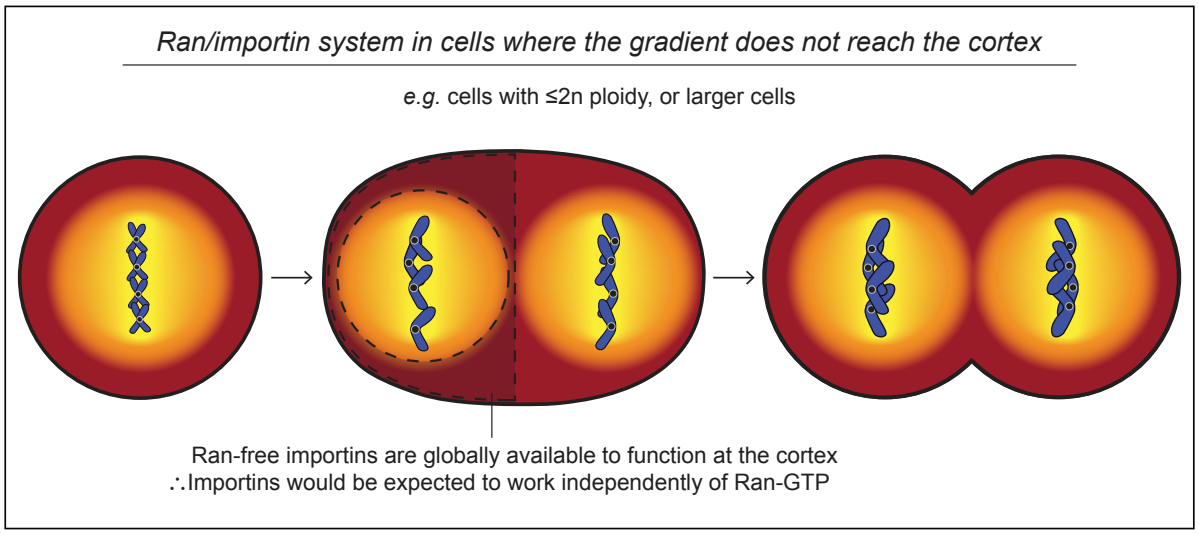
Ran/importin system in cells where the gradient does not reach the cortex
e.g. cells with ≤2n ploidy, or larger cells
Ran-free importins are globally available to function at the cortex
∴ Importins would be expected to work independently of Ran-GTP

Figure 17. Different models for Ran gradient function during cytokinesis. A) Cartoons show how in small cells or in cells with high ploidy, Ran-GTP levels would be strong, and importins may not reach sufficient levels at the cortex to recruit anillin during metaphase. During anaphase, as the sister chromatids segregate to opposite poles of the cell, a sufficient threshold of importins could be reached in the equatorial plane. B) Cartoons show how in large cells or in cells with low ploidy, the Ran-GTP gradient would not reach the cortex and importins would be able to recruit anillin uniformly to the cortex in metaphase and anaphase. In these cells, Ran-independent mechanisms would be required to spatially enrich anillin in the equatorial plane.

determining the division plane, requiring these cells to rely more heavily on other mechanisms **(Fig. 17B)**. Additional studies are needed to support this model by determining how the Ran pathway functions in more diverse cell types, and where ploidy, size and/or chromatin position can be altered.

4.4. CYTOKINESIS DIVERSITY AMONG MAMMALIAN CELLS

We were driven by the desire to study cytokinesis in more diverse mammalian cell types in Chapter 3. These studies used novel tools to reveal differences in the localization of key cytokinesis proteins and cytokinesis kinetics among different cell types. These studies were the first to show how endogenous cytokinesis proteins localize in human cells – all prior studies used overexpression or fixation. In HeLa cells, we observed that while their timing of cortical enrichment was similar, anillin and RhoA were more broadly localized to the equatorial cortex compared to Ect2, which was much narrower **(Fig. 14)**. Anillin has been previously shown to strongly colocalize with RhoA using immunofluorescence in fixed cells, and showing that endogenous proteins have similar breadth and timing of enrichment supports these previous studies (Piekny and Glotzer, 2008). Our methods do not distinguish active versus inactive pools of RhoA, however, we can assume that membrane-localized RhoA reflects the active pool. The relatively small pool of active RhoA likely reveals that low thresholds are needed to support ring assembly. The narrow pool of cortical Ect2 could be crucial to restrict RhoA activation to a small region. Comparative analysis of endogenous anillin localization between HeLa, HEK293, HCT116, HepG2 and MDCK cells also revealed interesting differences in how cytokinesis occurs among these cell types. While anillin localizes to a similar extent in HeLa, HEK293 and MDCK cells, it is significantly broader in HCT116 and narrower in HepG2 cells **(Figs 14 and 15)**. Interestingly,

this also correlated with the duration of ingression, while the amount of accumulated anillin in the furrow did not. The duration of ingression was similar for HeLa, HEK293 and MDCK cells, but shorter in HCT116 and longer in HepG2 cells **(Fig. 15)**. During ring assembly, having broader pools of anillin could generate flow to favor alignment of the actomyosin filaments, while during ingression, these broad pools of anillin could relieve tension generated by the ring by directing outflow to remove membrane microdomains, which could cause more efficient ingression (Carim et al., 2020).

The mechanisms controlling anillin localization is expected to vary among the cell types, and our results highlight the need to study different pathways controlling cytokinesis in more depth in different cell types. The cortical localization of anillin in metaphase, and broader equatorial localization of anillin in anaphase HCT116 cells could reflect their ploidy. These cells have lower net ploidy compared to other cell types, and thus may have uniform pools of cortical importins that recruit anillin. However, HeLa and HepG2 cells have higher ploidy, and importins may only reach a threshold capable of recruiting anillin in the equatorial plane during anaphase. Further differences in breadth in HeLa and HepG2 likely reflect differences in other spindle-dependent and -independent pathways that control ring assembly. HepG2 cells are a type of liver cancer cell, and hepatocytes were previously shown to gain ploidy via differences in the core machinery regulating cytokinesis which make them prone to failure (Margall-Ducos et al., 2007, De Santis Puzzonia et al., 2016, Lazaro-Dieguez and Musch, 2017). In addition, HEK293 cells also have higher ploidy, but have anillin localization that more closely resembles HCT116 cells, suggesting differences in mechanisms regulating anillin in this cell type. Although HEK293 cells have lost aspects of their polarity during transformation (e.g., E-cadherin is not localized properly), they could retain some mechanisms that differently influence cytokinesis compared to other cell types.

We speculate that the Ran-importin system could function in all cell types, but cells could rely differently on this mechanism based on factors such as cell shape, size, ploidy and fate. Cells could become particularly sensitized to this pathway with smaller size or higher ploidy where the gradient can influence the levels of importins at the cortex. However, to obtain more support for this model there is a need to visualize the gradient of importins in these cell types to compare how the gradient changes with size or ploidy, and to determine how different perturbations affect this gradient and ring assembly. The Ran-importin system could be critical for cytokinesis in cancer cells that gain ploidy and have over-expressed components of the pathway, and it will be exciting to see if any of these components could be druggable targets in the fight against cancer. Our discovery of the role of the Ran-importin mechanism regulating cytokinesis and differences in its requirement among cell types makes it clear that we need to step away from a "standardized cytokinesis" model to instead consider "precision cytokinesis". As we improve our understanding of how different healthy and diseased cell types divide, this information will guide the development of targeted therapies for cancer.

We also observed asymmetric ring closure in MDCK cells, even though they were not grown to confluency and would not be expected to be polarized. Our findings suggest that there is a distinct intrinsic mechanism controlling asymmetric ingression in this cell type, which should be studied further to identify this mechanism. Asymmetric ingression has been observed in other cell types and in other contexts, and the mechanisms and reason for this type of ingression remains poorly understood. Since asymmetric ingression occurs toward the apical cortex of epithelial cells, which have polarity and form junctions with neighbors, this process may protect cells from aneuploidy, retain memory of polarity and/or ensure maintenance of interactions with neighbours. Although reports of studies in *Drosophila* epithelial cells suggest that asymmetric ingression is

controlled by extrinsic mechanisms (Herszterg et al., 2014), our study as well as Paim and FitzHarris (2022) show that intrinsic mechanisms also control asymmetric ingression, and the mechanisms likely vary with cell type and tissue context. For example, mechanical inputs from cell-cell contacts with neighbouring cells or when cells are adhered to a substrate could have different effects on cytokinesis (Dix et al., 2018, Chaigne et al., 2021). These data highlight the need for additional studies to identify the mechanisms controlling cytokinesis differences between different cell types. While *in vivo* studies are also essential, the amenability of using cultured cells for studies at the subcellular level will continue to play an important role in revealing the mechanisms controlling cytokinesis. For example, future studies are required to determine how factors such as cell fate, size, or developmental stage influence ring closure kinetics.

4.5 FUTURE DIRECTIONS

After a century of research, we have gained extensive knowledge of cytokinesis. However, it is clear that there is more diversity in how the core machinery is expressed and regulated than was initially appreciated. This diversity is likely due to differences in intrinsic and extrinsic mechanisms controlling ring assembly and ingression, which is necessitated by the diversity in the cell types themselves. The mitotic spindle is crucial to successful division and could be considered the core mode of regulation, while the spindle-independent pathways could be thought of as the 'supporting cast' to tweak its cytokinetic modulation from what would be dictated by the spindle alone. In addition, how a cell combines different pathways of regulation may be much more relevant to cytokinetic success than whether a pathway is spindle-dependent or -independent. Timing also plays a factor, and with the different pathways of regulation kicking in at different

times during cytokinesis, cells pass the baton of regulation in both the temporal and spatial sense. Thus, the field stands to gain a much deeper understanding of cytokinetic regulation if we adopt a wider outlook on the interconnectivity of pathways.

The chromatin sensing pathway is one of the spindle-independent pathways that was elucidated in this thesis. We found that the pathway works differently in cells with different fates in the early *C. elegans* embryo, highlighting the need to do more studies to understand the full extent of how the Ran/importin system modulates cytokinesis. If we look to other forms of division, or consider the different characteristics of cells, it is likely that the chromatin sensing pathway does not function in a singular way. Importins show great flexibility in their roles. Based on the NLS-containing protein in question, they have an interesting ability to positively or negatively regulate protein function upon binding, alone or as an importin heterodimer (Ozugergin and Piekny, 2021). Thus, it is unlikely that the Ran/importin system functions in a 'one size fits all' manner across different cell types.

The findings reported in this thesis support that anillin is a target of the Ran pathway in AB cells but not in P_1 cells, where it functions to regulate the contractile ring through other targets. Importins may similarly regulate other key cytokinesis proteins which contain an NLS, such as Ect2, Cyk4 and MKLP1 (Deavours and Walker, 1999, Tatsumoto et al., 1999, Kawashima et al., 2009). It is an exciting possibility that the same mechanism of importin regulation could have opposite cytokinetic outcomes. While the Ran/importin system may boost cytokinesis kinetics through potential target proteins such as Ect2, it may decrease kinetics through other targets. For example, during cytokinesis in the *C. elegans* zygote, GCK III (discussed in section 1.2) slows down the speed of ring constriction (Bell et al., 2020), and mammalian GCK III proteins have an NLS (Pombo et al., 2007). An interesting speculation is that in the *C. elegans* zygote, and perhaps

other cell types, importins may be a part of setting up the necessary contractility for cytokinesis while also being a part of the negative feedback that prevents hypercontractility. Although anillin is currently the only known target of the Ran pathway during cytokinesis, future studies will likely identify other targets of the pathway and reveal whether the cortical functions of importins are only towards enhancing contractility.

Having built the foundation of knowledge necessary to understand how cytokinesis takes place, we now have enough understanding to break away from the 'one size fits all' approach to understanding metazoan cell cytokinesis. Here, we have reviewed and demonstrated some of the differences in how cytokinesis takes place and is regulated in various metazoan cell types, but this is presumably just the tip of the iceberg. Thus, it is likely not appropriate to presume that findings in one cell type would hold across different model organisms or other cell types, at least without considering the starting differences. The diversity described here also highlights that not all model organisms or cell types are appropriate to study certain facets of cytokinesis, and this should be considered before starting or interpreting studies.

Novel research avenues exploring organismal differences and/or factors such as cell size, fate or ploidy will be crucial to expanding our understanding of how cytokinesis can be 'personalized' to a cell type. In addition to a better comprehension of the pathways themselves, mechanistic studies of spindle-independent pathways may provide insight into when/where/how the many pathways collaborate with each other. It is not a given that any one of the pathways discussed in this thesis will behave the same way in one cell type versus another, so it is imperative that future studies address this knowledge gap by utilising a wider range of cell types – both cultured and *in vivo* – for the field to gain an appreciation of the cytokinetic diversity across life forms.

REFERENCES

ADRIAANS, I. E., BASANT, A., PONSIOEN, B., GLOTZER, M. & LENS, S. M. A. 2019. PLK1 plays dual roles in centralspindlin regulation during cytokinesis. *J Cell Biol,* 218**,** 1250-1264.

ALBERTSON, R., CAO, J., HSIEH, T. S. & SULLIVAN, W. 2008. Vesicles and actin are targeted to the cleavage furrow via furrow microtubules and the central spindle. *J Cell Biol,* 181**,** 777-90.

AMINI, R., GOUPIL, E., LABELLA, S., ZETKA, M., MADDOX, A. S., LABBE, J. C. & CHARTIER, N. T. 2014. C. elegans Anillin proteins regulate intercellular bridge stability and germline syncytial organization. *J Cell Biol,* 206**,** 129-43.

ASKJAER, P., GALY, V., HANNAK, E. & MATTAJ, I. W. 2002. Ran GTPase cycle and importins alpha and beta are essential for spindle formation and nuclear envelope assembly in living Caenorhabditis elegans embryos. *Mol Biol Cell,* 13**,** 4355-70.

BAI, X., MELESSE, M., SORENSEN TURPIN, C. G., SLOAN, D. E., CHEN, C. Y., WANG, W. C., LEE, P. Y., SIMMONS, J. R., NEBENFUEHR, B., MITCHELL, D., KLEBANOW, L. R., MATTSON, N., BETZIG, E., CHEN, B. C., CHEERAMBATHUR, D. & BEMBENEK, J. N. 2020. Aurora B functions at the apical surface after specialized cytokinesis during morphogenesis in C. elegans. *Development,* 147.

BALCAROVA-STANDER, J., PFEIFFER, S. E., FULLER, S. D. & SIMONS, K. 1984. Development of cell surface polarity in the epithelial Madin-Darby canine kidney (MDCK) cell line. *EMBO J,* 3**,** 2687-94.

BASANT, A. & GLOTZER, M. 2017. A GAP that Divides. *F1000Res,* 6**,** 1788.

BASANT, A. & GLOTZER, M. 2018. Spatiotemporal Regulation of RhoA during Cytokinesis. *Curr Biol,* 28**,** R570-R580.

BASANT, A., LEKOMTSEV, S., TSE, Y. C., ZHANG, D., LONGHINI, K. M., PETRONCZKI, M. & GLOTZER, M. 2015. Aurora B kinase promotes cytokinesis by inducing centralspindlin oligomers that associate with the plasma membrane. *Dev Cell,* 33**,** 204-15.

BASTOS, R. N., PENATE, X., BATES, M., HAMMOND, D. & BARR, F. A. 2012. CYK4 inhibits Rac1-dependent PAK1 and ARHGEF7 effector pathways during cytokinesis. *J Cell Biol,* 198**,** 865-80.

BAUER, J., POUPART, V., GOUPIL, E., NGUYEN, K. C. Q., HALL, D. H. & LABBE, J. C. 2021. The initial expansion of the C. elegans syncytial germ line is coupled to incomplete primordial germ cell cytokinesis. *Development,* 148.

BEAUDET, D., AKHSHI, T., PHILLIPP, J., LAW, C. & PIEKNY, A. 2017. Active Ran regulates anillin function during cytokinesis. *Mol Biol Cell,* 28**,** 3517-3531.

BEAUDET, D., PHAM, N., SKAIK, N. & PIEKNY, A. 2020. Importin binding mediates the intramolecular regulation of anillin during cytokinesis. *Mol Biol Cell,* 31**,** 1124-1139.

BELL, K. R., WERNER, M. E., DOSHI, A., CORTES, D. B., SATTLER, A., VUONG-BRENDER, T., LABOUESSE, M. & MADDOX, A. S. 2020. Novel cytokinetic ring components drive negative feedback in cortical contractility. *Mol Biol Cell,* 31**,** 1623-1636.

BEMENT, W. M., BENINK, H. A. & VON DASSOW, G. 2005. A microtubule-dependent zone of active RhoA during cleavage plane specification. *J Cell Biol,* 170**,** 91-101.

BOURDAGES, K. G., LACROIX, B., DORN, J. F., DESCOVICH, C. P. & MADDOX, A. S. 2014. Quantitative analysis of cytokinesis in situ during C. elegans postembryonic development. *PLoS One,* 9**,** e110689.

BRENNER, S. 1974. The genetics of Caenorhabditis elegans. *Genetics,* 77**,** 71-94.

BRINGMANN, H. & HYMAN, A. A. 2005. A cytokinesis furrow is positioned by two consecutive signals. *Nature,* 436**,** 731-4.

BROWNLEE, C. & HEALD, R. 2019. Importin alpha Partitioning to the Plasma Membrane Regulates Intracellular Scaling. *Cell,* 176**,** 805-815 e8.

BUCKLEY, C. E. & ST JOHNSTON, D. 2022. Apical-basal polarity and the control of epithelial form and function. *Nat Rev Mol Cell Biol*.

BUDNAR, S., HUSAIN, K. B., GOMEZ, G. A., NAGHIBOSADAT, M., VARMA, A., VERMA, S., HAMILTON, N. A., MORRIS, R. G. & YAP, A. S. 2019. Anillin Promotes Cell Contractility by Cyclic Resetting of RhoA Residence Kinetics. *Dev Cell,* 49**,** 894-906 e12.

BURDYNIUK, M., CALLEGARI, A., MORI, M., NEDELEC, F. & LENART, P. 2018. F-Actin nucleated on chromosomes coordinates their capture by microtubules in oocyte meiosis. *J Cell Biol,* 217**,** 2661-2674.

BURKARD, M. E., MACIEJOWSKI, J., RODRIGUEZ-BRAVO, V., REPKA, M., LOWERY, D. M., CLAUSER, K. R., ZHANG, C., SHOKAT, K. M., CARR, S. A., YAFFE, M. B. & JALLEPALLI, P. V. 2009. Plk1 self-organization and priming phosphorylation of HsCYK-4 at the spindle midzone regulate the onset of division in human cells. *PLoS Biol,* 7**,** e1000111.

CABERNARD, C., PREHODA, K. E. & DOE, C. Q. 2010. A spindle-independent cleavage furrow positioning pathway. *Nature,* 467**,** 91-4.

CANMAN, J. C., CAMERON, L. A., MADDOX, P. S., STRAIGHT, A., TIRNAUER, J. S., MITCHISON, T. J., FANG, G., KAPOOR, T. M. & SALMON, E. D. 2003. Determining the position of the cell division plane. *Nature,* 424**,** 1074-8.

CANMAN, J. C., HOFFMAN, D. B. & SALMON, E. D. 2000. The role of pre- and post-anaphase microtubules in the cytokinesis phase of the cell cycle. *Curr Biol,* 10**,** 611-4.

CANMAN, J. C., LEWELLYN, L., LABAND, K., SMERDON, S. J., DESAI, A., BOWERMAN, B. & OEGEMA, K. 2008. Inhibition of Rac by the GAP activity of centralspindlin is essential for cytokinesis. *Science,* 322**,** 1543-6.

CARIM, S. C., KECHAD, A. & HICKSON, G. R. X. 2020. Animal Cell Cytokinesis: The Rho-Dependent Actomyosin-Anilloseptin Contractile Ring as a Membrane Microdomain Gathering, Compressing, and Sorting Machine. *Front Cell Dev Biol,* 8**,** 575226.

CARRENO, S., KOURANTI, I., GLUSMAN, E. S., FULLER, M. T., ECHARD, A. & PAYRE, F. 2008. Moesin and its activating kinase Slik are required for cortical stability and microtubule organization in mitotic cells. *J Cell Biol,* 180**,** 739-46.

CARVALHO, A., DESAI, A. & OEGEMA, K. 2009. Structural memory in the contractile ring makes the duration of cytokinesis independent of cell size. *Cell,* 137**,** 926-37.

CHAIGNE, A., SMITH, M. B., LOPEZ CAVESTANY, R., HANNEZO, E., CHALUT, K. J. & PALUCH, E. K. 2021. Three-dimensional geometry controls division symmetry in stem cell colonies. *J Cell Sci,* 134.

CHALAMALASETTY, R. B., HUMMER, S., NIGG, E. A. & SILLJE, H. H. 2006. Influence of human Ect2 depletion and overexpression on cleavage furrow formation and abscission. *J Cell Sci,* 119**,** 3008-19.

CHAN, C. K. & JANS, D. A. 1999. Synergy of importin alpha recognition and DNA binding by the yeast transcriptional activator GAL4. *FEBS Lett,* 462**,** 221-4.

CHAN, F. Y., SILVA, A. M., SARAMAGO, J., PEREIRA-SOUSA, J., BRIGHTON, H. E., PEREIRA, M., OEGEMA, K., GASSMANN, R. & CARVALHO, A. X. 2019. The ARP2/3 complex prevents excessive formin activity during cytokinesis. *Mol Biol Cell,* 30**,** 96-107.

CHAZAUD, C. & YAMANAKA, Y. 2016. Lineage specification in the mouse preimplantation embryo. *Development,* 143**,** 1063-74.

CHEN, A., AKHSHI, T. K., LAVOIE, B. D. & WILDE, A. 2015. Importin beta2 Mediates the Spatio-temporal Regulation of Anillin through a Noncanonical Nuclear Localization Signal. *J Biol Chem,* 290**,** 13500-9.

CHEN, A., ARORA, P. D., MCCULLOCH, C. A. & WILDE, A. 2017. Cytokinesis requires localized beta-actin filament production by an actin isoform specific nucleator. *Nat Commun,* 8**,** 1530.

CHEN, A., ULLOA SEVERINO, L., PANAGIOTOU, T. C., MORAES, T. F., YUEN, D. A., LAVOIE, B. D. & WILDE, A. 2021. Inhibition of polar actin assembly by astral microtubules is required for cytokinesis. *Nat Commun,* 12**,** 2409.

CLARKE, E. K., RIVERA GOMEZ, K. A., MUSTACHI, Z., MURPH, M. C. & SCHVARZSTEIN, M. 2018. Manipulation of Ploidy in Caenorhabditis elegans. *J Vis Exp***,** 1-11.

CLARKE, P. R. & ZHANG, C. 2008. Spatial and temporal coordination of mitosis by Ran GTPase. *Nat Rev Mol Cell Biol,* 9**,** 464-77.

COMPTON, D. A. 2000. Spindle assembly in animal cells. *Annu Rev Biochem,* 69**,** 95-114.

CONG, L., RAN, F. A., COX, D., LIN, S., BARRETTO, R., HABIB, N., HSU, P. D., WU, X., JIANG, W., MARRAFFINI, L. A. & ZHANG, F. 2013. Multiplex genome engineering using CRISPR/Cas systems. *Science,* 339**,** 819-23.

COWAN, C. R. & HYMAN, A. A. 2007. Acto-myosin reorganization and PAR polarity in C. elegans. *Development,* 134**,** 1035-43.

D'AVINO, P. P., GIANSANTI, M. G. & PETRONCZKI, M. 2015. Cytokinesis in animal cells. *Cold Spring Harb Perspect Biol,* 7**,** a015834.

DAVIES, T., KIM, H. X., ROMANO SPICA, N., LESEA-PRINGLE, B. J., DUMONT, J., SHIRASU-HIZA, M. & CANMAN, J. C. 2018. Cell-intrinsic and -extrinsic mechanisms promote cell-type-specific cytokinetic diversity. *Elife,* 7.

DE MAN, S. M., ZWANENBURG, G., VAN DER WAL, T., HINK, M. A. & VAN AMERONGEN, R. 2021. Quantitative live-cell imaging and computational modeling shed new light on endogenous WNT/CTNNB1 signaling dynamics. *Elife,* 10.

DE SANTIS PUZZONIA, M., COZZOLINO, A. M., GRASSI, G., BISCEGLIA, F., STRIPPOLI, R., GUARGUAGLINI, G., CITARELLA, F., SACCHETTI, B., TRIPODI, M., MARCHETTI, A. & AMICONE, L. 2016. TGFbeta Induces Binucleation/Polyploidization in Hepatocytes through a Src-Dependent Cytokinesis Failure. *PLoS One,* 11**,** e0167158.

DEAVOURS, B. E. & WALKER, R. A. 1999. Nuclear localization of C-terminal domains of the kinesin-like protein MKLP-1. *Biochem Biophys Res Commun,* 260**,** 605-8.

DECHANT, R. & GLOTZER, M. 2003. Centrosome Separation and Central Spindle Assembly Act in Redundant Pathways that Regulate Microtubule Density and Trigger Cleavage Furrow Formation. *Dev Cell,* 4**,** 333-344.

DEHAPIOT, B., CARRIERE, V., CARROLL, J. & HALET, G. 2013. Polarized Cdc42 activation promotes polar body protrusion and asymmetric division in mouse oocytes. *Dev Biol,* 377**,** 202-12.

DELATTRE, M. & GOEHRING, N. W. 2021. The first steps in the life of a worm: Themes and variations in asymmetric division in C. elegans and other nematodes. *Curr Top Dev Biol,* 144**,** 269-308.

DENG, M., SURANENI, P., SCHULTZ, R. M. & LI, R. 2007. The Ran GTPase mediates chromatin signaling to control cortical polarity during polar body extrusion in mouse oocytes. *Dev Cell,* 12**,** 301-8.

DIX, C. L., MATTHEWS, H. K., UROZ, M., MCLAREN, S., WOLF, L., HEATLEY, N., WIN, Z., ALMADA, P., HENRIQUES, R., BOUTROS, M., TREPAT, X. & BAUM, B. 2018. The Role of Mitotic Cell-Substrate Adhesion Re-modeling in Animal Cell Division. *Dev Cell,* 45**,** 132-145 e3.

DORN, J. F., ZHANG, L., PHI, T. T., LACROIX, B., MADDOX, P. S., LIU, J. & MADDOX, A. S. 2016. A theoretical model of cytokinesis implicates feedback between membrane curvature and cytoskeletal organization in asymmetric cytokinetic furrowing. *Mol Biol Cell,* 27**,** 1286-99.

DOUGLAS, M. E., DAVIES, T., JOSEPH, N. & MISHIMA, M. 2010. Aurora B and 14-3-3 coordinately regulate clustering of centralspindlin during cytokinesis. *Curr Biol,* 20**,** 927-33.

DOYON, J. B., ZEITLER, B., CHENG, J., CHENG, A. T., CHERONE, J. M., SANTIAGO, Y., LEE, A. H., VO, T. D., DOYON, Y., MILLER, J. C., PASCHON, D. E., ZHANG, L., REBAR, E. J., GREGORY, P. D., URNOV, F. D. & DRUBIN, D. G. 2011. Rapid and efficient clathrin-mediated endocytosis revealed in genome-edited mammalian cells. *Nat Cell Biol,* 13**,** 331-7.

DRUBIN, D. G. & HYMAN, A. A. 2017. Stem cells: the new "model organism". *Mol Biol Cell,* 28**,** 1409-1411.

DUGINA, V., ZWAENEPOEL, I., GABBIANI, G., CLEMENT, S. & CHAPONNIER, C. 2009. Beta and gamma-cytoplasmic actins display distinct distribution and functional diversity. *J Cell Sci,* 122**,** 2980-8.

EL AMINE, N., KECHAD, A., JANANJI, S. & HICKSON, G. R. 2013. Opposing actions of septins and Sticky on Anillin promote the transition from contractile to midbody ring. *J Cell Biol,* 203**,** 487-504.

EVANS, T. C. 2006. Transformation and microinjection. *WormBook*.

FIELD, C. M. & ALBERTS, B. M. 1995. Anillin, a contractile ring protein that cycles from the nucleus to the cell cortex. *J Cell Biol,* 131**,** 165-78.

FOTOPOULOS, N., WERNIKE, D., CHEN, Y., MAKIL, N., MARTE, A. & PIEKNY, A. 2013. Caenorhabditis elegans anillin (ani-1) regulates neuroblast cytokinesis and epidermal morphogenesis during embryonic development. *Dev Biol,* 383**,** 61-74.

FOUNOUNOU, N., LOYER, N. & LE BORGNE, R. 2013. Septins regulate the contractility of the actomyosin ring to enable adherens junction remodeling during cytokinesis of epithelial cells. *Dev Cell,* 24**,** 242-55.

FRENETTE, P., HAINES, E., LOLOYAN, M., KINAL, M., PAKARIAN, P. & PIEKNY, A. 2012. An anillin-Ect2 complex stabilizes central spindle microtubules at the cortex during cytokinesis. *PLoS One,* 7**,** e34888.

GAN, W. J. & MOTEGI, F. 2020. Mechanochemical Control of Symmetry Breaking in the Caenorhabditis elegans Zygote. *Front Cell Dev Biol,* 8**,** 619869.

GELES, K. G. & ADAM, S. A. 2001. Germline and developmental roles of the nuclear transport factor importin alpha3 in C. elegans. *Development,* 128**,** 1817-30.

GIESECKE, A. & STEWART, M. 2010. Novel binding of the mitotic regulator TPX2 (target protein for Xenopus kinesin-like protein 2) to importin-alpha. *J Biol Chem,* 285**,** 17628-35.

GLOTZER, M. 2005. The molecular requirements for cytokinesis. *Science,* 307**,** 1735-9.

GLOTZER, M. 2009. The 3Ms of central spindle assembly: microtubules, motors and MAPs. *Nat Rev Mol Cell Biol,* 10**,** 9-20.

GLOTZER, M. 2017. Cytokinesis in Metazoa and Fungi. *Cold Spring Harb Perspect Biol,* 9**,** 9:a02234-9:a02234.

GOMEZ-CAVAZOS, J. S., LEE, K. Y., LARA-GONZALEZ, P., LI, Y., DESAI, A., SHIAU, A. K. & OEGEMA, K. 2020. A Non-canonical BRCT-Phosphopeptide Recognition Mechanism Underlies RhoA Activation in Cytokinesis. *Curr Biol,* 30**,** 3101-3115 e11.

GOUPIL, E., AMINI, R., HALL, D. H. & LABBE, J. C. 2017. Actomyosin contractility regulators stabilize the cytoplasmic bridge between the two primordial germ cells during Caenorhabditis elegans embryogenesis. *Mol Biol Cell,* 28**,** 3789-3800.

GREEN, R. A., PALUCH, E. & OEGEMA, K. 2012. Cytokinesis in animal cells. *Annu Rev Cell Dev Biol,* 28**,** 29-58.

GRILL, S. W., GONCZY, P., STELZER, E. H. K. & HYMAN, A. A. 2001. Polarity controls forces governing asymmetric spindle positioning in the Caenorhabditis elegans embryo. *Nature,* 409**,** 630-3.

GRUSS, O. J., CARAZO-SALAS, R. E., SCHATZ, C. A., GUARGUAGLINI, G., KAST, J., WILM, M., LE BOT, N., VERNOS, I., KARSENTI, E. & MATTAJ, I. W. 2001. Ran induces spindle assembly by reversing the inhibitory effect of importin alpha on TPX2 activity. *Cell,* 104**,** 83-93.

GUILLOT, C. & LECUIT, T. 2013. Adhesion disengagement uncouples intrinsic and extrinsic forces to drive cytokinesis in epithelial tissues. *Dev Cell,* 24**,** 227-41.

GUO, S. & KEMPHUES, K. J. 1996. A non-muscle myosin required for embryonic polarity in Caenorhabditis elegans.

GUSE, A., MISHIMA, M. & GLOTZER, M. 2005. Phosphorylation of ZEN-4/MKLP1 by aurora B regulates completion of cytokinesis. *Curr Biol,* 15**,** 778-86.

HASEGAWA, K., RYU, S. J. & KALAB, P. 2013. Chromosomal gain promotes formation of a steep RanGTP gradient that drives mitosis in aneuploid cells. *J Cell Biol,* 200**,** 151-61.

HERSZTERG, S., LEIBFRIED, A., BOSVELD, F., MARTIN, C. & BELLAICHE, Y. 2013. Interplay between the dividing cell and its neighbors regulates adherens junction formation during cytokinesis in epithelial tissue. *Dev Cell,* 24**,** 256-70.

HERSZTERG, S., PINHEIRO, D. & BELLAICHE, Y. 2014. A multicellular view of cytokinesis in epithelial tissue. *Trends Cell Biol,* 24**,** 285-93.

HICKSON, G. R. & O'FARRELL, P. H. 2008. Rho-dependent control of anillin behavior during cytokinesis. *J Cell Biol,* 180**,** 285-94.

HOEGE, C. & HYMAN, A. A. 2013. Principles of PAR polarity in Caenorhabditis elegans embryos. *Nat Rev Mol Cell Biol,* 14**,** 315-22.

HOLOPAINEN, S., HYTONEN, M. K., SYRJA, P., ARUMILLI, M., JARVINEN, A. K., RAJAMAKI, M. & LOHI, H. 2017. ANLN truncation causes a familial fatal acute respiratory distress syndrome in Dalmatian dogs. *PLoS Genet,* 13**,** e1006625.

HUSSER, M. C., SKAIK, N., MARTIN, V. J. J. & PIEKNY, A. 2021. CRISPR-Cas tools to study gene function in cytokinesis. *J Cell Sci,* 134.

HYMAN, A. H. & SIMONS, K. 2011. The new cell biology: Beyond HeLa cells. *Nature,* 480**,** 34.

ILLUKKUMBURA, R., BLAND, T. & GOEHRING, N. W. 2020. Patterning and polarization of cells by intracellular flows. *Curr Opin Cell Biol,* 62**,** 123-134.

IYER, S., MIR, A., VEGA-BADILLO, J., ROSCOE, B. P., IBRAHEIM, R., ZHU, L. J., LEE, J., LIU, P., LUK, K., MINTZER, E., SOARES DE BRITO, J., ZAMORE, P. D., SONTHEIMER, E. J. & WOLFE, S. A. 2019. Efficient Homology-directed Repair with Circular ssDNA Donors. *bioRxiv*.

JORDAN, S. N., DAVIES, T., ZHURAVLEV, Y., DUMONT, J., SHIRASU-HIZA, M. & CANMAN, J. C. 2016. Cortical PAR polarity proteins promote robust cytokinesis during asymmetric cell division. *J Cell Biol,* 212**,** 39-49.

KALAB, P. & HEALD, R. 2008. The RanGTP gradient - a GPS for the mitotic spindle. *J Cell Sci,* 121**,** 1577-86.

KALAB, P., PRALLE, A., ISACOFF, E. Y., HEALD, R. & WEIS, K. 2006. Analysis of a RanGTP-regulated gradient in mitotic somatic cells. *Nature,* 440**,** 697-701.

KALAB, P., WEIS, K. & HEALD, R. 2002. Visualization of a Ran-GTP gradient in interphase and mitotic Xenopus egg extracts. *Science,* 295**,** 2452-6.

KALETTA, T. & HENGARTNER, M. O. 2006. Finding function in novel targets: C. elegans as a model organism. *Nat Rev Drug Discov,* 5**,** 387-98.

KAMATH, R. S., MARTINEZ-CAMPOS, M., ZIPPERLEN, P., FRASER, A. G. & AHRINGER, J. 2001. Effectiveness of specific RNA-mediated interference through ingested double-stranded RNA in Caenorhabditis elegans. *Genome biology,* 2**,** 1-10.

KAMIJO, K., OHARA, N., ABE, M., UCHIMURA, T., HOSOYA, H., LEE, J. S. & MIKI, T. 2006. Dissecting the role of Rho-mediated signaling in contractile ring formation. *Mol Biol Cell,* 17**,** 43-55.

KAWASHIMA, T., BAO, Y. C., MINOSHIMA, Y., NOMURA, Y., HATORI, T., HORI, T., FUKAGAWA, T., FUKADA, T., TAKAHASHI, N., NOSAKA, T., INOUE, M., SATO, T., KUKIMOTO-NIINO, M., SHIROUZU, M., YOKOYAMA, S. & KITAMURA, T. 2009. A Rac GTPase-activating protein, MgcRacGAP, is a nuclear localizing signal-containing nuclear chaperone in the activation of STAT transcription factors. *Mol Cell Biol,* 29**,** 1796-813.

KEMPHUES, K. J., PRIESS, J. R., MORTON, D. G. & CHENG, N. S. 1988. Identification of genes required for cytoplasmic localization in early C. elegans embryos. *Cell,* 52**,** 311-20.

KHALIULLIN, R. N., GREEN, R. A., SHI, L. Z., GOMEZ-CAVAZOS, J. S., BERNS, M. W., DESAI, A. & OEGEMA, K. 2018. A positive-feedback-based mechanism for constriction rate acceleration during cytokinesis in Caenorhabditis elegans. *Elife,* 7.

KIM, J. E., BILLADEAU, D. D. & CHEN, J. 2005. The tandem BRCT domains of Ect2 are required for both negative and positive regulation of Ect2 in cytokinesis. *J Biol Chem,* 280**,** 5733-9.

KIMURA, K., TSUJI, T., TAKADA, Y., MIKI, T. & NARUMIYA, S. 2000. Accumulation of GTP-bound RhoA during cytokinesis and a critical role of ECT2 in this accumulation. *J Biol Chem,* 275**,** 17233-6.

KIYOMITSU, T. & CHEESEMAN, I. M. 2013. Cortical dynein and asymmetric membrane elongation coordinately position the spindle in anaphase. *Cell,* 154**,** 391-402.

KOH, S. P., PHAM, N. P. & PIEKNY, A. 2021. Seeing is believing: tools to study the role of Rho GTPases during cytokinesis. *Small GTPases***,** 1-14.

KOTADIA, S., MONTEMBAULT, E., SULLIVAN, W. & ROYOU, A. 2012. Cell elongation is an adaptive response for clearing long chromatid arms from the cleavage plane. *J Cell Biol,* 199**,** 745-53.

KOTYNKOVA, K., SU, K. C., WEST, S. C. & PETRONCZKI, M. 2016. Plasma Membrane Association but Not Midzone Recruitment of RhoGEF ECT2 Is Essential for Cytokinesis. *Cell Rep,* 17**,** 2672-2686.

KUNDA, P., PELLING, A. E., LIU, T. & BAUM, B. 2008. Moesin controls cortical rigidity, cell rounding, and spindle morphogenesis during mitosis. *Curr Biol,* 18**,** 91-101.

KUNDA, P., RODRIGUES, N. T., MOEENDARBARY, E., LIU, T., IVETIC, A., CHARRAS, G. & BAUM, B. 2012. PP1-mediated moesin dephosphorylation couples polar relaxation to mitotic exit. *Curr Biol,* 22**,** 231-6.

LABBE, J. C., MCCARTHY, E. K. & GOLDSTEIN, B. 2004. The forces that position a mitotic spindle asymmetrically are tethered until after the time of spindle assembly. *J Cell Biol,* 167**,** 245-56.

LACROIX, B. & MADDOX, A. S. 2012. Cytokinesis, ploidy and aneuploidy. *J Pathol,* 226**,** 338-51.

LANG, C. F. & MUNRO, E. 2017. The PAR proteins: from molecular circuits to dynamic self-stabilizing cell polarity. *Development,* 144**,** 3405-3416.

LANGE, A., MILLS, R. E., LANGE, C. J., STEWART, M., DEVINE, S. E. & CORBETT, A. H. 2007. Classical nuclear localization signals: definition, function, and interaction with importin alpha. *J Biol Chem,* 282**,** 5101-5.

LAZARO-DIEGUEZ, F. & MUSCH, A. 2017. Cell-cell adhesion accounts for the different orientation of columnar and hepatocytic cell divisions. *J Cell Biol,* 216**,** 3847-3859.

LECUIT, T. 2004. Junctions and vesicular trafficking during Drosophila cellularization. *J Cell Sci,* 117**,** 3427-33.

LEKOMTSEV, S., SU, K. C., PYE, V. E., BLIGHT, K., SUNDARAMOORTHY, S., TAKAKI, T., COLLINSON, L. M., CHEREPANOV, P., DIVECHA, N. & PETRONCZKI, M. 2012. Centralspindlin links the mitotic spindle to the plasma membrane during cytokinesis. *Nature,* 492**,** 276-9.

LEWELLYN, L., DUMONT, J., DESAI, A. & OEGEMA, K. 2010. Analyzing the effects of delaying aster separation on furrow formation during cytokinesis in the Caenorhabditis elegans embryo. *Mol Biol Cell,* 21**,** 50-62.

LORIA, A., LONGHINI, K. M. & GLOTZER, M. 2012. The RhoGAP domain of CYK-4 has an essential role in RhoA activation. *Curr Biol,* 22**,** 213-9.

MADDOX, A. S., HABERMANN, B., DESAI, A. & OEGEMA, K. 2005. Distinct roles for two C. elegans anillins in the gonad and early embryo. *Development,* 132**,** 2837-48.

MADDOX, A. S., LEWELLYN, L., DESAI, A. & OEGEMA, K. 2007. Anillin and the septins promote asymmetric ingression of the cytokinetic furrow. *Dev Cell,* 12**,** 827-35.

MAHEN, R., KOCH, B., WACHSMUTH, M., POLITI, A. Z., PEREZ-GONZALEZ, A., MERGENTHALER, J., CAI, Y. & ELLENBERG, J. 2014. Comparative assessment of fluorescent transgene methods for quantitative imaging in human cells. *Mol Biol Cell,* 25**,** 3610-8.

MALI, P., YANG, L., ESVELT, K. M., AACH, J., GUELL, M., DICARLO, J. E., NORVILLE, J. E. & CHURCH, G. M. 2013. RNA-guided human genome engineering via Cas9. *Science,* 339**,** 823-6.

MANGAL, S., SACHER, J., KIM, T., OSORIO, D. S., MOTEGI, F., CARVALHO, A. X., OEGEMA, K. & ZANIN, E. 2018. TPXL-1 activates Aurora A to clear contractile ring components from the polar cortex during cytokinesis. *J Cell Biol,* 217**,** 837-848.

MANN, B. J. & WADSWORTH, P. 2018. Distribution of Eg5 and TPX2 in mitosis: Insight from CRISPR tagged cells. *Cytoskeleton (Hoboken),* 75**,** 508-521.

MARGALL-DUCOS, G., CELTON-MORIZUR, S., COUTON, D., BREGERIE, O. & DESDOUETS, C. 2007. Liver tetraploidization is controlled by a new process of incomplete cytokinesis. *J Cell Sci,* 120**,** 3633-9.

MAUPIN, P., PHILLIPS, C. L., ADELSTEIN, R. S. & POLLARD, T. D. 1994. Differential localization of myosin-II isozymes in human cultured cells and blood cells. *J Cell Sci,* 107 (Pt 11)**,** 3077-90.

MAZUMDAR, A. & MAZUMDAR, M. 2002. How one becomes many: blastoderm cellularization in Drosophila melanogaster. *Bioessays,* 24**,** 1012-22.

MCNEELY, K. C. & DWYER, N. D. 2021. Cytokinetic Abscission Regulation in Neural Stem Cells and Tissue Development. *Current Stem Cell Reports,* 7**,** 161-173.

MIKI, T., SMITH, C. L., LONG, J. E., EVA, A. & FLEMING, T. P. 1993. Oncogene ect2 is related to regulators of small GTP-binding proteins. *Nature,* 362**,** 462-5.

MISHIMA, M., KAITNA, S. & GLOTZER, M. 2002. Central spindle assembly and cytokinesis require a kinesin-like protein/RhoGAP complex with microtubule bundling activity. *Dev Cell,* 2**,** 41-54.

MISHIMA, M., PAVICIC, V., GRUNEBERG, U., NIGG, E. A. & GLOTZER, M. 2004. Cell cycle regulation of central spindle assembly. *Nature,* 430**,** 908-13.

MONTEMBAULT, E., CLAVERIE, M. C., BOUIT, L., LANDMANN, C., JENKINS, J., TSANKOVA, A., CABERNARD, C. & ROYOU, A. 2017. Myosin efflux promotes cell elongation to coordinate chromosome segregation with cell cleavage. *Nat Commun,* 8**,** 326.

MORAIS-DE-SA, E. & SUNKEL, C. 2013. Adherens junctions determine the apical position of the midbody during follicular epithelial cell division. *EMBO Rep,* 14**,** 696-703.

MUNRO, E., NANCE, J. & PRIESS, J. R. 2004. Cortical flows powered by asymmetrical contraction transport PAR proteins to establish and maintain anterior-posterior polarity in the early C. elegans embryo. *Dev Cell,* 7**,** 413-24.

MURTHY, K. & WADSWORTH, P. 2008. Dual role for microtubules in regulating cortical contractility during cytokinesis. *J Cell Sci,* 121**,** 2350-9.

NACHURY, M. V., MARESCA, T. J., SALMON, W. C., WATERMAN-STORER, C. M., HEALD, R. & WEIS, K. 2001. Importin β Is a Mitotic Target of the Small GTPase Ran in Spindle Assembly. *Cell,* 104**,** 95-106.

NISHIMURA, Y. & YONEMURA, S. 2006. Centralspindlin regulates ECT2 and RhoA accumulation at the equatorial cortex during cytokinesis. *J Cell Sci,* 119**,** 104-14.

OEGEMA, K., SAVOIAN, M. S., MITCHISON, T. J. & FIELD, C. M. 2000. Functional analysis of a human homologue of the Drosophila actin binding protein anillin suggests a role in cytokinesis. *J Cell Biol,* 150**,** 539-52.

OSORIO, D. S., CHAN, F. Y., SARAMAGO, J., LEITE, J., SILVA, A. M., SOBRAL, A. F., GASSMANN, R. & CARVALHO, A. X. 2019. Crosslinking activity of non-muscle myosin II is not sufficient for embryonic cytokinesis in C. elegans. *Development,* 146.

OSSWALD, M. & MORAIS-DE-SA, E. 2019. Dealing with apical-basal polarity and intercellular junctions: a multidimensional challenge for epithelial cell division. *Curr Opin Cell Biol,* 60**,** 75-83.

OZUGERGIN, I., MASTRONARDI, K., LAW, C. & PIEKNY, A. 2022. Diverse mechanisms regulate contractile ring assembly for cytokinesis in the two-cell Caenorhabditis elegans embryo. *J Cell Sci,* 135.

OZUGERGIN, I. & PIEKNY, A. 2021. Complementary functions for the Ran gradient during division. *Small GTPases,* 12**,** 177-187.

PAIM, L. M. G. & FITZHARRIS, G. 2022. Cell size and polarization determine cytokinesis furrow ingression dynamics in mouse embryos. *Proc Natl Acad Sci U S A,* 119**,** e2119381119.

PETERMAN, E., VALIUS, M. & PREKERIS, R. 2020. CLIC4 is a cytokinetic cleavage furrow protein that regulates cortical cytoskeleton stability during cell division. *J Cell Sci,* 133.

PETRONCZKI, M., GLOTZER, M., KRAUT, N. & PETERS, J. M. 2007. Polo-like kinase 1 triggers the initiation of cytokinesis in human cells by promoting recruitment of the RhoGEF Ect2 to the central spindle. *Dev Cell,* 12**,** 713-25.

PICKAR-OLIVER, A. & GERSBACH, C. A. 2019. The next generation of CRISPR-Cas technologies and applications. *Nat Rev Mol Cell Biol,* 20**,** 490-507.

PIEKNY, A., WERNER, M. & GLOTZER, M. 2005. Cytokinesis: welcome to the Rho zone. *Trends Cell Biol,* 15**,** 651-8.

PIEKNY, A. J. & GLOTZER, M. 2008. Anillin is a scaffold protein that links RhoA, actin, and myosin during cytokinesis. *Curr Biol,* 18**,** 30-6.

PIEKNY, A. J. & MADDOX, A. S. 2010. The myriad roles of Anillin during cytokinesis. *Semin Cell Dev Biol,* 21**,** 881-91.

PIMPALE, L. G., MIDDELKOOP, T. C., MIETKE, A. & GRILL, S. W. 2020. Cell lineage-dependent chiral actomyosin flows drive cellular rearrangements in early Caenorhabditis elegans development. *Elife,* 9.

PINDER, J., SALSMAN, J. & DELLAIRE, G. 2015. Nuclear domain 'knock-in' screen for the evaluation and identification of small molecule enhancers of CRISPR-based genome editing. *Nucleic Acids Res,* 43**,** 9379-92.

PINTARD, L. & BOWERMAN, B. 2019. Mitotic Cell Division in *Caenorhabditis elegans*. *Genetics,* 211**,** 35-73.

PITTMAN, K. J. & SKOP, A. R. 2012. Anterior PAR proteins function during cytokinesis and maintain DYN-1 at the cleavage furrow in Caenorhabditis elegans. *Cytoskeleton (Hoboken),* 69**,** 826-39.

PO'UHA, S. T. & KAVALLARIS, M. 2015. Gamma-actin is involved in regulating centrosome function and mitotic progression in cancer cells. *Cell Cycle,* 14**,** 3908-19.

POLLARD, T. D. & O'SHAUGHNESSY, B. 2019. Molecular Mechanism of Cytokinesis. *Annu Rev Biochem,* 88**,** 661-689.

POMBO, C. M., FORCE, T., KYRIAKIS, J., NOGUEIRA, E., FIDALGO, M. & ZALVIDE, J. 2007. The GCK II and III subfamilies of the STE20 group kinases. *Front Biosci,* 12**,** 850-9.

PRICE, K. L. & ROSE, L. S. 2017. LET-99 functions in the astral furrowing pathway, where it is required for myosin enrichment in the contractile ring. *Mol Biol Cell,* 28**,** 2360-2373.

PROKOPENKO, S. N., BRUMBY, A., O'KEEFE, L., PRIOR, L., HE, Y., SAINT, R. & BELLEN, H. J. 1999. A putative exchange factor for Rho1 GTPase is required for initiation of cytokinesis in Drosophila. *Genes Dev,* 13**,** 2301-14.

RAPPAPORT, R. 1961. Experiments concerning the cleavage stimulus in sand dollar eggs. *J Exp Zool,* 148**,** 81-9.

REHAIN-BELL, K., LOVE, A., WERNER, M. E., MACLEOD, I., YATES, J. R., 3RD & MADDOX, A. S. 2017. A Sterile 20 Family Kinase and Its Co-factor CCM-3 Regulate Contractile Ring Proteins on Germline Intercellular Bridges. *Curr Biol,* 27**,** 860-867.

REYES, C. C., JIN, M., BREZNAU, E. B., ESPINO, R., DELGADO-GONZALO, R., GORYACHEV, A. B. & MILLER, A. L. 2014. Anillin regulates cell-cell junction

integrity by organizing junctional accumulation of Rho-GTP and actomyosin. *Curr Biol,* 24**,** 1263-70.

REYMANN, A. C., STANISCIA, F., ERZBERGER, A., SALBREUX, G. & GRILL, S. W. 2016. Cortical flow aligns actin filaments to form a furrow. *Elife,* 5.

ROBERTS, B., HAUPT, A., TUCKER, A., GRANCHAROVA, T., ARAKAKI, J., FUQUA, M. A., NELSON, A., HOOKWAY, C., LUDMANN, S. A., MUELLER, I. A., YANG, R., HORWITZ, R., RAFELSKI, S. M. & GUNAWARDANE, R. N. 2017. Systematic gene tagging using CRISPR/Cas9 in human stem cells to illuminate cell organization. *Mol Biol Cell,* 28**,** 2854-2874.

RODRIGUES, N. T., LEKOMTSEV, S., JANANJI, S., KRISTON-VIZI, J., HICKSON, G. R. & BAUM, B. 2015. Kinetochore-localized PP1-Sds22 couples chromosome segregation to polar relaxation. *Nature,* 524**,** 489-92.

ROSE, L. & GONCZY, P. 2014. Polarity establishment, asymmetric division and segregation of fate determinants in early C. elegans embryos. *WormBook***,** 1-43.

ROUBINET, C., DECELLE, B., CHICANNE, G., DORN, J. F., PAYRASTRE, B., PAYRE, F. & CARRENO, S. 2011. Molecular networks linked by Moesin drive remodeling of the cell cortex during mitosis. *J Cell Biol,* 195**,** 99-112.

SAKUMA, T., NAKADE, S., SAKANE, Y., SUZUKI, K. T. & YAMAMOTO, T. 2016. MMEJ-assisted gene knock-in using TALENs and CRISPR-Cas9 with the PITCh systems. *Nat Protoc,* 11**,** 118-33.

SAVIC, D., PARTRIDGE, E. C., NEWBERRY, K. M., SMITH, S. B., MEADOWS, S. K., ROBERTS, B. S., MACKIEWICZ, M., MENDENHALL, E. M. & MYERS, R. M. 2015.

CETCh-seq: CRISPR epitope tagging ChIP-seq of DNA-binding proteins. *Genome Res,* 25**,** 1581-9.

SCHATZ, C. A., SANTARELLA, R., HOENGER, A., KARSENTI, E., MATTAJ, I. W., GRUSS, O. J. & CARAZO-SALAS, R. E. 2003. Importin alpha-regulated nucleation of microtubules by TPX2. *EMBO J,* 22**,** 2060-70.

SCHENK, C., BRINGMANN, H., HYMAN, A. A. & COWAN, C. R. 2010. Cortical domain correction repositions the polarity boundary to match the cytokinesis furrow in C. elegans embryos. *Development,* 137**,** 1743-53.

SCHNEID, S., WOLFF, F., BUCHNER, K., BERTRAM, N., BAYGUN, S., BARBOSA, P., MANGAL, S. & ZANIN, E. 2021. The BRCT domains of ECT2 have distinct functions during cytokinesis. *Cell Rep,* 34**,** 108805.

SCULLY, R., PANDAY, A., ELANGO, R. & WILLIS, N. A. 2019. DNA double-strand break repair-pathway choice in somatic mammalian cells. *Nat Rev Mol Cell Biol,* 20**,** 698-714.

SEDZINSKI, J., BIRO, M., OSWALD, A., TINEVEZ, J. Y., SALBREUX, G. & PALUCH, E. 2011. Polar actomyosin contractility destabilizes the position of the cytokinetic furrow. *Nature,* 476**,** 462-6.

SILLJE, H. H., NAGEL, S., KORNER, R. & NIGG, E. A. 2006. HURP is a Ran-importin beta-regulated protein that stabilizes kinetochore microtubules in the vicinity of chromosomes. *Curr Biol,* 16**,** 731-42.

SILVA, A. M., OSORIO, D. S., PEREIRA, A. J., MAIATO, H., PINTO, I. M., RUBINSTEIN, B., GASSMANN, R., TELLEY, I. A. & CARVALHO, A. X. 2016. Robust gap repair in the contractile ring ensures timely completion of cytokinesis. *J Cell Biol,* 215**,** 789-799.

SILVERMAN-GAVRILA, R. V., HALES, K. G. & WILDE, A. 2008. Anillin-mediated targeting of peanut to pseudocleavage furrows is regulated by the GTPase Ran. *Mol Biol Cell,* 19**,** 3735-44.

SINGH, D. & POHL, C. 2014. Coupling of rotational cortical flow, asymmetric midbody positioning, and spindle rotation mediates dorsoventral axis formation in C. elegans. *Dev Cell,* 28**,** 253-67.

SOMERS, W. G. & SAINT, R. 2003. A RhoGEF and Rho Family GTPase-Activating Protein Complex Links the Contractile Ring to Cortical Microtubules at the Onset of Cytokinesis. *Dev Cell,* 4**,** 29-39.

STEIGEMANN, P., WURZENBERGER, C., SCHMITZ, M. H., HELD, M., GUIZETTI, J., MAAR, S. & GERLICH, D. W. 2009. Aurora B-mediated abscission checkpoint protects against tetraploidization. *Cell,* 136**,** 473-84.

STRAIGHT, A. F., FIELD, C. M. & MITCHISON, T. J. 2005. Anillin binds nonmuscle myosin II and regulates the contractile ring. *Mol Biol Cell,* 16**,** 193-201.

STROME, S. & WOOD, W. B. 1982. Immunofluorescence visualization of germ-line-specific cytoplasmic granules in embryos, larvae, and adults of Caenorhabditis elegans. *Proc Natl Acad Sci U S A,* 79**,** 1558-62.

SU, K. C., TAKAKI, T. & PETRONCZKI, M. 2011. Targeting of the RhoGEF Ect2 to the equatorial membrane controls cleavage furrow formation during cytokinesis. *Dev Cell,* 21**,** 1104-15.

SUN, D., EVANS, L., PERRONE, F., SOKLEVA, V., LIM, K., REZAKHANI, S., LUTOLF, M., ZILBAUER, M. & RAWLINS, E. L. 2021. A functional genetic toolbox for human tissue-derived organoids. *Elife,* 10.

SUN, L., GUAN, R., LEE, I. J., LIU, Y., CHEN, M., WANG, J., WU, J. Q. & CHEN, Z. 2015. Mechanistic insights into the anchorage of the contractile ring by anillin and Mid1. *Dev Cell,* 33**,** 413-26.

TATSUMOTO, T., XIE, X., BLUMENTHAL, R., OKAMOTO, I. & MIKI, T. 1999. Human ECT2 is an exchange factor for Rho GTPases, phosphorylated in G2/M phases, and involved in cytokinesis. *J Cell Biol,* 147**,** 921-8.

TOKUNAGA, M., IMAMOTO, N. & SAKATA-SOGAWA, K. 2008. Highly inclined thin illumination enables clear single-molecule imaging in cells. *Nat Methods,* 5**,** 159-61.

TSE, Y. C., PIEKNY, A. & GLOTZER, M. 2011. Anillin promotes astral microtubule-directed cortical myosin polarization. *Mol Biol Cell,* 22**,** 3165-75.

TSE, Y. C., WERNER, M., LONGHINI, K. M., LABBE, J. C., GOLDSTEIN, B. & GLOTZER, M. 2012. RhoA activation during polarization and cytokinesis of the early Caenorhabditis elegans embryo is differentially dependent on NOP-1 and CYK-4. *Mol Biol Cell,* 23**,** 4020-31.

URETMEN KAGIALI, Z. C., SANER, N., AKDAG, M., SANAL, E., DEGIRMENCI, B. S., MOLLAOGLU, G. & OZLU, N. 2020. CLIC4 and CLIC1 bridge plasma membrane and cortical actin network for a successful cytokinesis. *Life Sci Alliance,* 3.

VAN OOSTENDE TRIPLET, C., JARAMILLO GARCIA, M., HAJI BIK, H., BEAUDET, D. & PIEKNY, A. 2014. Anillin interacts with microtubules and is part of the astral pathway that defines cortical domains. *J Cell Sci,* 127**,** 3699-710.

VERBRUGGHE, K. J. & WHITE, J. G. 2004. SPD-1 is required for the formation of the spindle midzone but is not essential for the completion of cytokinesis in C. elegans embryos. *Curr Biol,* 14**,** 1755-60.

VERMA, N., ZHU, Z. & HUANGFU, D. 2017. CRISPR/Cas-Mediated Knockin in Human Pluripotent Stem Cells. *Methods Mol Biol,* 1513**,** 119-140.

VON DASSOW, G., VERBRUGGHE, K. J., MILLER, A. L., SIDER, J. R. & BEMENT, W. M. 2009. Action at a distance during cytokinesis. *J Cell Biol,* 187**,** 831-45.

WALCZAK, C. E. & HEALD, R. 2008. Mechanisms of mitotic spindle assembly and function. *Int Rev Cytol,* 265**,** 111-58.

WANG, H., LA RUSSA, M. & QI, L. S. 2016. CRISPR/Cas9 in Genome Editing and Beyond. *Annu Rev Biochem,* 85**,** 227-64.

WERNER, M., MUNRO, E. & GLOTZER, M. 2007. Astral signals spatially bias cortical myosin recruitment to break symmetry and promote cytokinesis. *Curr Biol,* 17**,** 1286-97.

WERNIKE, D., CHEN, Y., MASTRONARDI, K., MAKIL, N. & PIEKNY, A. 2016. Mechanical forces drive neuroblast morphogenesis and are required for epidermal closure. *Dev Biol,* 412**,** 261-77.

WIESE, C., WILDE, A., MOORE, M. S., ADAM, S. A., MERDES, A. & ZHENG, Y. 2001. Role of importin-beta in coupling Ran to downstream targets in microtubule assembly. *Science,* 291**,** 653-6.

WOLFE, B. A., TAKAKI, T., PETRONCZKI, M. & GLOTZER, M. 2009. Polo-like kinase 1 directs assembly of the HsCyk-4 RhoGAP/Ect2 RhoGEF complex to initiate cleavage furrow formation. *PLoS Biol,* 7**,** e1000110.

WRIGHT, W. D., SHAH, S. S. & HEYER, W. D. 2018. Homologous recombination and the repair of DNA double-strand breaks. *J Biol Chem,* 293**,** 10524-10535.

XU, L. & MASSAGUE, J. 2004. Nucleocytoplasmic shuttling of signal transducers. *Nat Rev Mol Cell Biol,* 5**,** 209-19.

YAMAMOTO, K., OTOMO, K., NEMOTO, T., ISHIHARA, S., HAGA, H., NAGASAKI, A., MURAKAMI, Y. & TAKAHASHI, M. 2019. Differential contributions of nonmuscle myosin IIA and IIB to cytokinesis in human immortalized fibroblasts. *Exp Cell Res,* 376**,** 67-76.

YI, K., UNRUH, J. R., DENG, M., SLAUGHTER, B. D., RUBINSTEIN, B. & LI, R. 2011. Dynamic maintenance of asymmetric meiotic spindle position through Arp2/3-complex-driven cytoplasmic streaming in mouse oocytes. *Nat Cell Biol,* 13**,** 1252-8.

YONEMURA, S., HIRAO-MINAKUCHI, K. & NISHIMURA, Y. 2004. Rho localization in cells and tissues. *Exp Cell Res,* 295**,** 300-14.

YUCE, O., PIEKNY, A. & GLOTZER, M. 2005. An ECT2-centralspindlin complex regulates the localization and function of RhoA. *J Cell Biol,* 170**,** 571-82.

ZANIN, E., DESAI, A., POSER, I., TOYODA, Y., ANDREE, C., MOEBIUS, C., BICKLE, M., CONRADT, B., PIEKNY, A. & OEGEMA, K. 2013. A conserved RhoGAP limits M phase contractility and coordinates with microtubule asters to confine RhoA during cytokinesis. *Dev Cell,* 26**,** 496-510.

ZAVORTINK, M., CONTRERAS, N., ADDY, T., BEJSOVEC, A. & SAINT, R. 2005. Tum/RacGAP50C provides a critical link between anaphase microtubules and the assembly of the contractile ring in Drosophila melanogaster. *J Cell Sci,* 118**,** 5381-92.

ZHANG, D. & GLOTZER, M. 2015. The RhoGAP activity of CYK-4/MgcRacGAP functions non-canonically by promoting RhoA activation during cytokinesis. *Elife,* 4.

ZHAO, W. M. & FANG, G. 2005a. Anillin is a substrate of anaphase-promoting complex/cyclosome (APC/C) that controls spatial contractility of myosin during late cytokinesis. *J Biol Chem,* 280**,** 33516-24.

ZHAO, W. M. & FANG, G. 2005b. MgcRacGAP controls the assembly of the contractile ring and the initiation of cytokinesis. *Proc Natl Acad Sci U S A,* 102**,** 13158-63.

ZHURAVLEV, Y., HIRSCH, S. M., JORDAN, S. N., DUMONT, J., SHIRASU-HIZA, M. & CANMAN, J. C. 2017. CYK-4 regulates Rac, but not Rho, during cytokinesis. *Mol Biol Cell,* 28**,** 1258-1270.

SUPPLEMENTAL FIGURES

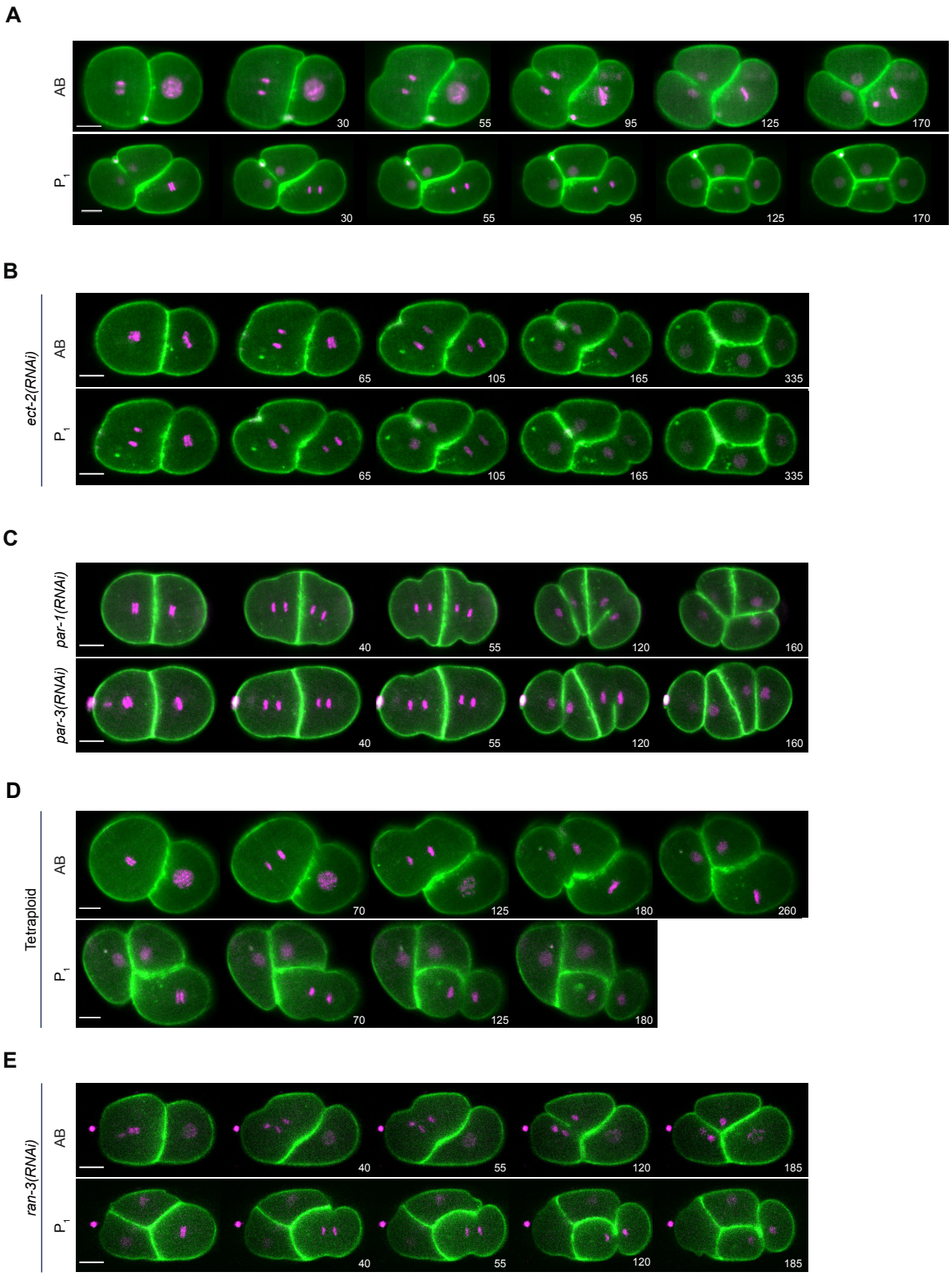

Figure S1. Comparison of cytokinesis in AB and P_1 cells. Timelapse images of A) control (also shown in Figure 1A), B) *ect-2(RNAi)*, C) *par-1(RNAi)* (top) and *par-3(RNAi)* (bottom), D) tetraploid and E) *ran-3(RNAi)* embryos co-expressing mCherry::HIS-58; GFP::PH (A, E) or mCherry::HIS-58 and mNeonGreen::PH (B-D). All scale bars are 10 μm.

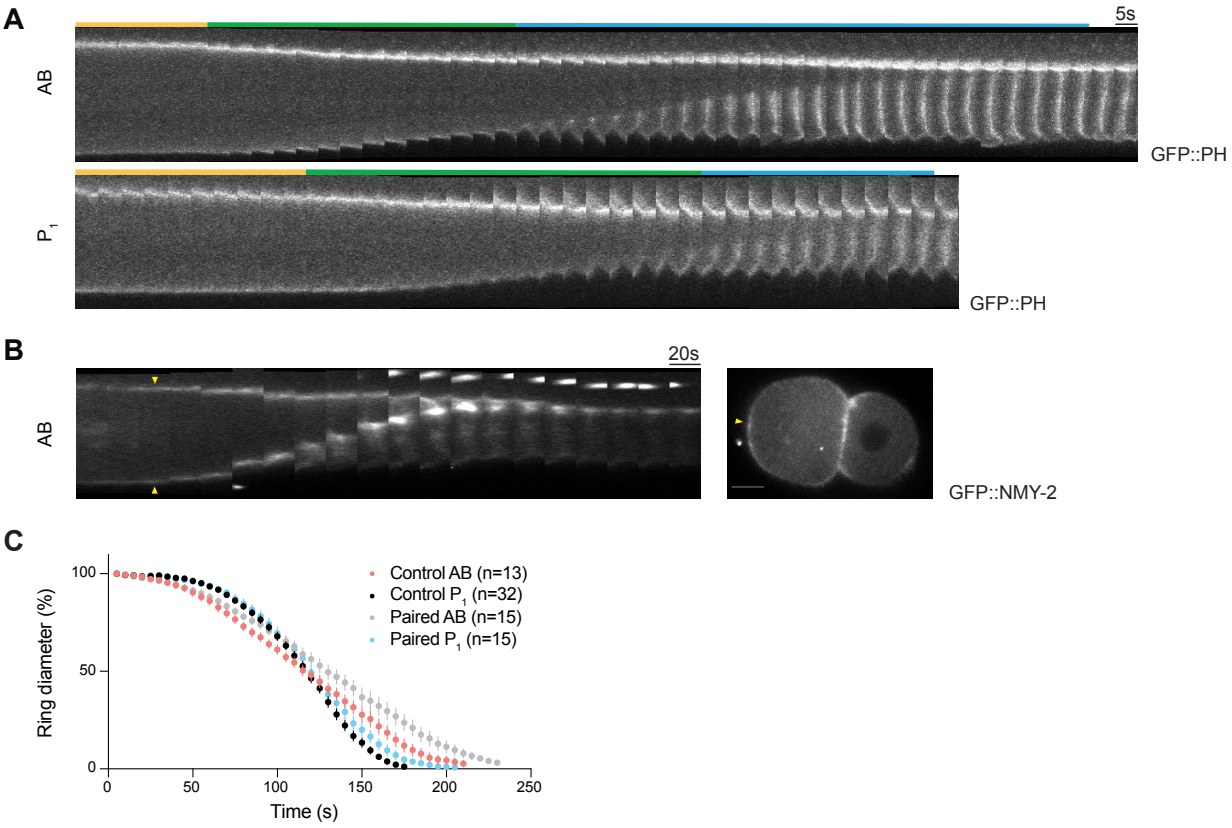
A
5s
AB
GFP::PH
P1
GFP::PH
B
20s
AB
GFP::NMY-2
C
Ring diameter (%)
100
50
0
0
50
100
150
200
250
Time (s)
Control AB (n=13)
Control P1 (n=32)
Paired AB (n=15)
Paired P1 (n=15)

Figure S2. AB and P_1 cells have distinct cytokinesis phases. A) Kymographs were generated from the furrow region in AB (top) and P_1 (bottom) cells, from images acquired at 5-second intervals from anaphase onset until closure. The bars indicate the duration of ring assembly (yellow), furrow initiation (green) and ring constriction (yellow) phases. B) Left: a kymograph was generated from a cell expressing GFP::NMY-2, from images acquired at 20-second intervals. Right: image shows myosin localization during ring assembly, before furrow initiation. Yellow arrowheads point to myosin accumulation. C) A graph shows average ring closure in control AB and P_1 cells (shown in main figures) compared to paired (*i.e.* sister cells from the same embryo) AB and P_1 cells. The sample sizes are indicated (n) and error bars show s.e.m.

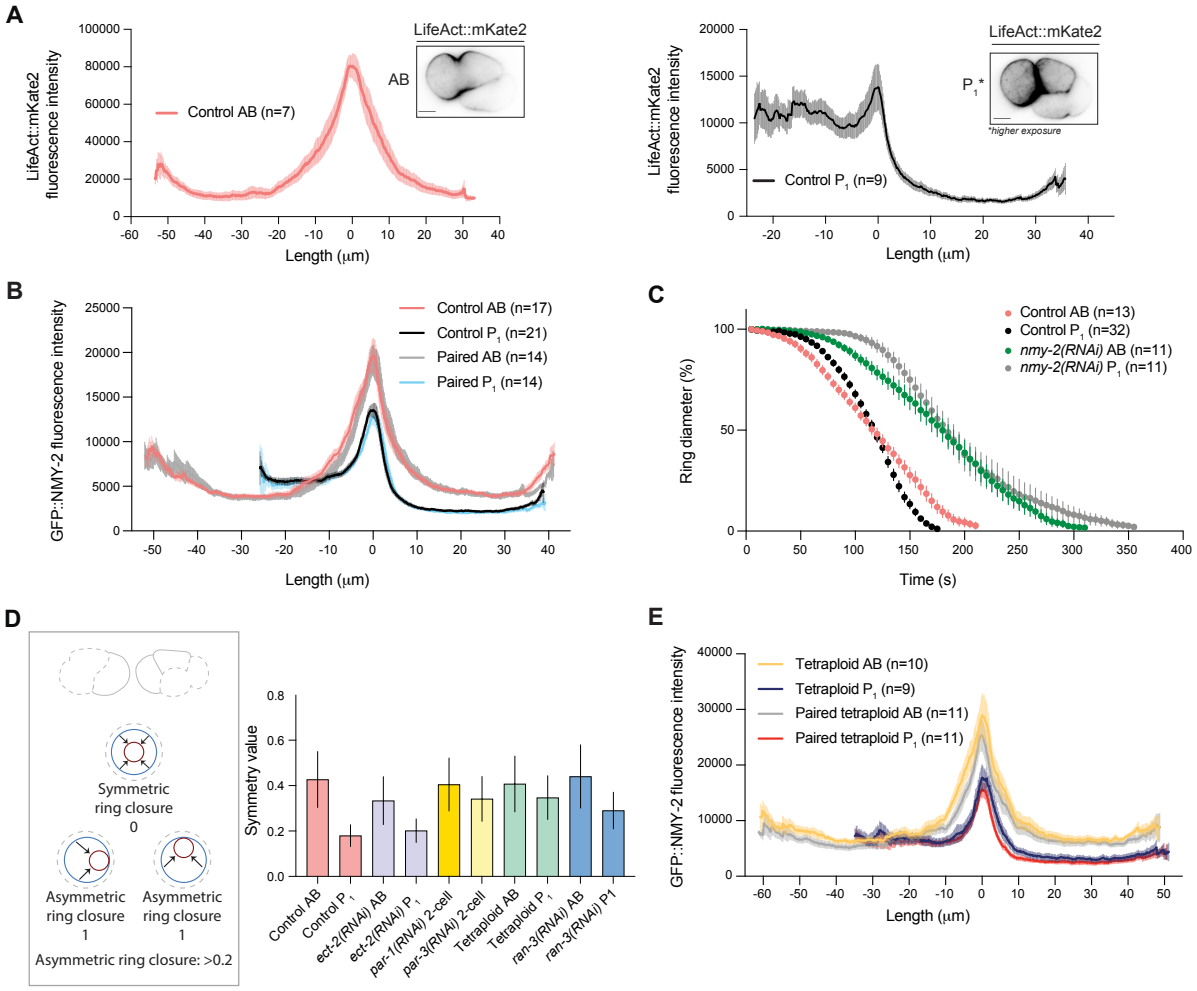
A
LifeAct::mKate2 fluorescence intensity
Control AB (n=7)
AB
LifeAct::mKate2
Length (μm)
Control P1 (n=9)
P1*
*higher exposure
B
GFP::NMY-2 fluorescence intensity
Control AB (n=17)
Control P1 (n=21)
Paired AB (n=14)
Paired P1 (n=14)
C
Ring diameter (%)
Control AB (n=13)
Control P1 (n=32)
nmy-2(RNAi) AB (n=11)
nmy-2(RNAi) P1 (n=11)
Time (s)
D
Symmetric ring closure 0
Asymmetric ring closure 1
Asymmetric ring closure 1
Asymmetric ring closure: >0.2
Symmetry value
Control AB
Control P1
ect-2(RNAi) AB
ect-2(RNAi) P1
par-1(RNAi) 2-cell
par-3(RNAi) 2-cell
Tetraploid AB
Tetraploid P1
ran-3(RNAi) AB
ran-3(RNAi) P1
E
GFP::NMY-2 fluorescence intensity
Tetraploid AB (n=10)
Tetraploid P1 (n=9)
Paired tetraploid AB (n=11)
Paired tetraploid P1 (n=11)
Length (μm)

Figure S3. Characterization of cytokinesis shows differences in actomyosin, and asymmetric ring closure in AB and P_1 cells. A) Inverted images show LifeAct::mKate2 localization in control AB and P_1 cells. Graphs show the average accumulation of LifeAct::mKate2 at the midplane cortex of AB (left) and P_1 (right) cells. B) A graph shows GFP::NMY-2 levels at the midplane cortex of control AB and P_1 cells (shown in main figures) compared to paired cells. C) A graph shows ring closure in *nmy-2(RNAi)* AB and P_1 cells compared to control. D) Left: Cartoon embryos and end-on views show how the symmetry of ring closure was quantified. Values closer to 1 are asymmetric (along the x or y-axis), while those closest to 0 are symmetric. Right: graph shows the symmetry measurements for control embryos, after *ect-2*, *par-1*, *par-3* or *ran-3(RNAi)*, and in tetraploid embryos. E) A graph shows GFP::NMY-2 levels at the midplane cortex of tetraploid AB and P_1 cells (shown in main figures) compared to paired tetraploid cells. For all graphs, n's are indicated, and error bars show s.e.m. All scale bars are 10 μm.

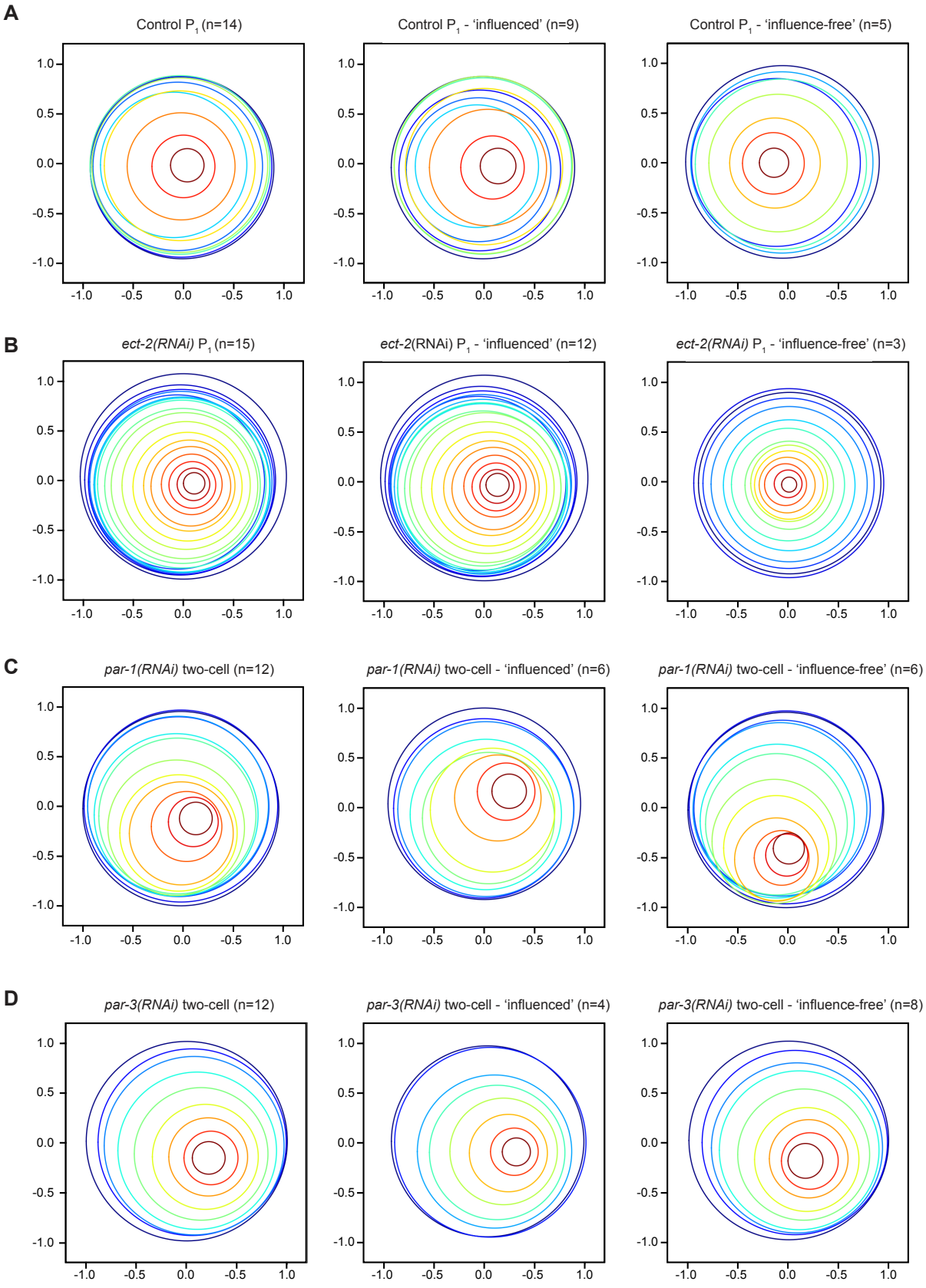
A
Control P1 (n=14)
Control P1 - 'influenced' (n=9)
Control P1 - 'influence-free' (n=5)
B
ect-2(RNAi) P1 (n=15)
ect-2(RNAi) P1 - 'influenced' (n=12)
ect-2(RNAi) P1 - 'influence-free' (n=3)
C
par-1(RNAi) two-cell (n=12)
par-1(RNAi) two-cell - 'influenced' (n=6)
par-1(RNAi) two-cell - 'influence-free' (n=6)
D
par-3(RNAi) two-cell (n=12)
par-3(RNAi) two-cell - 'influenced' (n=4)
par-3(RNAi) two-cell - 'influence-free' (n=8)
1.0
0.5
0.0
-0.5
-1.0

Figure S4. Symmetry of ring closure is similar between influenced and influence-free P_1 cells. Ring closure is shown over time for A) control, B) *ect-2(RNAi),* C) *par-1(RNAi),* and D) *par-3(RNAi)* P_1 cells, with each timepoint as a different color. Average ring closure for all n's is shown in the left column. The middle column is the average ring closure for influenced P_1 cells, and the right column is the average ring closure for influence-free P_1 cells. The x and y-axis indicate ratios of the distance from the starting position (0).

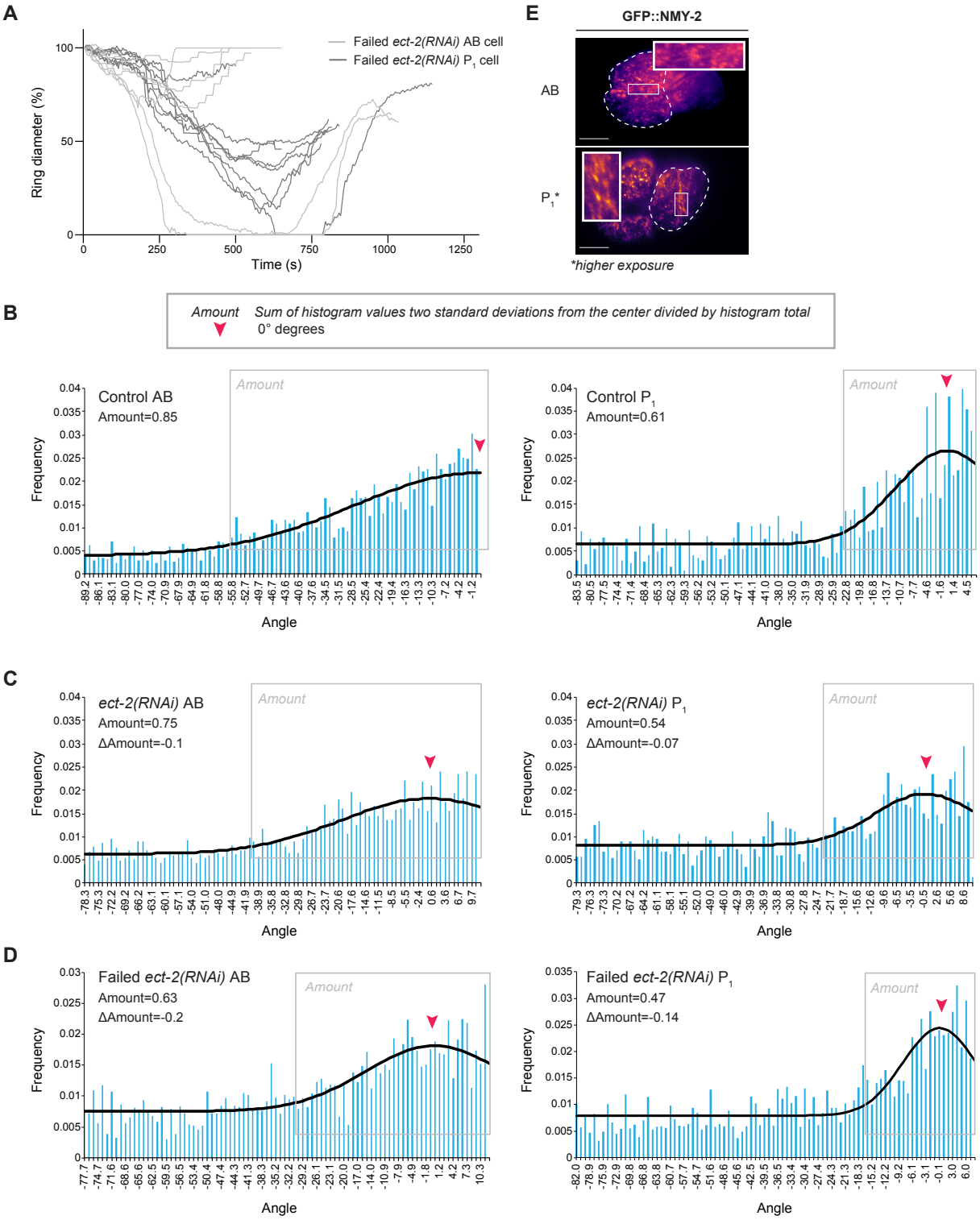
A
Failed ect-2(RNAi) AB cell
Failed ect-2(RNAi) P1 cell
Ring diameter (%)
Time (s)
E
GFP::NMY-2
AB
P1*
*higher exposure
B
Amount
Sum of histogram values two standard deviations from the center divided by histogram total
0° degrees
Control AB
Amount=0.85
Control P1
Amount=0.61
C
ect-2(RNAi) AB
Amount=0.75
ΔAmount=-0.1
ect-2(RNAi) P1
Amount=0.54
ΔAmount=-0.07
D
Failed ect-2(RNAi) AB
Amount=0.63
ΔAmount=-0.2
Failed ect-2(RNAi) P1
Amount=0.47
ΔAmount=-0.14
Frequency
Angle

Figure S5. Myosin filaments are less-well organized and aligned in *ect-2(RNAi)* AB and P_1 cells. A) A graph shows partial ring closure and regression for *ect-2(RNAi)* AB and P_1 cells that fail cytokinesis. B-D) Histograms show the frequency distribution (y-axis) of myosin filament bundles at different angles (x-axis) in AB and P_1 cells. Measurements were taken in the furrow region of B) control cells (shown in Figure 6E), C) *ect-2(RNAi)* cells that complete cytokinesis (shown in Figure 7H) and D) *ect-2(RNAi)* cells that fail cytokinesis (shown in Figure S5E). Well-aligned filament bundles are close to 0° (red arrowhead). The proportion of filament bundles within two standard deviations of the highest frequency peak, outlined by the grey boxes, is indicated as 'Amount' on each graph. E) Pseudocolored HILO images show GFP::NMY-2 in *ect-2(RNAi)* AB and P_1 cells (outlined by the dashed line) that fail cytokinesis.

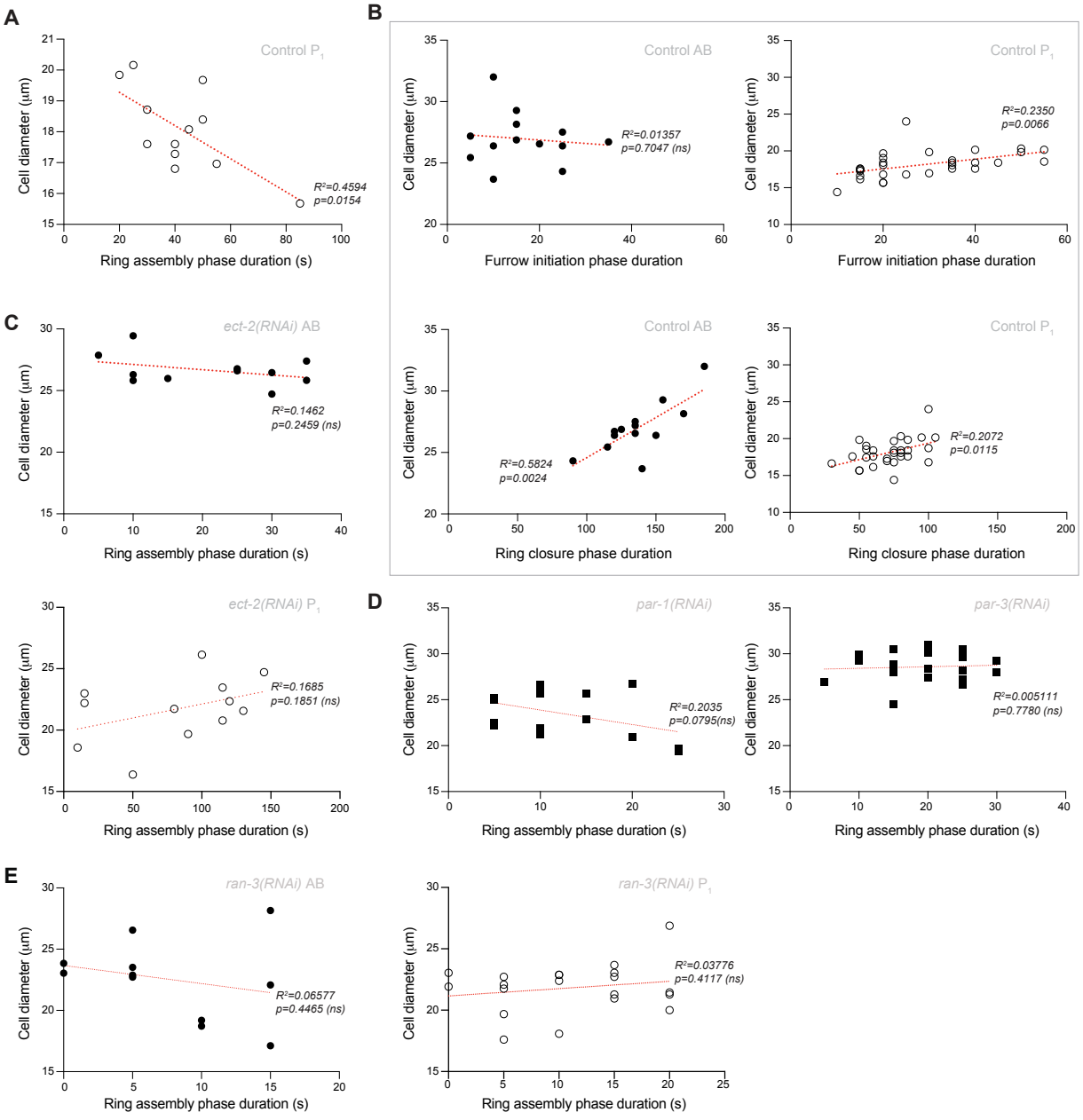
A
Control P1
Cell diameter (µm)
Ring assembly phase duration (s)
R²=0.4594
p=0.0154
B
Control AB
Furrow initiation phase duration
R²=0.01357
p=0.7047 (ns)
Control P1
R²=0.2350
p=0.0066
Control AB
Ring closure phase duration
R²=0.5824
p=0.0024
Control P1
R²=0.2072
p=0.0115
C
ect-2(RNAi) AB
R²=0.1462
p=0.2459 (ns)
ect-2(RNAi) P1
R²=0.1685
p=0.1851 (ns)
D
par-1(RNAi)
R²=0.2035
p=0.0795(ns)
par-3(RNAi)
R²=0.005111
p=0.7780 (ns)
E
ran-3(RNAi) AB
R²=0.06577
p=0.4465 (ns)
ran-3(RNAi) P1
R²=0.03776
p=0.4117 (ns)

Figure S6. There is no correlation between the duration of ring assembly and cell size after ECT-2 depletion, disruption of cell fate or lowering Ran-GTP in P_1 cells. A) A graph shows the correlation between the duration of ring assembly and diameter for twelve randomly selected P_1 cells. B) Graphs show the correlation between the duration of furrow initiation (top) or ring closure (bottom) phases and cell diameter. C) Graphs show the correlation between the duration of ring assembly and diameter for AB (top) and P_1 (bottom) cells in *ect-2(RNAi)* cells. D) Graphs show the correlation between the duration of ring assembly and diameter for *par-1(RNAi)* (left) and *par-3(RNAi)* (right) P_0 daughter cells. D) Graphs show the correlation between the duration of ring assembly and diameter for AB (left) and P_1 (right) cells in *ran-3(RNAi)* cells. For all graphs, the red lines show simple linear regression (R^2 and *p* are shown; ns is not significant).

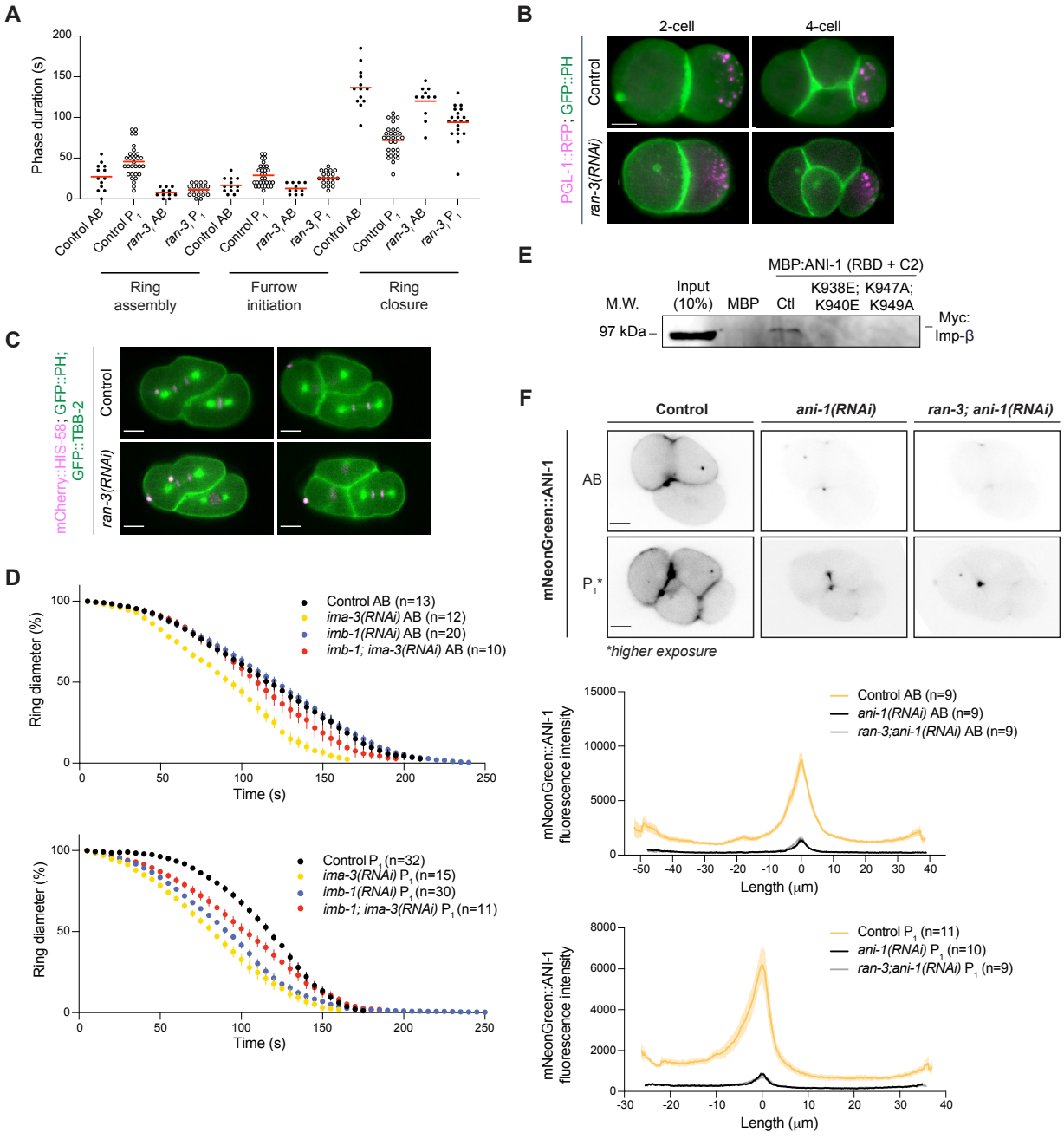
A
Phase duration (s)
Control AB
Control P1
ran-3 AB
ran-3 P1
Ring assembly
Furrow initiation
Ring closure
B
2-cell
4-cell
Control
ran-3(RNAi)
PGL-1::RFP; GFP::PH
C
mCherry::HIS-58; GFP::PH; GFP::TBB-2
D
Ring diameter (%)
Time (s)
Control AB (n=13)
ima-3(RNAi) AB (n=12)
imb-1(RNAi) AB (n=20)
imb-1; ima-3(RNAi) AB (n=10)
Control P1 (n=32)
ima-3(RNAi) P1 (n=15)
imb-1(RNAi) P1 (n=30)
imb-1; ima-3(RNAi) P1 (n=11)
E
MBP:ANI-1 (RBD + C2)
M.W.
Input (10%)
MBP
Ctl
K938E; K940E
K947A; K949A
97 kDa
Myc: Imp-β
F
Control
ani-1(RNAi)
ran-3; ani-1(RNAi)
mNeonGreen::ANI-1
AB
P1*
*higher exposure
mNeonGreen::ANI-1 fluorescence intensity
Length (μm)
Control AB (n=9)
ani-1(RNAi) AB (n=9)
ran-3;ani-1(RNAi) AB (n=9)
Control P1 (n=11)
ani-1(RNAi) P1 (n=10)
ran-3;ani-1(RNAi) P1 (n=9)

Figure S7. Different thresholds of importin-α and -β control cytokinesis in AB and P_1 cells. A) A plot shows the duration of ring assembly, furrow initiation and ring closure phases for individual control and *ran-3(RNAi)* AB and P_1 cells (average, red lines). B) Images show embryos co-expressing PGL-1::RFP and GFP::PH in 2-cell and 4-cell control (top) and *ran-3(RNAi)* (bottom) embryos. C) Images show divisions of AB and P_1 cells in control (top) and *ran-3(RNAi)* (bottom) embryos co-expressing mCherry-HIS::58, GFP::PH and GFP::TBB-2. D) Graphs show ring closure in AB (top) and P_1 (bottom) cells in control embryos or after *ima-3(RNAi)*, *imb-1(RNAi)* and *imb-1(RNAi); ima-3(RNAi)*. E) A western blot shows Myc-tagged importin-β from HeLa cell lysates (input) and after pull-down with recombinant, purified MBP or MBP-tagged ANI-1 (RBD + C2) containing mutations K938E; K940E or K947A; K949A. F) Inverted images show dividing AB (top) or P_1 (bottom) cells in embryos where endogenous ANI-1 is tagged with mNeonGreen (mNeonGreen::ANI-1), and after *ani-1(RNAi)* or *ran-3; ani-1(RNAi)*. The graphs show mNeonGreen::ANI-1 levels at the midplane cortex in control compared to RNAi-treated cells. All error bars show s.e.m. All scale bars are 10 μm.

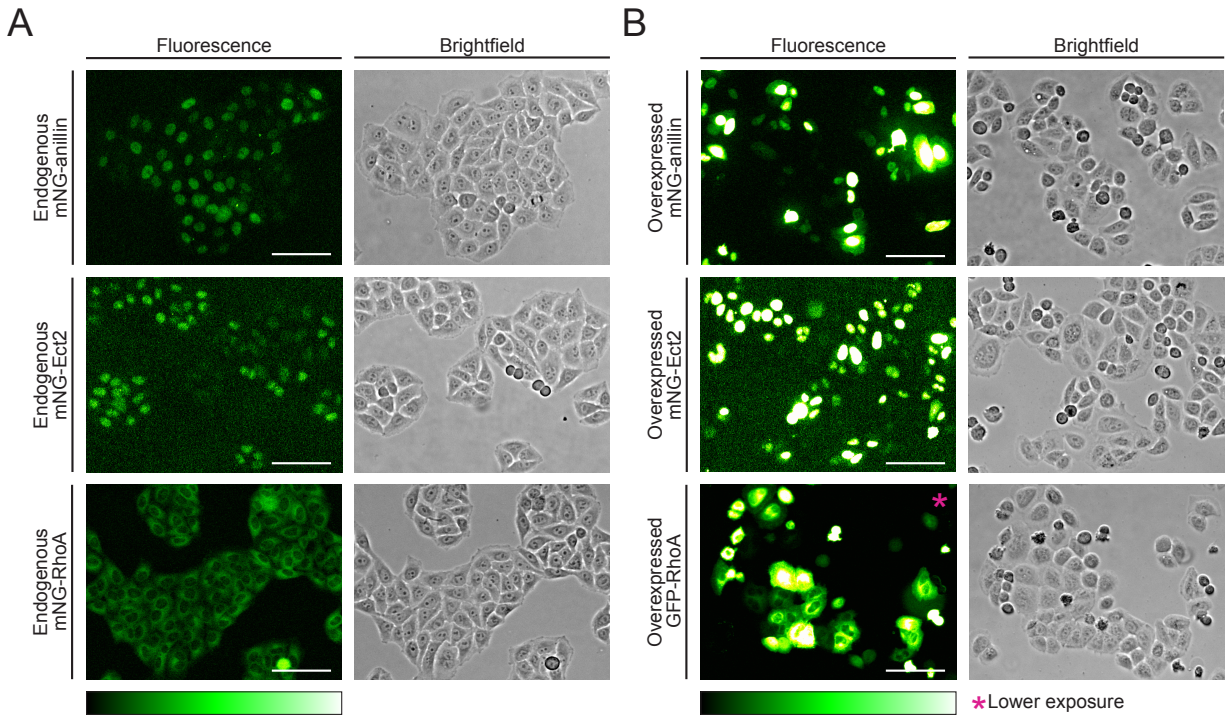
A
Fluorescence
Brightfield
Endogenous mNG-anillin
Endogenous mNG-Ect2
Endogenous mNG-RhoA
B
Fluorescence
Brightfield
Overexpressed mNG-anillin
Overexpressed mNG-Ect2
Overexpressed GFP-RhoA
*
*Lower exposure

Figure S8. Comparison of endogenous tags with transient overexpression. A) Fluorescence (left) and corresponding brightfield (right) images of HeLa cells where anillin (top), Ect2 (middle) and RhoA (bottom) are endogenously tagged with mNeonGreen. B) Fluorescence (left) and corresponding brightfield (right) images of HeLa cells where mNeonGreen-anillin (top), mNeonGreen-Ect2 (middle) and GFP-RhoA (bottom) are exogenously expressed, 24 hours after transfection. *Image taken with a lower exposure time. Scale bars are 100 μm. Relative intensity for mNeonGreen is shown in the corresponding scales.

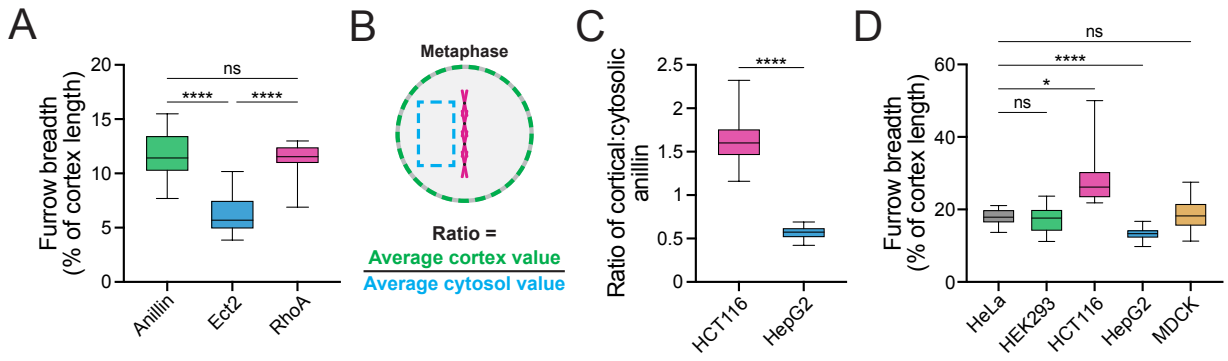
A
Furrow breadth (% of cortex length)
20
15
10
5
0
ns
****
****
Anillin
Ect2
RhoA
B
Metaphase
Ratio =
Average cortex value
Average cytosol value
C
Ratio of cortical:cytosolic anillin
2.5
2
1.5
1
0.5
0
****
HCT116
HepG2
D
Furrow breadth (% of cortex length)
60
40
20
0
ns
****
*
ns
HeLa
HEK293
HCT116
HepG2
MDCK

Figure S9. Characterization of endogenous mNeonGreen-anillin, Ect2 and RhoA localization during cytokinesis. A) A box plot shows the breadth of mNeonGreen-anillin (*n*=16), -Ect2 (*n*=10) and -RhoA (*n*=10) in HeLa cells relative to cortical length. B) A schematic shows how the ratio of cortical to cytosolic mNeonGreen-anillin was measured for C. C) A box plot shows the enrichment of mNeonGreen-anillin at the cortex relative to the cytosol during metaphase in HCT116 (*n*=8) and HepG2 (*n*=12) cells. D) A box plot shows the breadth of mNeonGreen-anillin in HeLa (*n*=16), HEK293 (*n*=9), HCT116 (*n*=11), HepG2 (*n*=13), and MDCK (*n*=10) cells relative to cortical length. Box plots in A, C and D show the median line, quartile box edges and minimum and maximum whiskers. Statistical significance was determined by one-way ANOVA in A and D, and Welch's *t*-test in C (ns, not significant; **P*≤0.05; ***P*≤0.01; ****P*≤0.001; *****P*≤0.0001).

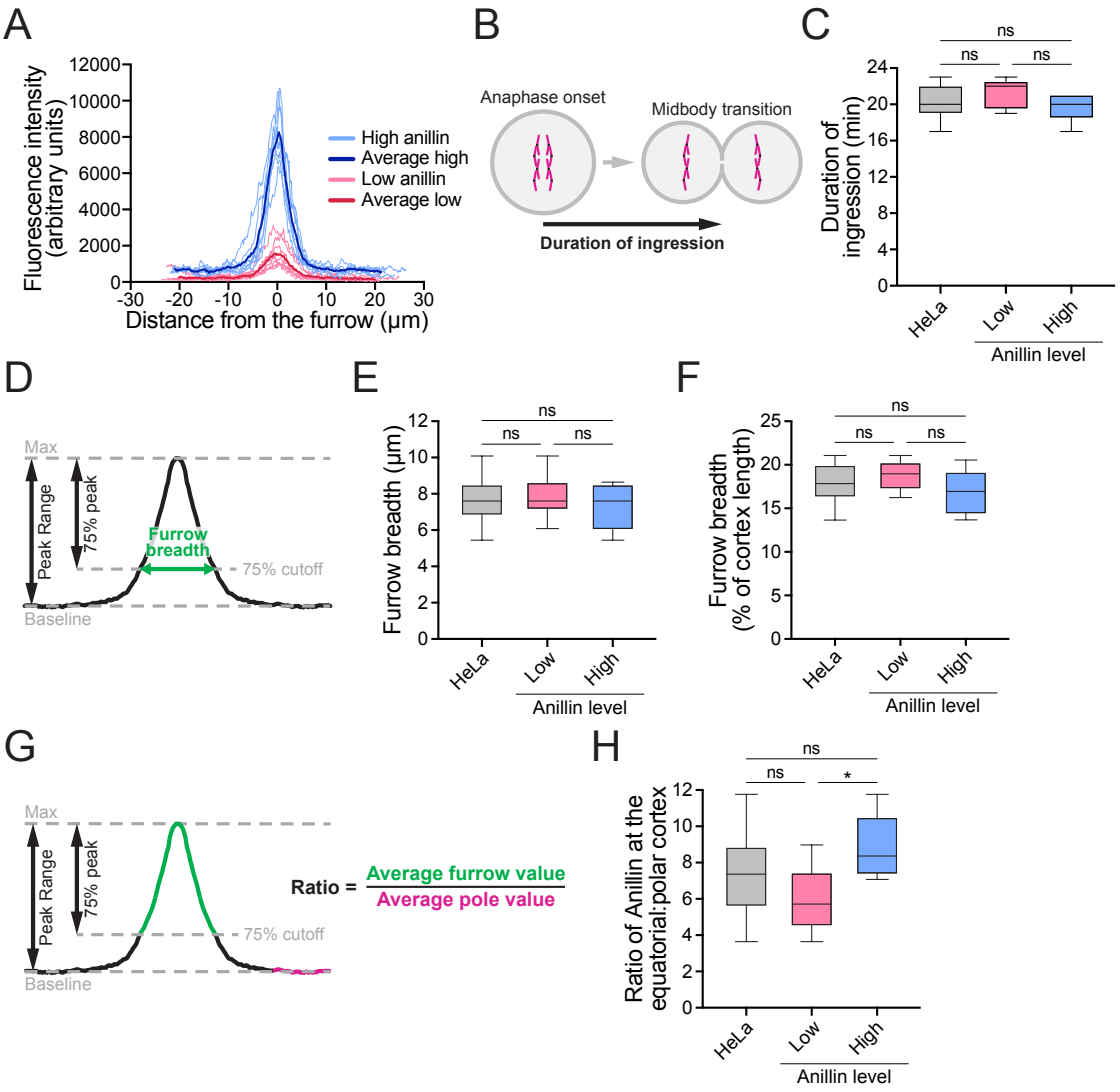
A
Fluorescence intensity (arbitrary units)
12000
10000
8000
6000
4000
2000
0
-30
-20
-10
0
10
20
30
Distance from the furrow (µm)
High anillin
Average high
Low anillin
Average low
B
Anaphase onset
Midbody transition
Duration of ingression
C
ns
ns
ns
Duration of ingression (min)
24
20
16
12
8
4
0
HeLa
Low
High
Anillin level
D
Max
Peak Range
75% peak
Furrow breadth
75% cutoff
Baseline
E
ns
ns
ns
Furrow breadth (µm)
12
10
8
6
4
2
0
HeLa
Low
High
Anillin level
F
ns
ns
ns
Furrow breadth (% of cortex length)
25
20
15
10
5
0
HeLa
Low
High
Anillin level
G
Max
Peak Range
75% peak
75% cutoff
Baseline
Ratio = Average furrow value / Average pole value
H
ns
ns
*
Ratio of Anillin at the equatorial:polar cortex
12
10
8
6
4
2
0
HeLa
Low
High
Anillin level

Figure S10. Comparison of HeLa cells expressing high and low levels of mNeonGreen-anillin. A) A graph shows two sets of linescans to highlight the differences in fluorescence intensity of mNeonGreen-anillin along the cortex of 'high' (blue, *n*=8) and 'low' (red, *n*=8) expressing HeLa cells. Individual cells are shown in light colors and the average for each population is shown in dark colors. B) A schematic shows how ingression time was measured for C. C) A box plot shows the duration of ingression in high- (*n*=6) and low- (*n*=5) expressing mNeonGreen-anillin HeLa cells compared to combined populations. D) A schematic shows how the breadth at the equatorial cortex was calculated for E and F. E) A box plot shows the breadth of mNeonGreen-anillin peaks in high- (*n*=8) and low- (*n*=8) expressing HeLa cells compared to combined populations. F) A box plot shows the breadth of mNeonGreen-anillin peaks relative to cortical length in high- (*n*=8) and low- (*n*=8) expressing HeLa cells compared to combined populations. G) A schematic shows how the ratio of protein in the furrow relative to the polar cortex was calculated for H. H) A box plot shows the ratio of mNeonGreen-anillin in the furrow relative to the polar cortex in high- (*n*=8) and low- (*n*=8) expressing HeLa cells compared to combined populations. Box plots in C, E, F and H show the median line, quartile box edges and minimum and maximum whiskers. Statistical significance was determined by one-way ANOVA (ns, not significant; **P*≤0.05; ***P*≤0.01; ****P*≤0.001; *****P*≤0.0001).

SUPPLEMENTAL TABLES

Table S1. *C. elegans* strains used in this study.

Strain	Genotype	Notes
UM463	*cpIs42[Pmex-5::mNeonGreen::PLCδ-PH::tbb-2 3'UTR; unc-119(+)] II; ltIs37[pAA64; Ppie-1::mCherry::HIS-58; unc-119(+)] IV*	Also used to generate a tetraploid strain.
OD95	*ItIs37 [(pAA64 Ppie-1::mCherry::HIS-58 + unc-119(+)]; ItIs38 [pie-1p::GFP::PH(PLC1delta1) + unc-119(+)] III*	
SWG001	*mex-5p::Lifeact::mKate2*	
LP162	*cp13[nmy-2::gfp + LoxP]) I.*	Also used to generate a tetraploid strain.
MDX29	*ani-1(mon7[mNeonGreen^3xFlag::ani-1]) III*	

APPENDIX

Manuscript published as: OZUGERGIN, I. & PIEKNY, A. 2021. Complementary functions for the Ran gradient during division. *Small GTPases,* 12**,** 177-187.

SMALL GTPASES
2021, VOL. 12, NO. 3, 177–187
https://doi.org/10.1080/21541248.2020.1725371

Taylor & Francis
Taylor & Francis Group

REVIEWS

Complementary functions for the Ran gradient during division

Imge Ozugergin and Alisa Piekny

Department of Biology, Concordia University, Montreal, QC, Canada

ABSTRACT

The Ran pathway has a well-described function in nucleocytoplasmic transport, where active Ran dissociates importin/karyopherin-bound cargo containing a nuclear localization signal (NLS) in the nucleus. As cells enter mitosis, the nuclear envelope breaks down and a gradient of active Ran forms where levels are highest near chromatin. This gradient plays a crucial role in regulating mitotic spindle assembly, where active Ran binds to and releases importins from NLS-containing spindle assembly factors. An emerging theme is that the Ran gradient also regulates the actomyosin cortex for processes including polar body extrusion during meiosis, and cytokinesis. For these events, active Ran could play an inhibitory role, where importin-binding may help promote or stabilize a conformation or interaction that favours the recruitment and function of cortical regulators. For either spindle assembly or cortical polarity, the gradient of active Ran determines the extent of importin-binding, the effects of which could vary for different proteins.

ARTICLE HISTORY
Received 28 October 2019
Revised 26 January 2020
Accepted 28 January 2020

KEYWORDS
Ran; importin-α; importin-β; mitosis; cytokinesis

In addition to its well-described function in nucleocytoplasmic transport, the Ran gradient regulates mitotic spindle assembly and cortical actomyosin-dependent events. These cortical processes include cellularization, polar body extrusion and cytokinesis. The mechanisms by which the gradient facilitates spindle assembly are well-described. However, importin-α and/or -β also can localize to the cortex and regulate the function of cortical proteins [Kiyomitsu & Cheeseman 2013, 1,2]. In this review we describe how during division, the Ran gradient plays complementary roles to spatially and temporally regulate spindle assembly and cortical regulation.

Nucleocytoplasmic transport is the best-known function for the small GTPase Ran and importins [3]. The role of karyopherins in nucleocytoplasmic transport has been reviewed extensively [e.g. 4–10]. If a message needs to be relayed to the nucleus, or if proteins or RNA need to be nuclear-localized, the nuclear envelope poses a logistical challenge [4,10,11]. The nuclear pore, a large multicomplex structure that spans the double membrane of the nucleus, serves as a selective gateway to allow for communication between the cytoplasm and the nucleus. Karyopherins, which includes the family of importins, are able to traverse the nuclear pore to bring proteins into or out of the nucleus [6]. Broadly speaking, the process of nucleocytoplasmic shuttling involves the interplay between importins, Ran and exportins [10]. Importins bind to proteins through their nuclear localization signal (NLS) and transport them into the nucleus. Active Ran triggers their dissociation causing NLS-proteins to remain in the nucleus while importins return to the cytoplasm [4–10]. In addition, some proteins bind to exportins and Ran-GTP for transport out of the nucleus.

This review highlights recent data describing the roles of Ran and importins beyond their transport functions. Many proteins that regulate mitotic spindle assembly and cytokinesis have NLS sequences that may regulate their activity via importin-binding (Table 1). Collectively, studies support a model where the Ran/importin gradient is an elegantly balanced system with dual control of processes close to and away from chromatin – a biological example of the principle of yin and yang. We aim to highlight emerging evidence supporting that the functions of Ran-GTP at the two ends of the gradient are interrelated and complementary functions of one system. Although much remains to be explored, we postulate that the Ran gradient acts as a sliding scale. Our current knowledge supports Ran-GTP as a spatial and temporal cue that influences a variety of processes along the length of its gradient across the cell.

Ran-mediated regulation of the mitotic spindle

The regulation of mitotic spindle assembly is one of the prevalent non-transport functions of importins. The Heald group showed that a gradient of active Ran

CONTACT Alisa Piekny alisa.piekny@concordia.ca Department of Biology, Concordia University, 7141 Sherbrooke St. W. Montreal, QC H4B 1R6, Canada

Table 1. Ran-GTP regulation of proteins through importins.

Protein	Protein Function	Interacting Importin	Reference
RCC1	RanGEF	Importin α3 Importin β1	[101,102]
HURP		Importin β1	[33]
Kid		Importin α1 Importin β1	[103,104]
NuMA	Spindle Assembly Factor	Importin α1 Importin β1	[30–32]
TPX2		Importin α1 Importin β1	[27–29]
XCTK2		Importin α1 Importin β1	[105]
Cdc7	Serine/threonine kinase	Importin α2 Importin β1	[39,106]
PTHrP	Various functions	Importin α1 Importin β1	[40,107]
Snail	Transcription factor	Importin α1 Importin α3 Importin α5 Importin β1	[41]
TRF1	Regulator of telomere length	Importin α1 Importin β1	[42]
Ect2	RhoGEF	Importin α* Importin β1	[83,92]
Anillin	Scaffold for the contractile ring	Importin α Importin β1 Importin β2	[1,58,80]
Cyk-4/ MgcRacGAP	Forms central spindle	Importin α1 Importin β1	[88]
MKLP1	Forms central spindle	Unknown	[87,90,91]
GAL4	Transcription factor	Importin α1 Importin β1	[43,108]
N-WASP	Activator of Arp2/3	Importin α1 Importin α5	[51]
GCK-III	Subgroup of Ste20-like serine/ threonine kinases	Unknown	[84]

*Ect2 contains a classic NLS, and though direct importin-α interaction was not demonstrated, heterodimer interaction was inferred through importin-β binding.

forms in the vicinity of chromatin, which controls the release of importin-bound spindle assembly factors [SAFs; 12–14]. In interphase cells, RCC1, the RanGEF (guanine nucleotide exchange factor), is enriched in the nucleus, and RanGAP (GTPase-activating protein), is in the cytoplasm [10,15]. Their differential localization creates a gradient of active Ran that is high in the nucleus and low in the cytoplasm. This gradient persists after nuclear envelope breakdown, as RCC1 remains associated with chromatin [13, 16, Figure 1(a)]. Importin-α binds to the classical NLS of SAFs and serves as an adaptor for importin-β via its autoinhibitory IBB (importin-β binding) domain [10,11,15,17–19]. Importin-β-binding causes a conformational change that displaces the IBB and relieves autoinhibition to permit cargo-binding [18–20]. The working model is that binding of the α/β heterodimer impedes SAF function by hindering binding to proteins required for their function in bipolar spindle assembly. When Ran-GTP binds to the importin-SAF complex in the vicinity of chromatin, the SAF is released to carry out its function [7,10,21]. As a result, cells have a gradient of SAF-bound importins that is inverse, although not necessarily proportional to the active Ran gradient (Figure 1(a,b)).

The Ran-GTP gradient was demonstrated in several model systems by the Heald lab [12,13,16]. They generated a fluorescence resonance energy transfer (FRET) probe termed Rango (Ran-regulated importin-β cargo) that indirectly shows Ran-GTP levels. Strikingly, they showed that a gradient of active Ran persists after nuclear envelope breakdown in mitotic *Xenopus laevis* egg extracts and in HeLa cells [13,16]. In both systems, the Ran-GTP gradient is steep with high concentrations near chromatin, and lower concentrations over the length of the spindle, followed by a sharp decrease at spindle poles [13,16]. Importantly, the steepness of the gradient is not the same in every cell, and at least partly depends on ploidy, with chromosomal gain driving a steeper gradient [22]. It will be interesting to determine how the regulation of RCC1 or RanGAP gene expression compares between different cell types, which could indicate different threshold requirements for the Ran-regulation of spindle assembly. For example, this pathway could be more dominant in aneuploid cancer cells to help them avoid mitotic catastrophe.

Several reviews have highlighted how the Ran gradient regulates the function of SAFs [e.g. 23,14]. Spindle assembly requires the coordinated function of MAPs (microtubule associated proteins) required for microtubule nucleation, stability, bundling and/or motors to generate force [23,24]. As cells enter mitosis, centrosomes mature, nucleate microtubules and separate. The length and kinetics of microtubules must be controlled to ensure the formation of stable microtubule attachments at kinetochores, which is necessary for proper chromosome alignment and subsequent separation as cells exit mitosis [25,26]. Factors such as TPX2, NuMA and HURP, which regulate microtubule nucleation, bundling and stability, are all negatively regulated by importin-binding [14,23]. TPX2 is directly inhibited by importin-α of the heterodimer [27–29], while NuMA is sterically hindered by importin-β of the heterodimer [30–32], and HURP is directly inhibited by importin-β-binding [33, Figure 2]. Thus, different SAFs are regulated differently by importin-α, importin-β, or the heterodimer. Since each could have unique contact sites when bound to cargo, their effect on intra- or intermolecular interactions could be different [7,15,30,34]. This fits with the concept that not all SAFs have the same spatial or temporal functional requirements [35].

Different SAFs function in different locations of the cell for mitotic spindle assembly. The mitotic spindle

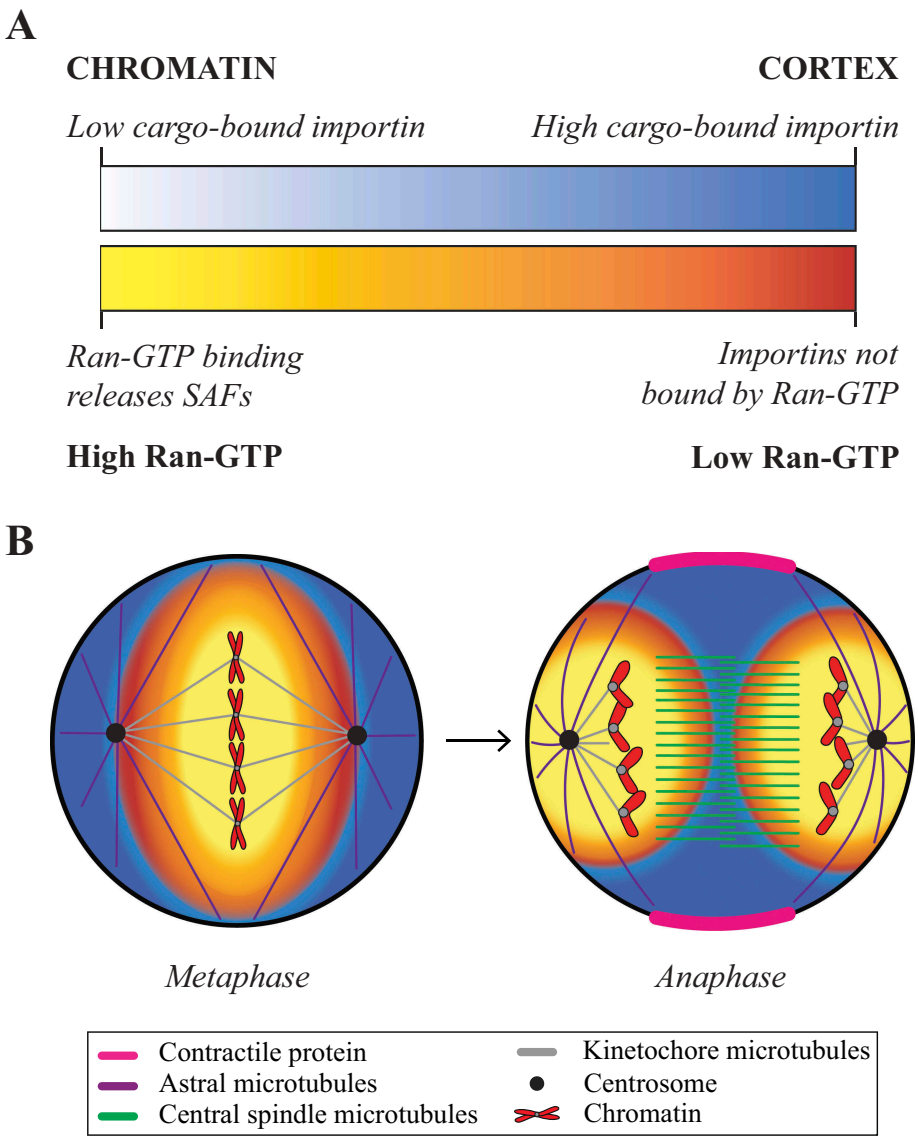

Figure 1. The Ran gradient regulates different stages of mitosis. (a) Following nuclear envelope breakdown, active Ran (Ran-GTP) levels remain as a gradient that decreases from chromatin towards the cortex (orange gradient – dark orange is low) [13,16]. RCC1, the RanGEF that generates active Ran, remains associated with chromatin, while RanGAP generates inactive Ran (Ran-GDP) and is cytosolic [12]. There is an inverse gradient of importins bound to NLS-containing proteins, which is highest near the cortex (blue gradient – dark blue is high) [4]. (b) Cartoon schematics show a cell in metaphase (left) and anaphase (right) with the relative locations of active Ran (orange gradient) and importin-bound proteins (blue gradient) [13,16]. The legend indicates the components of the cell with chromatin (red), centrosome (black), central spindle microtubules (green), astral microtubules (purple), kinetochore microtubules (grey) and contractile proteins (pink). During metaphase, the spindle is controlled by the high levels of Ran-GTP around chromatin, while in anaphase, importin-binding facilitates the cortical localization of proteins such as anillin to control polarity [1,12].

occupies a large proportion of the cell, with the spindle poles positioned away from chromatin where Ran-GTP levels are highest [13]. Some SAFs are required close to chromatin for chromosome alignment, such as HURP and the chromokinesin Kid, while others function at the poles and/or over a larger distance, such as XCTK2, TPX2 and NuMA for minus end stability and/or microtubule nucleation [12,35,36]. The spatial and temporal control of SAFs could be achieved through their different binding affinities for importin-α, -β, or the heterodimer, or steepness of the Ran-GTP gradient. Our understanding of the spatial requirements for the Ran/importin gradients could benefit from computational models of spindle assembly [37,38]. Further, visualizing these gradients in different cell types and cell cycle stages would help verify and improve these models, and predict where they function.

The formation of importin-SAF complexes also could vary depending on intra-/intermolecular inhibition or post-translational modifications. A recent study

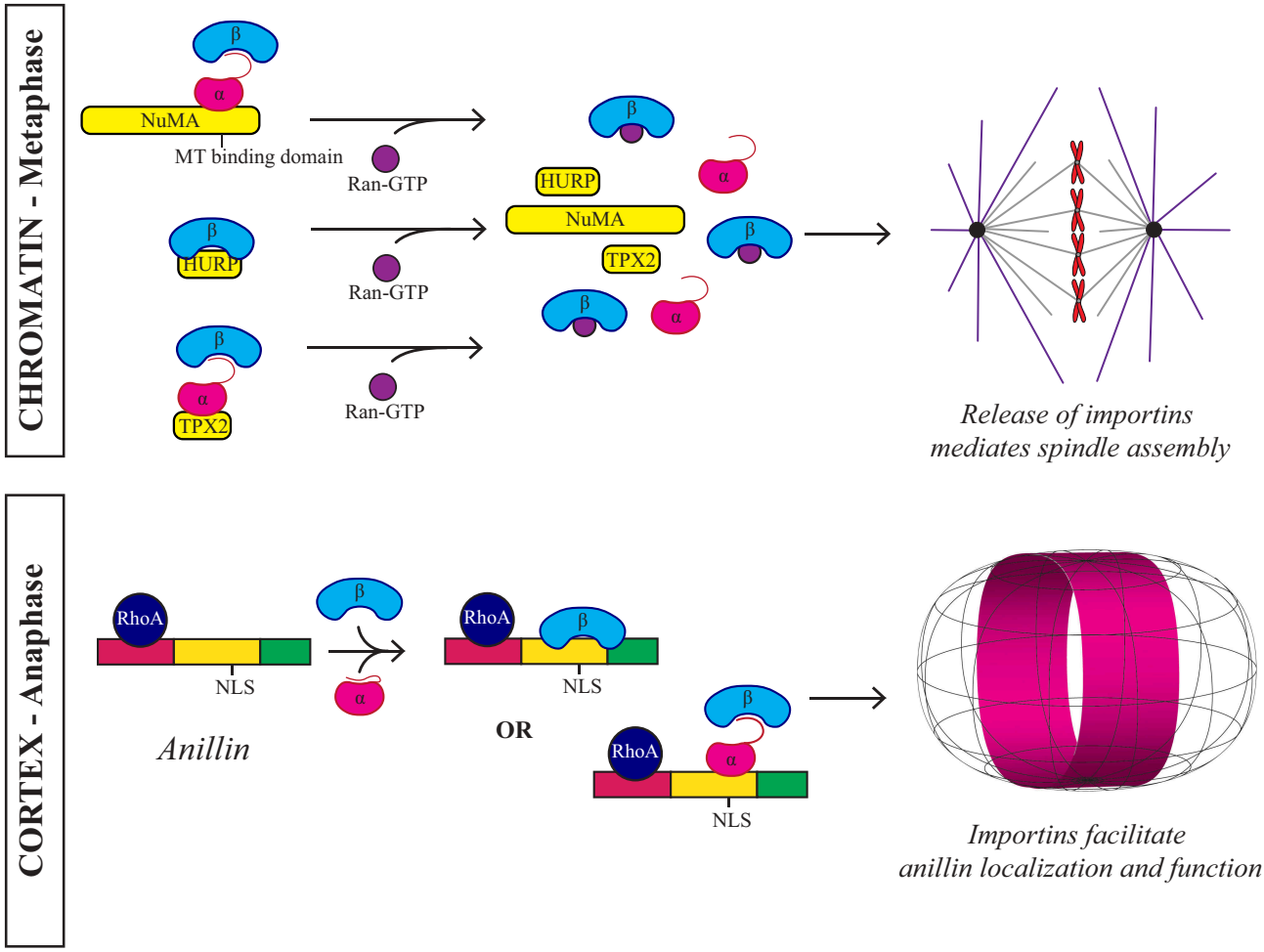

Figure 2. Ran regulates proteins required for spindle assembly and cortical polarity. During metaphase, the Ran gradient regulates spindle assembly in the vicinity of chromatin. Among other proteins, importin-binding inhibits the function of TPX2, NuMA and HURP (all in light yellow), although the mechanism by which this occurs differs for each protein [14,23]. The microtubule-bundling activity of HURP is directly inhibited by importin-β (blue) binding [33], whereas the α/β heterodimer inhibits TPX2 and NuMA. In the heterodimer, importin-β sterically hinders the microtubule binding site of NuMA [30–32]. Importin-α (pink) directly inhibits TPX2, but requires importin-β for TPX2-binding [27–29]. The release of SAFs from importins by Ran-GTP (purple) permits them to carry out their function in spindle assembly [12]. The spatial location of cargo release from importins would depend on various factors including binding affinity to importins (-α, -β or the heterodimer) and post-translational modifications. Thus, where the importin and Ran gradients are functionally relevant, as well as the gradient steepness and length-scale of these gradients could be unique to each NLS-containing cargo. During anaphase, importin-binding regulates cortical proteins [1]. In particular, anillin is a conserved protein that crosslinks components of the contractile ring for cytokinesis. The C-terminus of anillin contains a RhoA-GTP Binding Domain (RBD; red), a C2 domain (yellow), and a Pleckstrin homology domain (PH; green) [95]. RhoA-GTP (dark blue) binds to the RBD, causing a conformational change that relieves autoinhibition of the NLS in the neighbouring C2 domain. This domain also contains binding sites for phospholipids, microtubules and Ect2, the GEF required for RhoA activation. Importin-β-binding facilitates cortical recruitment, by stabilizing a conformation that may favour these other interactions [1]. We propose that other NLS-containing contractile proteins could similarly be regulated by importin-binding.

showed that a fraction of importin-α is palmitoylated and associated with the plasma membrane [2]. Hyper-palmitoylation caused a decrease in spindle and nuclear size, suggesting that sequestering importin-α at the membrane reduces the cytosolic pool regulating SAF function and nuclear import [2]. However, hyper-palmitoylation did not prevent a bipolar spindle from forming, suggesting that many SAFs remained functional likely because they are regulated directly by importin-β. This also raises the question as to whether importin-β binds to palmitoylated -α. This study highlights the unique localization and/or functions of importin-α, and it would be interesting to understand the different threshold requirements for the function of importin-α or -β as monomers vs. the heterodimer.

An increasing number of studies is requiring us to re-evaluate the conventional view on how the Ran/importin system regulates NLS-containing proteins.

For example, several studies showed that the importin-β-mediated nuclear localization of proteins such as Cdc7 [39], PTHrP [40], Snail [41] and TRF1 [42] is inhibited by importin-α. Another study showed that importin-α acts as a coactivator of the transcriptional activator GAL4 when it is bound to DNA [43]. Thus, importins can play negative or positive roles in different contexts, and the binding of importin-α and/or -β does not have to impede the function of a target protein, but rather could facilitate conformational changes that are favourable for binding to other partners and/or function. As discussed in the following sections, the location of a particular protein along the Ran gradient could also correlate with whether importins positively vs. negatively regulate protein function.

Ran-mediated regulation of the cortex

Ran in meiosis

The Ran-GTP gradient also regulates polar body formation in mouse oocytes. During meiosis, polar bodies extrude complements of DNA to reduce ploidy [reviewed in 44, 45]. The small, acentrosomal meiotic spindle forms near the cortex and positions the chromosomes for segregation into the polar body (Figure 3(a)). Prior to extrusion of the polar body, the cortex is polarized by the formation of an F-actin cap [44,45]. Dumont et al. [46] used the previously mentioned FRET probe Rango to show that a Ran-GTP gradient forms around meiotic DNA in the mouse oocyte. In a separate study, Deng et al. [47] showed that Ran-GTP is required to establish cortical polarity and induce the formation of the cortical F-actin cap. By injecting beads coated with bacterial or yeast plasmid DNA into MII oocytes, they found that the cap could still form in response to any type of DNA. Interestingly, the elicited response was both DNA-dosage and -distance dependent. Both the amount of input DNA and the distance of DNA to the cortex correlated with the magnitude of response; one DNA bead induced a smaller cortical cap than three beads, and three DNA beads could elicit a response within 10 μm of the cortex, less so at 20 μm, and not at 30 μm. Thus, the authors hypothesized that the Ran-GTP gradient helps cells sense chromatin position by serving as a molecular ruler.

Additional studies revealed that there could be crosstalk between Ran and Cdc42, although they did not explore the mechanism by which this occurs [48]. Active Cdc42 recruits N-WASP to regulate Arp2/3 for the nucleation of actin filaments that form the cortical cap [49]. N-WASP has an NLS and it would be interesting to determine if it can be directly regulated by importin-binding [50,51]. Burdyniuk et al. [52] proposed a unique role for Ran-GTP in regulating F-actin for chromosome alignment in starfish oocytes. They found that an Arp2/3-nucleated F-actin network forms around chromosomes during meiosis in a Ran-GTP-dependent manner to collect chromosomes scattered over a large distance [52]. Since these F-actin patches prevent microtubule-kinetochore attachments, they must disassemble before attachments can be made, which would help prevent aneuploidy.

In addition to regulating chromosome alignment, having a cue associated with meiotic chromatin that regulates the cortex would ensure that actin and myosin assembly for polar body formation occurs only when chromatin is at an ideal distance to the cortex to prevent aneuploidy. Deng et al. [47] also reported that injection of constitutively active Ran^{Q69L} inhibited cap formation rather than inducing larger or multiple caps, which is similar to observations from studies on the role of Ran in cytokinesis [1]. Further studies using ooctyes that vary in size, and from different species, will expand our knowledge of the molecular mechanisms of the Ran pathway in meiosis.

Importins in cellularization

Another cortical process that was shown to be regulated by importins is cellularization in *Drosophila* (Figure 3(b)). After 9 mitotic divisions, the nuclei of the syncytial embryo migrate to the periphery and subsequently become separated by membranes via a process of cellularization, which begins during the 14th division [e.g. 53, 54, 55]. This process gives rise to a layer of polarized epithelial cells connected via adherens junctions, and occurs due to the trafficking of vesicles for directed membrane growth [56]. The end-stages of cellularization have some similarity to cytokinesis. Anillin, a scaffold protein that binds to actin, myosin and septins and has well-described roles in cytokinesis, is also required for cellularization, although its role in this process is not well-understood [57]. Silverman-Gavrila et al. [58] showed that importins could regulate anillin's localization during cellularization. They found that over-expression of importin-α decreases anillin's cortical localization, and showed that importin-α/β could outcompete the septin Peanut for anillin-binding [58]. However, since the nuclei are enclosed during cellularization and Ran-GTP would be sequestered, it is not clear how importin-binding regulates anillin localization. Based on our studies of anillin in cytokinesis (see below), one hypothesis is that cytosolic importins promote anillin's recruitment to the cortex by modulating its conformation for septin and/or lipid-binding, but its enrichment to precise locations is governed by binding to active RhoA.

Other studies showed that importins can regulate proteins independently of Ran for mitotic Golgi

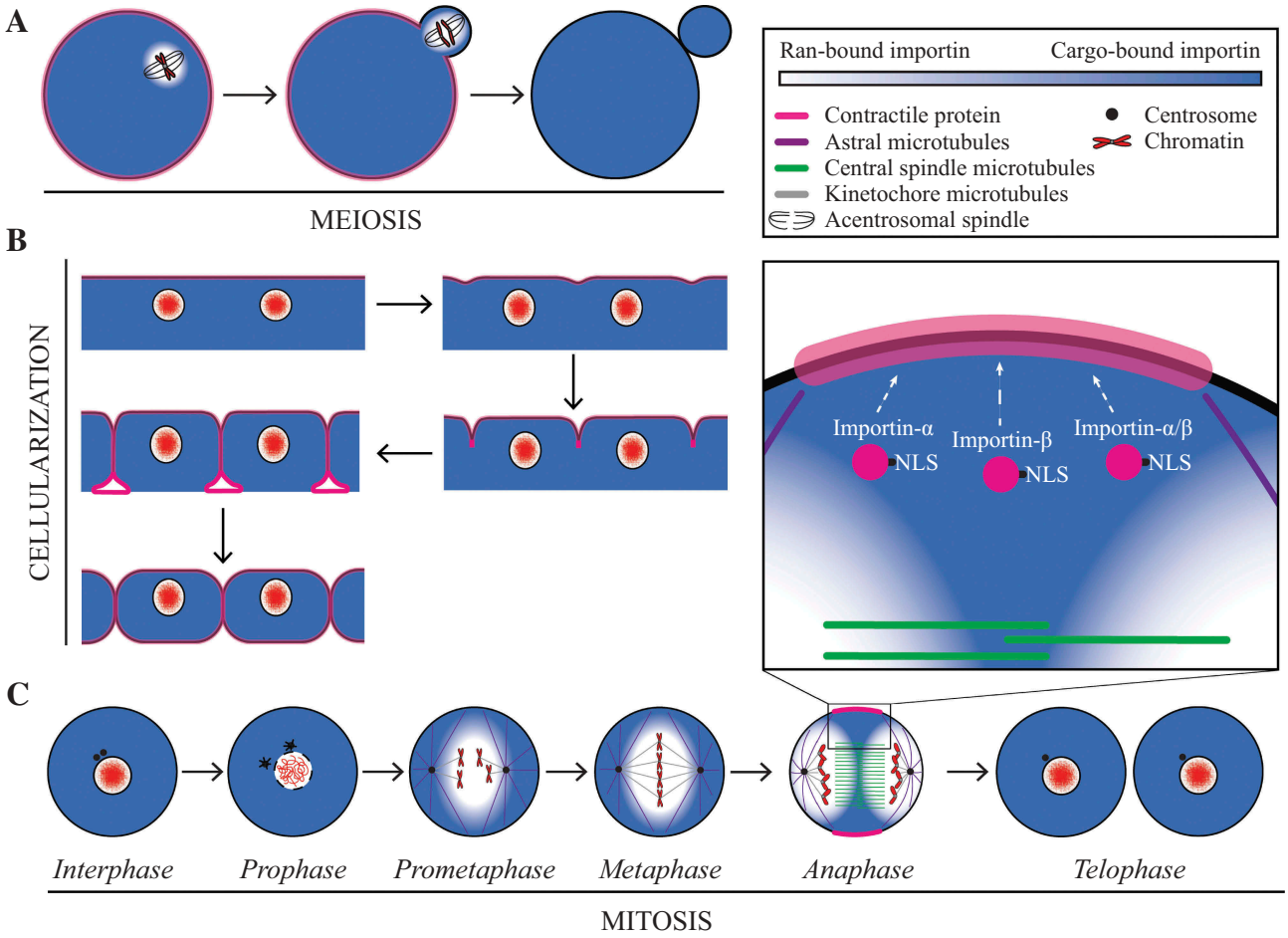

Figure 3. The Ran gradient regulates cortical proteins. (a) Cartoon schematics show an oocyte undergoing polar body extrusion. The legend describes the cell components for the cells in (a–c); contractile proteins (pink), astral microtubules (purple), central spindle microtubules (green), kinetochore microtubules (grey), centrosome (black) and chromatin (red). The Ran gradient is enriched around chromatin, which is positioned close to the cortex and functions as a molecular ruler to direct actin cap formation [47]. (b) During cellularization, Ran-GTP is sequestered in closed nuclei, and importin-binding could increase the localization of proteins at the cortex. The enrichment of proteins at the ingressing membrane would be directed by other factors. (c) In mitotic somatic cells Ran-GTP is generated at chromatin by RCC1 (RanGEF), which is hydrolysed by RanGAP in the cytosol to form a gradient. An inverse gradient of importin-bound proteins forms so that they are high near the cortex. In prometaphase and metaphase, Ran-GTP regulates spindle formation by releasing active spindle assembly factors from importin-binding [12]. In anaphase, importin-binding facilitates anillin's localization to the equatorial cortex for cytokinesis, and we propose that other cortical proteins could similarly be regulated by importin-binding [1]. Ran-GTP is sequestered in the nucleus in telophase as the nuclear envelope reforms (Clarke & Zhang, 2008, 4).

disassembly [59]. Importin-α and other karyopherins may thus have interactions and functions that occur outside of the Ran pathway. This raises the possibility that in the context of cellularization – a closed system in which little to no Ran would be found in the cytoplasm – importins could be functioning at the cortex in a Ran-independent manner to form separate cells.

Ran in cytokinesis

Cytokinesis occurs at the end of mitosis to separate a cell into two daughters (Figure 3(c)). This highly conserved process must occur with high precision to avoid aneuploidy or changes in cell fate [60–62]. Multiple pathways regulate cytokinesis, and can be microtubule-dependent or -independent [60,62]. While these pathways likely function redundantly in symmetrically dividing cells, the preference for one over another may depend on cell fate, architecture, or ploidy. Cytokinesis occurs due to the ingression of a RhoA-dependent contractile ring. The central spindle, which arises between segregating chromatids in anaphase, stimulates the accumulation of active RhoA in the equatorial cortex via the regulation of cortical complexes that activate Ect2, a RhoA guanine nucleotide exchange factor [GEF; e.g. reviewed by 60–62]. Ect2 forms an anaphase-dependent complex with Cyk-4/

MgcRacGAP and MKLP1 at the cortex, which potentiates its activity [61,63–65]. Astral microtubules, which emanate from the centrosomes towards the polar cortex, globally inhibit cortical contractility, leading to the equatorial accumulation of contractile proteins as the spindle elongates [61,62,66]. In addition, MP-GAP globally inhibits RhoA and functions together with astral microtubules to ensure that cortical contractility is dampened outside the equatorial plane [67]. p190RhoGAP also controls contractility in the division plane by modulating RhoA activity [68–71]. It is not clear how astral microtubules regulate cytokinesis, although data supports that these microtubules could sequester anillin, which has a microtubule-binding domain [72,73]. As shown in *C. elegans* embryos, another mechanism could involve the TPXL-1 (TPX2)-mediated polar clearance of contractile proteins by Aurora A kinase [74]. Microtubule-independent pathways also regulate cytokinesis, by signalling through the centrosomes, kinetochores and chromosomes [1,47,58,67,75–79]. In particular, sensing chromatin position could help prevent aneuploidy, especially in asymmetrically dividing cells, and will be discussed below.

In mammalian cells, several studies demonstrated a correlation between chromatin position and cortical contractility during anaphase [1,77,79]. The Ran gradient persists into anaphase (Figures 1(a,b) and 3(c)), and Kiyomitsu & Cheeseman [77] showed that elongation of the cortex occurs in response to spindle positioning. In particular, the site of ingression shifts to recover the equatorial plane when the spindle is displaced towards one of the poles. They proposed that cortical proteins are negatively regulated by Ran-GTP associated with chromatin. In support of this model, they found that cortical proteins polarize in response to chromatin position in BHK (baby hamster kidney epithelial) cells with depolymerized microtubules forced to exit mitosis, which fail to occur upon loss of RCC1 [77]. Overall, this data showed that Ran-GTP inhibits contractility at the cortex, although the mechanism by which it does this was not known [77].

A more recent study by our group offers insight into the molecular mechanism of how Ran-GTP regulates the cortex for cytokinesis [1]. We found that importin-β binds to a conserved C-terminal NLS in anillin, and point mutations that disrupt importin-binding decrease anillin's cortical affinity and function for cytokinesis (Figure 2). The NLS, which is in the C2 domain, is autoinhibited by the neighbouring RhoA-GTP binding domain (RBD). This led us to propose a model where active RhoA initially induces conformational changes in anillin, that then could be stabilized by importin-binding (Figures 2 and 3(c)). Our model also considers that importins optimally regulate anillin function at an ideal concentration. Similar to the findings from Silverman-Gavrila et al. [58] for cellularization, over-expressing importin-β also decreases anillin's cortical affinity during cytokinesis [1]. We propose that anillin's affinity for importins is lower than that of its other binding partners such as phospholipids, RhoA regulators and septins to permit a 'hand-off' from importins to these other components at the equatorial membrane.

Several cytokinesis regulators have at least one NLS that mediates nuclear localization during interphase, and it would be exciting to explore their regulation by the Ran pathway during mitotic exit [i.e. 80–83]. For example, mammalian GCK-III proteins have an NLS [84], and recent studies showed that GCK-1 (*C. elegans*) may counteract active RhoA by restricting the amount of anillin and myosin in the contractile ring to brake contractility [85,86]. Other key cytokinesis regulators with an NLS include Ect2, Cyk-4, and MKLP1 [83,87,88]. Having an NLS could permit the regulation of cytokinesis proteins in various ways by importin-binding. For example, Ect2 and MKLP1 have phosphorylation sites for cell cycle kinases in/near their NLS's, and phosphorylation could affect importin-binding, causing them to accumulate in the cytosol during prophase and/or prevent their sequestration after nuclear reformation [89–92]. However, another role to consider for importin-binding could be to control their cortical localization and function. Interestingly, human anillin has more than one NLS; the N-terminal NLS mediates nucleocytoplasmic transport through importin-β2-binding, while the highly-conserved C-terminal bipartite classic NLS binds to importin-β for anillin's cortical recruitment and function in cytokinesis [1,80]. This raises an interesting question as to whether the highly conserved, C-terminal NLS initially arose in metazoans to mediate nuclear localization, but then was co-opted into a second function of controlling cortical localization and function, or vice-versa.

In a biological context, there are many advantages to having the Ran pathway regulate cytokinesis proteins. The enrichment of importins available to bind to NLS-containing proteins near the cortex can facilitate the recruitment of cortical regulators prior to central spindle-dependent mechanisms. In cells where chromatin is asymmetrically positioned, this can create an asymmetric distribution of contractile proteins for asymmetric furrow ingression. In cells where ploidy is high, this could delay contractile protein recruitment until chromosomes have already begun segregating

towards their poles, which could tightly couple ingression with chromosome segregation to prevent aneuploidy.

Most of our knowledge of cytokinesis is from studies done using cultured cells, either from *Drosophila* (S2 cells) or mammalian cells (HeLa cells), or in the one-celled *C. elegans* or sea urchin embryo [e.g. 93–95, 64]. It is assumed that the preference for different mechanisms regulating cytokinesis depends on the organism, but this could also be due to differences in cell fate, geometry, ploidy or the number of neighbouring cells. For example, the central spindle is quite small in the early embryo relative to cell size in *C. elegans*, echinoderms and *Xenopus*, and the astral spindle pathway more dominantly regulates cytokinesis in these cells [76,96,97]. A recent study by Davies et al. [98] showed that P_2 and EMS cells rely differently on F-actin-dependent mechanisms, as well as intrinsic vs. extrinsic cues. This highlights the need to explore mechanisms regulating cytokinesis of cells in their native tissue and in developmental contexts. Since few studies have explored the role of the Ran pathway in cytokinesis, we are studying its role in regulating cytokinesis of AB and P_1 cells in early *C. elegans* embryos. The AB cell, which is larger and divides first, is fated to be many tissues of the body, while the P_1 cell is fated to become the germline [99]. It will be interesting to determine if the Ran pathway differently regulates cortical contractility for cytokinesis in these cells.

Concluding remarks

To summarize, the Ran/importin gradient is a beautiful example of the principle of yin and yang where the cortex and spindle are regulated in opposing, but complementary ways by the same system. Cortical regulation and spindle assembly occur at opposite ends of the gradient, which acts as a sliding scale that ties these functions together. However, the gradient likely is not linear and the impact on proteins will vary depending on their binding affinities for importin-α, -β or the heterodimer, post-translational modifications, and accessibility or levels at particular cellular locations. Also, since few cortical targets have been identified, the extent to which the gradient regulates cortical polarity is not clear. The finding that RanBP1 (Ran-binding protein 1) controls cortical neuron polarity via regulating LKB1/Par4 [100] suggests that other Ran pathway components also influence protein function. Thus, there may be many layers of complexity in how the Ran pathway regulates polarization in different cell types.

Disclosure statement

No potential conflict of interest was reported by the authors.

Funding

This work was supported by the Natural Sciences and Engineering Research Council of Canada [RGPIN-2017-04161].

References

[1] Beaudet D, Akhshi T, Phillipp J, et al. Active Ran regulates anillin function during cytokinesis. Mol Biol Cell. 2017;28(24):3517–3531.
[2] Brownlee C, Heald R. Importin α partitioning to the plasma membrane regulates intracellular scaling. Cell. 2019;176(4):805–815.
[3] Moore MS, Blobel G. The GTP-binding protein Ran/TC4 is required for protein import into the nucleus. Nature. 1993;365(6447):661–663.
[4] Clarke PR, Zhang C. Spatial and temporal coordination of mitosis by Ran GTPase. Nat Rev Mol Cell Biol. 2008;9(6):464–477.
[5] Güttler T, Görlich D. Ran-dependent nuclear export mediators: a structural perspective. Embo J. 2011;30(17):3457–3474.
[6] Harel A, Forbes DJ. Importin beta: conducting a much larger cellular symphony. Mol Cell. 2004;16(3):319–330.
[7] Lange A, Mills RE, Lange CJ, et al. Classical nuclear localization signals: definition, function, and interaction with importin-α. J Biol Chem. 2007;282(8):5101–5105.
[8] Matsuura Y. Mechanistic insights from structural analyses of Ran-GTPase-driven nuclear export of proteins and RNAs. J Mol Biol. 2016;428(10Pt A):2025–2039.
[9] Oka M, Yoneda Y. Importin α: functions as a nuclear transport factor and beyond. Proc Jpn Acad Ser B Phys Biol Sci. 2018;94(7):259–274.
[10] Xu L, Massagué J. Nucleocytoplasmic shuttling of signal transducers. Nat Rev Mol Cell Biol. 2004;5(3):209–219.
[11] Kimura M, Imamoto N. Biological significance of the importin-β family-dependent nucleocytoplasmic transport pathways. Traffic. 2014;15(7):727–748.
[12] Kaláb P, Heald R. The RanGTP gradient - a GPS for the mitotic spindle. J Cell Sci. 2008;121:1577–1586.
[13] Kaláb P, Pralle A, Isacoff EY, et al. Analysis of a RanGTP-regulated gradient in mitotic somatic cells. Nature. 2006;440(7084):697–701.
[14] Weaver LN, Walczak CE. Spatial gradients controlling spindle assembly. Biochem Soc Trans. 2015;43(1):7–12.
[15] Cook A, Bono F, Jinek M, et al. Structural biology of nucleocytoplasmic transport. Annu Rev Biochem. 2007;76:647–671.
[16] Kaláb P, Weis K, Heald R. Visualization of a Ran-GTP gradient in interphase and mitotic *Xenopus* egg extracts. Science. 2002;295(5564):2452–2456.

[17] Cingolani G, Petosa C, Weis K, et al. Structure of importin-β bound to the IBB domain of importin-α. Nature. 1999;399(6733):221–229.
[18] Goldfarb DS, Corbett AH, Mason DA, et al. Importin α: a multipurpose nuclear-transport receptor. Trends Cell Biol. 2004;14(9):505–514.
[19] Kobe B. Autoinhibition by an internal nuclear localization signal revealed by the crystal structure of mammalian importin α. Nat Struct Biol. 1999;6(4):388–397.
[20] Fanara P, Hodel MR, Corbett AH, et al. Quantitative analysis of nuclear localization signal (NLS)-importin α interaction through fluorescence depolarization. Evidence for auto-inhibitory regulation of NLS binding. J Biol Chem. 2000;275(28):21218–21223.
[21] Görlich D, Panté N, Kutay U, et al. Identification of different roles for RanGDP and RanGTP in nuclear protein import. Embo J. 1996;15(20):5584–5594.
[22] Hasegawa K, Ryu SJ, Kaláb P. Chromosomal gain promotes formation of a steep RanGTP gradient that drives mitosis in aneuploid cells. J Cell Biol. 2013;200 (2):151–161.
[23] Forbes DJ, Travesa A, Nord MS, et al. Nuclear transport factors: global regulation of mitosis. Curr Opin Cell Biol. 2015;35:78–90.
[24] Compton DA. Spindle assembly in animal cells. Annu Rev Biochem. 2000;69:95–114.
[25] Gadde S, Heald R. Mechanisms and molecules of the mitotic spindle. Curr Biol. 2004;14(18):R797–805.
[26] Walczak CE, Cai S, Khodjakov A. Mechanisms of chromosome behaviour during mitosis. Nat Rev Mol Cell Biol. 2010;11(2):91–102.
[27] Giesecke A, Stewart M. Novel binding of the mitotic regulator TPX2 (target protein for *Xenopus* kinesin-like protein 2) to importin-α. J Biol Chem. 2010;285 (23):17628–17635.
[28] Gruss OJ, Carazo-Salas RE, Schatz CA, et al. Ran induces spindle assembly by reversing the inhibitory effect of importin α on TPX2 activity. Cell. 2001;104 (1):83–93.
[29] Schatz CA, Santarella R, Hoenger A, et al. Importin α-regulated nucleation of microtubules by TPX2. Embo J. 2003;22(9):2060–2070.
[30] Chang -C-C, Huang T-L, Shimamoto Y, et al. Regulation of mitotic spindle assembly factor NuMA by importin- β. J Cell Biol. 2017;216(11):3453–3462.
[31] Nachury MV, Maresca TJ, Salmon WC, et al. Importin β is a mitotic target of the small GTPase Ran in spindle assembly. Cell. 2001;104(1):95–106.
[32] Wiese C, Wilde A, Moore MS, et al. Role of importin-β in coupling Ran to downstream targets in microtubule assembly. Science. 2001;291(5504):653–656.
[33] Silljé HHW, Nagel S, Körner R, et al. HURP is a Ran-importin β-regulated protein that stabilizes kinetochore microtubules in the vicinity of chromosomes. Curr Biol. 2006;16(8):731–742.
[34] Miyamoto Y, Yamada K, Yoneda Y. Importin α: a key molecule in nuclear transport and non-transport functions. J Biochem. 2016;160(2):69–75.
[35] Gruss OJ, Vernos I. The mechanism of spindle assembly: functions of Ran and its target TPX2. J Cell Biol. 2004;166(7):949–955.
[36] Petry S. Mechanisms of mitotic spindle assembly. Annu Rev Biochem. 2016;85:659–683.
[37] Caudron M, Bunt G, Bastiaens P, et al. Spatial coordination of spindle assembly by chromosome-mediated signaling gradients. Science. 2005;309 (5739):1373–1376.
[38] Loughlin R, Heald R, Nédélec F. A computational model predicts *Xenopus* meiotic spindle organization. J Cell Biol. 2010;191(7):1239–1249.
[39] Kim BJ, Lee H. Importin-β mediates Cdc7 nuclear import by binding to the kinase insert II domain, which can be antagonized by importin-α. J Biol Chem. 2006;281(17):12041–12049.
[40] Lam MHC, Briggs LJ, Hu W, et al. Importin β recognizes parathyroid hormone-related protein with high affinity and mediates its nuclear import in the absence of importin α. J Biol Chem. 1999;274(11):7391–7398.
[41] Sekimoto T, Miyamoto Y, Arai S, et al. Importin α protein acts as a negative regulator for snail protein nuclear import. J Biol Chem. 2011;286(17):15126–15131.
[42] Forwood JK, Jans DA. Nuclear import pathway of the telomere elongation supressor TRF1: inhibition by importin α. Biochemistry. 2002;41(30):9333–9340.
[43] Chan C-K, Jans DA. Synergy of importin α recognition and DNA binding by the yeast transcriptional activator GAL4. FEBS Lett. 1999;462(1–2):221–224.
[44] Bennabi I, Terret M-E, Verlhac M-H. Meiotic spindle assembly and chromosome segregation in oocytes. J Cell Biol. 2016;215(5):611–619.
[45] Maddox AS, Azoury J, Dumont J. Polar body cytokinesis. Cytoskeleton. 2012;69(11):855–868.
[46] Dumont J, Petri S, Pellegrin F, et al. A centriole- and RanGTP-independent spindle assembly pathway in meiosis I of vertebrate oocytes. J Cell Biol. 2007;176 (3):295–305.
[47] Deng M, Suraneni P, Schultz RM, et al. The Ran GTPase mediates chromatin signaling to control cortical polarity during polar body extrusion in mouse oocytes. Dev Cell. 2007;12(2):301–308.
[48] Dehapiot B, Carrière V, Carroll J, et al. Polarized Cdc42 activation promotes polar body protrusion and asymmetric division in mouse oocytes. Dev Biol. 2013;377(1):202–212.
[49] Yi K, Unruh JR, Deng M, et al. Dynamic maintenance of asymmetric meiotic spindle position through Arp2/3-complex-driven cytoplasmic streaming in mouse oocytes. Nat Cell Biol. 2011;13(10):1252–1258.
[50] Suetsugu S, Takenawa T. Translocation of N-WASP by nuclear localization and export signals into the nucleus modulates expression of HSP90. J Biol Chem. 2003;278 (43):42515–42523.
[51] Wu X, Suetsugu S, Cooper LA, et al. Focal adhesion kinase regulation of N-WASP subcellular localization and function. J Biol Chem. 2004;279(10):9565–9576.
[52] Burdyniuk M, Callegari A, Mori M, et al. F-actin nucleated on chromosomes coordinates their capture by microtubules in oocyte meiosis. J Cell Biol. 2018;217(8):2661–2674.
[53] Lecuit T, Wieschaus E. Polarized insertion of new membrane from a cytoplasmic reservoir during cleavage of the *Drosophila* embryo. J Cell Biol. 2000;150 (4):849–860.

[54] Loncar D, Singer SJ. Cell membrane formation during the cellularization of the syncytial blastoderm of *Drosophila*. Proc Nat Acad Sci. 1995;92(6):2199–2203.
[55] Sisson JC, Field C, Ventura R, et al. Lava lamp, a novel peripheral Golgi protein, is required for *Drosophila melanogaster* cellularization. J Cell Biol. 2000;151(4):905–918.
[56] Lecuit T. Junctions and vesicular trafficking during *Drosophila* cellularization. J Cell Sci. 2004;117:34 27–3433.
[57] Field CM, Coughlin M, Doberstein S, et al. Characterization of *anillin* mutants reveals essential roles in septin localization and plasma membrane integrity. Development. 2005;132(12):2849–2860.
[58] Silverman-Gavrila RV, Hales KG, Wilde A. Anillin-mediated targeting of peanut to pseudocleavage furrows is regulated by the GTPase Ran. Mol Biol Cell. 2008;19(9):3735–3744.
[59] Chang -C-C, Chen C-J, Grauffel C, et al. Ran pathway-independent regulation of mitotic golgi disassembly by importin-α. Nat Commun. 2019;10(1):1–16.
[60] Glotzer M. Cytokinesis in metazoa and fungi. Cold Spring Harb Perspect Biol. 2017;9(10):9:a02234.
[61] Green RA, Paluch E, Oegema K. Cytokinesis in animal cells. Annu Rev Cell Dev Biol. 2012;28:29–58.
[62] Pollard TD, O'Shaughnessy B. Molecular mechanism of cytokinesis. Annu Rev Biochem. 2019;88:661–689.
[63] Hara T, Abe M, Inoue H, et al. Cytokinesis regulator ECT2 changes its conformation through phosphorylation at Thr-341 in G2/M phase. Oncogene. 2006;25 (4):566–578.
[64] Somers WG, Saint R. A RhoGEF and Rho family GTPase-activating protein complex links the contractile ring to cortical microtubules at the onset of cytokinesis. Dev Cell. 2003;4(1):29–39.
[65] Yüce Ö, Piekny A, Glotzer M. An ECT2-centralspindlin complex regulates the localization and function of RhoA. J Cell Biol. 2005;170 (4):571–582.
[66] Murthy K, Wadsworth P. Dual role for microtubules in regulating cortical contractility during cytokinesis. J Cell Sci. 2008;121:2350–2359.
[67] Zanin E, Desai A, Poser I, et al. A conserved RhoGAP limits M phase contractility and coordinates with microtubule asters to confine RhoA during cytokinesis. Dev Cell. 2013;26(5):496–510.
[68] Manchinelly SAS, Miller JA, Su L, et al. Mitotic down-regulation of p190RhoGAP is required for the successful completion of cytokinesis. J Biol Chem. 2010;285(35):26923–26932.
[69] Manukyan A, Ludwig K, Sanchez-Manchinelly S, et al. A complex of p190RhoGAP-A and anillin modulates RhoA-GTP and the cytokinetic furrow in human cells. J Cell Sci. 2015;128(1):50–60.
[70] Mikawa M, Su L, Parsons SJ. Opposing roles of pl90RhoGAP and Ect2 RhoGEF in regulating cytokinesis. Cell Cycle. 2008;7(13):2003–2012.
[71] Su L, Agati JM, Parsons SJ. p190RhoGAP is cell cycle regulated and affects cytokinesis. J Cell Biol. 2003;163 (3):571–582.
[72] Tse YC, Piekny A, Glotzer M. Anillin promotes astral microtubule-directed cortical myosin polarization. Mol Biol Cell. 2011;22(17):3165–3175.
[73] van Oostende Triplet C, Jaramillo Garcia M, Haji Bik H, et al. Anillin interacts with microtubules and is part of the astral pathway that defines cortical domains. J Cell Sci. 2014;127:3699–3710.
[74] Mangal S, Sacher J, Kim T, et al. TPXL-1 activates Aurora A to clear contractile ring components from the polar cortex during cytokinesis. J Cell Biol. 2018;217(3):837–848.
[75] Cabernard C, Prehoda KE, Doe CQ. A spindle-independent cleavage furrow positioning pathway. Nature. 2010;467(7311):91–94.
[76] Dechant R, Glotzer M. Centrosome separation and central spindle assembly act in redundant pathways that regulate microtubule density and trigger cleavage furrow formation. Dev Cell. 2003;4(3):333–344.
[77] Kiyomitsu T, Cheeseman IM. Cortical dynein and asymmetric membrane elongation coordinately position the spindle in anaphase. Cell. 2013;154 (2):391–402.
[78] Petronczki M, Glotzer M, Kraut N, et al. Polo-like kinase 1 triggers the initiation of cytokinesis in human cells by promoting recruitment of the RhoGEF Ect2 to the central spindle. Dev Cell. 2007;12(5):713–725.
[79] Rodrigues NTL, Lekomtsev S, Jananji S, et al. Kinetochore-localized PP1-Sds22 couples chromosome segregation to polar relaxation. Nature. 2015;524 (7566):489–492.
[80] Chen A, Akhshi TK, Lavoie BD, et al. Importin-β2 mediates the spatio-temporal regulation of anillin through a noncanonical nuclear localization signal. J Biol Chem. 2015;290(21):13500–13509.
[81] Lagana A, Dorn JF, De Rop V, et al. A small GTPase molecular switch regulates epigenetic centromere maintenance by stabilizing newly incorporated CENP-A. Nat Cell Biol. 2010;12(12):1186–1193.
[82] Oegema K, Savoian MS, Mitchison TJ, et al. Functional analysis of a human homologue of the *Drosophila* actin binding protein anillin suggests a role in cytokinesis. J Cell Biol. 2000;150(3):539–552.
[83] Tatsumoto T, Xie X, Blumenthal R, et al. Human ECT2 is an exchange factor for Rho GTPases, phosphorylated in G2/M phases, and involved in cytokinesis. J Cell Biol. 1999;147(5):921–927.
[84] Pombo CM, Force T, Kyriakis J, et al. The GCK II and III subfamilies of the STE20 group kinases. Front Biosci. 2007;12:850–859.
[85] Bell K, Werner ME, Doshi A, et al. Novel cytokinetic ring components limit RhoA activity and contractility. BioRxiv. 2019. DOI:10.1101/633743
[86] Rehain-Bell K, Love A, Werner ME, et al. A sterile 20 family kinase and its co-factor CCM-3 regulate contractile ring proteins on germline intercellular bridges. Curr Biol. 2017;27(6):860–867.
[87] Deavours BE, Walker RA. Nuclear localization of C-terminal domains of the kinesin-like protein MKLP-1. Biochem Biophys Res Commun. 1999;260 (3):605–608.
[88] Kawashima T, Bao YC, Minoshima Y, et al. A Rac GTPase-activating protein, MgcRacGAP, is a nuclear localizing signal-containing nuclear chaperone in the activation of STAT transcription factors. Mol Cell Biol. 2009;29(7):1796–1813.

[89] Guse A, Mishima M, Glotzer M. Phosphorylation of ZEN-4/MKLP1 by Aurora B regulates completion of cytokinesis. Curr Biol. 2005;15(8):778–786.
[90] Liu X, Erikson RL. The nuclear localization signal of mitotic kinesin-like protein Mklp-1: effect on Mklp-1 function during cytokinesis. Biochem Biophys Res Commun. 2007;353(4):960–964.
[91] Neef R, Klein UR, Kopajtich R, et al. Cooperation between mitotic kinesins controls the late stages of cytokinesis. Curr Biol. 2006;16(3):301–307.
[92] Suzuki K, Sako K, Akiyama K, et al. Identification of non-Ser/Thr-Pro consensus motifs for Cdk1 and their roles in mitotic regulation of C2H2 zinc finger proteins and Ect2. Sci Rep. 2015;5:1–9.
[93] Bement WM, Benink HA, von Dassow G. A microtubule-dependent zone of active RhoA during cleavage plane specification. J Cell Biol. 2005;170 (1):91–101.
[94] Lewellyn L, Dumont J, Desai A, et al. Analyzing the effects of delaying aster separation on furrow formation during cytokinesis in the *Caenorhabditis elegans* embryo. Mol Biol Cell. 2010;21(1):50–62.
[95] Piekny AJ, Glotzer M. Anillin is a scaffold protein that links RhoA, actin, and myosin during cytokinesis. Curr Biol. 2008;18(1):30–36.
[96] Takayama M, Noguchi T, Yamashiro S, et al. Microtuble organization in *Xenopus* eggs during the first cleavage and its role in cytokinesis. Cell Struct Funct. 2002;27(4):163–171.
[97] von Dassow G, Verbrugghe KJC, Miller AL, et al. Action at a distance during cytokinesis. J Cell Biol. 2009;187(6):831–845.
[98] Davies T, Kim HX, Spica NR, et al. Cell-intrinsic and -extrinsic mechanisms promote cell-type-specific cytokinetic diversity. ELife. 2018;7:e36204.
[99] Rose L, Gönczy P. Polarity establishment, asymmetric division and segregation of fate determinants in early *C. elegans* embryos. WormBook. 2014:1–43. DOI:10.1895/wormbook.1.30.2
[100] Mencarelli C, Nitarska J, Kroecher T, et al. RanBP1 couples nuclear export and Golgi regulation through LKB1 to promote cortical neuron polarity. Cell Rep. 2018;24(10):2529–2539.e4.
[101] Nemergut ME, Macara IG. Nuclear import of the Ran exchange factor, RCC1, is mediated by at least two distinct mechanisms. J Cell Biol. 2000;149(4):835–849.
[102] Talcott B, Moore MS. The nuclear import of RCC1 requires a specific nuclear localization sequence receptor, karyopherin α3/Qip. J Biol Chem. 2000;275 (14):10099–10104.
[103] Trieselmann N, Armstrong S, Rauw J, et al. Ran modulates spindle assembly by regulating a subset of TPX2 and Kid activities including Aurora A activation. J Cell Sci. 2003;116(23):4791–4798.
[104] Tahara K, Takagi M, Ohsugi M, et al. Importin-β and the small guanosine triphosphatase Ran mediate chromosome loading of the human chromokinesin Kid. J Cell Biol. 2008;180(3):493–506.
[105] Ems-McClung SC, Zheng Y, Walczak CE. Importin α/β and Ran-GTP regulate XCTK2 microtubule binding through a bipartite nuclear localization signal. Mol Biol Cell. 2004;15(1):46–57.
[106] Kim BJ, Kim S-Y, Lee H. Identification and characterization of human Cdc7 nuclear retention and export sequences in the context of chromatin binding. J Biol Chem. 2007;282(41):30029–30038.
[107] Cingolani G, Bednenko J, Gillespie MT, et al. Molecular basis for the recognition of a nonclassical nuclear localization signal by importin β. Mol Cell. 2002;10(6):1345–1353.
[108] Chan CK, Hübner S, Hu W, et al. Mutual exclusivity of DNA binding and nuclear localization signal recognition by the yeast transcription factor GAL4: implications for nonviral DNA delivery. Gene Ther. 1998;5(9):1204–1212.